

**DEVELOPMENT OF A BIOHYBRID LUNG**

by

Alexa Ann Polk

B.S. in Biomedical Engineering, University of Miami, 2001

Submitted to the Graduate Faculty of  
School of Engineering in partial fulfillment  
of the requirements for the degree of  
Doctor of Philosophy

University of Pittsburgh

2006

UNIVERSITY OF PITTSBURGH

SCHOOL OF ENGINEERING

This dissertation was presented

by

Alexa Ann Polk

It was defended on

July 10, 2006

and approved by

Donna Beer-Stolz, Ph.D.

Research Assistant Professor, Department of Cell Biology and Physiology

Harvey S. Borovetz, Ph.D.

Professor, Departments of Bioengineering and Surgery

William J. Federspiel, Ph.D.

Associate Professor, Departments of Chemical Engineering, Bioengineering and  
Surgery

Bruce R. Pitt, Ph.D.

Professor and EOH Chair, Departments of Environmental and Occupational Health

Dissertation Director: William R. Wagner, Ph.D.

Associate Professor, Departments of Surgery, Bioengineering and Chemical Engineering

Copyright © by Alexa Ann Polk

2006

## DEVELOPMENT OF A BIOHYBRID LUNG

Alexa Ann Polk, PhD

University of Pittsburgh, 2006

Therapy for patients suffering from acute respiratory distress syndrome (ARDS) is substantially inadequate, resulting in a 40% mortality rate. A biohybrid lung prototype consisting of a rotating endothelialized microporous hollow fiber (MHF) bundle was studied as an alternative solution for improved patient outcome. It is hypothesized that endothelialized MHFs could present a surface mimicking the native vascular lining to reduce thrombotic deposition on underlying MHF. Such an approach might thus allow blood oxygenation and CO<sub>2</sub> removal for extended periods with reduced anticoagulation requirements. Development of the biohybrid lung prototype, evaluation of endothelial cell (EC) response to shear stress, influence of endothelialization on gas transfer, and impact of bundle rotational speed on gas transfer and alterations in EC phenotype were studied.

MHF's were surface modified to promote EC attachment and proliferation. Endothelialized MHF bundles were rotated in the biohybrid lung prototype up to 1500 RPM (29.6 dynes/cm<sup>2</sup>). Blood-surface biocompatibility testing was performed on MHFs and MHF bundles in the biohybrid lung prototype, with or without ECs. Partial O<sub>2</sub> pressures were recorded for blood samples to measure oxygen buildup within the biohybrid lung. Scanning electron micrographs (SEMs) of thrombotic deposition were taken. Upregulation of e-selectin and p-selectin on ECs were assessed for indication of an inflammatory EC phenotype.

ECs maintained near confluent coverage on MHFs under rotation at the tested speeds, and showed minimal p-selectin expression subsequent to rotation. It was observed that even low to moderate levels of EC coverage greatly reduced thrombotic deposition on MHFs. Statistically significant differences in oxygen accumulation between MHF bundles with or without endothelialization in the presence of 95% O<sub>2</sub> were not found. Thrombotic deposition on endothelialized MHF bundles was less than or equivalent to thrombotic deposition on non-endothelialized MHF bundles following rotation. Low levels of e-selectin and p-selectin expression were observed following 24 hr hyperoxia.

These results suggest that endothelialized MHFs may serve to improve blood-surface biocompatibility in the presence of hyperoxia. Although further development and testing is required, a biohybrid lung employing endothelialized MHFs and a rotating fiber bundle may provide an alternative therapy for patients suffering from ARDS.

## TABLE OF CONTENTS

<b>PREFACE.....</b>	<b>XV</b>
<b>1.0 INTRODUCTION.....</b>	<b>1</b>
<b>1.1 OXYGENATION IN THE NATURAL LUNGS .....</b>	<b>1</b>
<b>1.2 ACUTE RESPIRATORY DISTRESS SYNDROME.....</b>	<b>1</b>
<b>1.3 MECHANICAL VENTILATION.....</b>	<b>2</b>
<b>1.3.1 Advancements in mechanical ventilation.....</b>	<b>4</b>
<b>1.3.2 Pharmacological therapies .....</b>	<b>4</b>
<b>1.3.3 Nitric oxide .....</b>	<b>5</b>
<b>1.4 EXTRACORPOREAL MEMBRANE OXYGENATION.....</b>	<b>6</b>
<b>1.4.1 Microporous hollow fiber membranes.....</b>	<b>7</b>
<b>1.4.1.1 Microporous hollow fiber membrane permeance .....</b>	<b>8</b>
<b>1.4.1.2 Microporous hollow fiber membrane failure.....</b>	<b>9</b>
<b>1.4.2 Standard blood oxygenators and microporous hollow fibers .....</b>	<b>12</b>
<b>1.4.3 Mass transfer augmenting blood oxygenators .....</b>	<b>15</b>
<b>1.4.4 Ongoing research for improved oxygenator biocompatibility.....</b>	<b>16</b>
<b>1.5 EC CONSIDERATIONS .....</b>	<b>17</b>
<b>1.5.1 EC inflammatory phenotype.....</b>	<b>17</b>
<b>1.5.2 Coatings for EC attachment .....</b>	<b>18</b>

1.5.3	Shear stress exposure.....	20
1.5.4	Hyperoxia and ECs.....	21
1.6	<b>THE BIOHYBRID LUNG APPROACH .....</b>	<b>22</b>
1.6.1	Significance of the biohybrid lung.....	22
1.6.2	Surface modification of microporous hollow fiber membranes .....	24
1.6.3	Specific aim #1: bioreactor development.....	24
1.6.4	Specific aim #2: ECs conditioned to shear stress .....	25
1.6.5	Specific aim #3: thrombotic deposition and inflammation in the biohybrid lung prototype.....	26
1.6.6	Specific aim #4: hyperoxia in the biohybrid lung prototype.....	27
2.0	<b>SURFACE MODIFICATION OF MICROPOROUS HOLLOW FIBER MEMBRANES .....</b>	<b>29</b>
2.1	<b>INTRODUCTION .....</b>	<b>29</b>
2.2	<b>METHODS.....</b>	<b>30</b>
2.2.1	Surface modification of MHFs to support HUVEC growth .....	30
2.2.2	Surface modification of PMP MHFs to support BAEC growth.....	32
2.2.3	Statistics for MHFs to support HUVEC growth.....	32
2.2.4	Statistics for PMP MHFs to support BAEC growth.....	33
2.3	<b>RESULTS .....</b>	<b>33</b>
2.3.1	Surface modification of MHFs to support HUVEC growth .....	33
2.3.2	Surface modification of PMP MHFs to support BAEC growth.....	36
2.4	<b>DISCUSSION.....</b>	<b>37</b>
3.0	<b>BIOREACTOR DEVELOPMENT .....</b>	<b>39</b>
3.1	<b>INTRODUCTION .....</b>	<b>39</b>
3.2	<b>METHODS.....</b>	<b>40</b>

3.2.1	Biohybrid lung prototype design and development.....	40
3.2.2	Bioreactor Sterility and Assembly.....	42
3.2.3	Shear Stress Calculations for Rotation of a MHF Bundle .....	43
3.3	RESULTS .....	45
3.3.1	Biohybrid lung prototype design and development.....	45
3.3.2	Shear Stress Calculations.....	49
3.4	DISCUSSION.....	50
4.0	ENDOTHELIALIZATION AND ROTATION OF MHF BUNDLES .....	53
4.1	INTRODUCTION .....	53
4.2	METHODS.....	54
4.2.1	Endothelialization of MHF bundles .....	54
4.2.2	Rotation of endothelialized MHF bundles.....	54
4.3	RESULTS .....	56
4.3.1	Endothelialization of MHF bundles .....	56
4.3.2	Rotation of endothelialized MHF bundles.....	58
4.4	DISCUSSION.....	62
5.0	THROMBOTIC DEPOSITION AND INFLAMMATION IN THE BIOHBRID LUNG PROTOTYPE.....	64
5.1	INTRODUCTION .....	64
5.2	METHODS.....	65
5.2.1	Bovine blood collection and preparation .....	65
5.2.2	MHF patches exposed to bovine blood.....	66
5.2.3	MHF bundles exposed to bovine blood .....	67
5.2.4	Statistics .....	68
5.3	RESULTS.....	68

5.3.1	Bovine blood collection and preparation .....	68
5.3.2	MHF patches exposed to bovine blood.....	69
5.3.3	MHF bundles exposed to bovine blood .....	73
5.4	DISCUSSION.....	77
6.0	HYPEROXIA IN THE BIOHYBRID LUNG PROTOTYPE.....	80
6.1	INTRODUCTION .....	80
6.2	METHODS.....	80
6.2.1	Oxygen accumulation in cell culture medium in the biohybrid lung prototype .....	80
6.2.2	Bovine blood collection and preparation .....	81
6.2.3	Oxygen accumulation in bovine blood in the biohybrid lung prototype	81
6.2.4	Evaluation of endothelialized MHF bundles following hyperoxia and bovine blood exposure .....	82
6.2.5	Statistics .....	83
6.3	RESULTS .....	83
6.3.1	Oxygen accumulation in cell culture medium in the biohybrid lung prototype .....	83
6.3.2	Oxygen accumulation in bovine blood in the biohybrid lung prototype	85
6.3.3	Evaluation of endothelialized MHF bundles following hyperoxia and bovine blood exposure .....	87
6.4	DISCUSSION.....	93
6.4.1	Oxygen accumulation in the biohybrid lung prototype .....	93
6.4.2	Evaluation of endothelialized MHF bundles following hyperoxia and bovine blood exposure .....	95
7.0	SUMMARY .....	97
7.1	CONCLUSIONS .....	97

<b>7.2</b>	<b>FUTURE WORK.....</b>	<b>99</b>
<b>APPENDIX A .....</b>	<b>101</b>	
<b>APPENDIX B .....</b>	<b>105</b>	
<b>APPENDIX C .....</b>	<b>107</b>	
<b>APPENDIX D .....</b>	<b>109</b>	
<b>APPENDIX E .....</b>	<b>111</b>	
<b>APPENDIX F .....</b>	<b>113</b>	
<b>BIBLIOGRAPHY.....</b>	<b>117</b>	

## LIST OF TABLES

Table 1 Nine MHF oxygenators .....	12
Table 2 Hemoglobin and platelet levels in nine MHF oxygenators .....	13
Table 3 Shear stress calculations .....	49
Table 4 Taylor number for corresponding RPM in the biohybrid lung prototype.....	110

## LIST OF FIGURES

Figure 2-1	Fibronectin effect on HUVEC growth on PP and PDMS MHFs .....	34
Figure 2-2	Collagen and matrigel effect on HUVEC growth on PDMS MHFs .....	35
Figure 2-3	RGDS effect on HUVEC growth on PDMS MHFs .....	36
Figure 2-4	BAEC coverage on PMP MHF patches of varying surface modification .....	37
Figure 3-1	Schematic of biohybrid lung prototype .....	41
Figure 3-2	Original biohybrid lung prototype .....	45
Figure 3-3	Original biohybrid lung prototype stainless steel components .....	46
Figure 3-4	Vyton seal exhibited debris in the original biohybrid lung prototype .....	46
Figure 3-5	Finalized biohybrid lung prototype .....	47
Figure 3-6	Microporous hollow fiber bundle and seeding tube .....	48
Figure 4-1	Protocol for acceleration of an endothelialized MHF bundle in the biohybrid lung prototype .....	55
Figure 4-2	Endothelialized microporous hollow fiber bundle, without rotation .....	57
Figure 4-3	Endothelialized microporous hollow fiber bundle without rotation .....	58
Figure 4-4	Endothelialized microporous hollow fiber bundles with rotation .....	60
Figure 4-5	Outer layer of endothelialized microporous hollow fiber bundles, with rotation ....	61
Figure 5-1	Thrombotic deposition shown on MHF patches with light microscopy .....	69
Figure 5-2	Thrombotic deposition on MHF patches shown by SEM .....	70

Figure 5-3 Thrombotic deposition on endothelialized PMP MHF patches.....	71
Figure 5-4 Electron micrographs of MHF bundles following rotation at 250 RPM and bovine blood exposure .....	74
Figure 5-5 Electron micrographs of MHF bundles following rotation at 750 RPM and bovine blood exposure .....	75
Figure 5-6 P-selectin expression for control BAECs from tissue culture flasks.....	76
Figure 5-7 P-selectin expression by BAECs from endothelialized MHF bundles.....	77
Figure 6-1 Oxygen accumulation in the biohybrid lung prototype in cell culture medium.....	84
Figure 6-2 Carbon dioxide accumulation in the biohybrid lung prototype in cell culture medium .....	85
Figure 6-3 Oxygen accumulation in the biohybrid lung prototype in blood.....	86
Figure 6-4 Carbon dioxide accumulation in the biohybrid lung prototype in blood.....	87
Figure 6-5 Electron micrographs of MHF modules rotated at 250 RPM exposed to bovine blood and hyperoxia.....	88
Figure 6-6 Electron micrographs of MHF modules rotated at 750 RPM exposed to bovine blood and hyperoxia.....	89
Figure 6-7 Confocal images of positive and negative immunofluorescent controls for e-selectin .....	90
Figure 6-8 E-selectin expression by ECs on the biohybrid lung prototype MHFs under hyperoxia at 250 RPM .....	91
Figure 6-9 E- selectin expression in the biohybrid lung prototype under hyperoxia at 750 RPM .....	92
Figure 6-10 P-selectin expression for BAECs from endothelialized MHF bundles .....	93
Figure 7-1 PECAM-1 expression by BAECs on MHF bundles exposed to bovine blood.....	111
Figure 7-2 PECAM-1 expression by BAECs on MHF bundles exposed to bovine blood and hyperoxia.....	112
Figure 7-3 Permeance test system.....	114

Figure 7-4 Oxygen permeance of polypropylene and PMP MHFs in water..... 115

## PREFACE

I would like to thank my Ph.D. advisor, William R. Wagner, for great mentorship, patience, funding and providing a good work environment. Working for Dr. Wagner was both an honor and a pleasure. I would also like to thank my committee members for guidance. Special appreciation is given to Donna Stolz and the Center for Biological Imaging at the University of Pittsburgh for assistance with fluorescent labeling and imaging. Appreciation is also given to William J. Federspiel and Bruce Pitt for assistance in the area of oxygenation.

Deep appreciation and thanks is given to Daniel T. McKeel for his machining work and dedication to this project. Appreciation is also given to Brian Frankowski for machining work and ongoing assistance.

Gratitude is expressed to lab mates (Kristie Burgess, Tim Deglau, Jianjun Guan, Yi Hong, Carl Johnson, Priya Ramaswami, Trevor Snyder, John Stankus, Eric Tom, Gregory Weller, and Joshua Woolley) for experimental assistance and brainstorming as needed. Special thanks to Dr. Jianjun Guan and Dr. Trevor Snyder for additional mentorship. Appreciation is also given to undergraduate students, especially Craig A. Lehocky, Michael B Audette and Bradley C. Lomago.

I would also like to acknowledge sources of funding, the Commonwealth of Pennsylvania and the CATER program. The CATER program was helpful in my overall education and graduate experience. Appreciation is given to the Animal Facility and MIRM at the University of Pittsburgh for use of equipment.

## **1.0 INTRODUCTION**

### **1.1 OXYGENATION IN THE NATURAL LUNGS**

The natural lung has a tidal volume of approximately 500 mL, which is the total volume of gas inspired or expired during each respiratory cycle [1]. Of the total gas, a 70 kg man at rest is estimated to produce 240 mL/min of carbon dioxide and consume 270 mL/min of oxygen [2]. Blood flows through capillaries in the alveoli to make this exchange possible. Oxygen and carbon dioxide exchange occurs across a barrier of capillary endothelial cells (ECs) and mucopolysaccharide hydrogel film. A membrane of 0.4-2  $\mu\text{m}$  thickness separates air-carrying alveoli from the pulmonary capillaries. Deoxygenated blood from the right side of the heart passes through this membrane of the lungs. Oxygen then diffuses across the membrane into the blood stream. Carbon dioxide is removed from the blood, into the alveoli, for exhalation [1]. The natural membrane appears as a porous, open-cell foam. The surface area of this membrane is estimated to be between 70  $\text{m}^2$  and 90  $\text{m}^2$  [1, 3].

### **1.2 ACUTE RESPIRATORY DISTRESS SYNDROME**

Acute Respiratory Distress Syndrome (ARDS) is an inflammatory lung condition that affects nearly 150,000 patients per year in the U.S. [4]. Mortality exceeds 40%, while survivors may suffer permanent lung damage and memory loss due to oxygen deprivation during lung dysfunction [5, 6]. ARDS is not a disease itself, but a syndrome associated with a variety of diseases such as pneumonia, shock, sepsis or trauma, resulting from direct physical or toxic injury to the lungs. Common modalities of injury include severe chest blows and aspiration. ARDS may also result from an indirect bloodborne injury to the lungs, such as sepsis [7, 8].

Characteristics common to ARDS patients include loss of lung compliance, diffuse alveolar infiltration and surfactant dysfunction. An increase in surface tension of the lungs results in atelectasis, pulmonary edema and ultimately hypoxemia. This state of deteriorated respiratory function requires mechanical ventilation. The condition may persist for several days to months [9].

ARDS is generally characterized by three sequential stages. First, the oxidative stage, is described by accumulation of excess fluid and protein in the alveolus. Inflammatory cells from the alveolar capillaries infiltrate the alveoli of the lung. Alveoli will rupture as a result of fluid buildup, and subsequently leak into the surrounding tissue. The loss of functional alveoli and continued fluid accumulation in the lungs results in diminished gas exchange. Second, in the fibroproliferative stage, proliferation of connective tissue and other structural elements of the lung occur. Continuing inflammation causes the lung tissue to fibrose. There is an increased risk for pneumonia, sepsis and rupture of the lungs. As ARDS progresses damage to vital organs may occur. The third stage, resolution and recovery, involves reorganization of the lung, which can lead to different levels of pulmonary recovery. The lungs may recover completely, respiratory dysfunction may persist, or death may occur [7, 8].

### **1.3 MECHANICAL VENTILATION**

Treatment of ARDS consists of mechanical ventilation to aid in lung recovery, oxygen delivery and carbon dioxide removal, while the underlying medical condition is also treated. Patients are often sedated into a drug-induced coma to ensure maximal oxygenation of vital organs. The mechanical ventilator forces oxygen into the lungs at concentrations that will maintain patient saturated oxygen content of the blood ( $\text{SaO}_2$ ) levels of greater than 95%. [10]. Mechanical ventilation relieves the pulmonary musculature and diaphragm, which would otherwise fatigue in an effort to supply oxygen to the body [7, 8].

Mechanical ventilation can be damaging to the lungs after prolonged use. Extended support cannot be maintained without the risk of mechanically induced tissue damage from supraphysiologic airway pressures, as well as biologically induced tissue damage from high oxygen concentrations [7, 8, 11-13]. Ventilation is performed either with a fixed tidal volume or

a fixed pressure applied to fully ventilate the lungs. Lungs of ARDS patients require substantially higher pressure settings in comparison to healthy lungs due to lower dispensability of the pulmonary tissue [8, 9]. Volutrauma is one of the most common complications resulting from mechanical ventilation of ARDS patients. This condition arises from over expansion of the alveoli, and may be reduced by decreasing the tidal volume [8]. However, healthier areas of lung tissue will be distended much further than damaged or fibrosed lung tissue due to lower compliance, resulting in over-distension of the healthy tissue [9]. Pneumothorax may also occur in patients as a result of high ventilator pressure or volume settings. This condition is the product of lung tissue rupture from over expansion of the alveoli. In combination, high volumes and pressures from mechanical ventilation lead to enhanced edema in the injured lung [8]. Barotrauma may occur with increased ventilator pressures. Other complications include bacterial infections and multiple organ dysfunction or failure.

The high mortality rate associated with ARDS is linked to multi-organ failure, rather than hypoxemia [9]. There is evidence that mechanical ventilation may aggravate or even initiate pulmonary inflammation [14]. Proinflammatory cytokines, such as tumor necrosis factor (TNF)- $\alpha$ , interleukin (IL)-1 and IL-6 are upregulated with hyperoxia and released during the initial phase of the inflammatory response [13]. Proinflammatory cytokines are elevated within 1 hr of conventional lung ventilation for ARDS patients [9]. In patients with healthy lungs, proinflammatory cytokines have not been shown to increase following 1 hr of conventional ventilation [9]. The inflammatory response becomes decompartmentalized following the rupture of alveoli and fluid leakage into the circulatory system, with systemic inflammation following.

Septic patients experience a decline in levels of natural anticoagulants, such as activated protein C (APC), antithrombin (AT) and tissue factor pathway inhibitor (TFPI) [14]. Tissue factor (TF, a membrane protein and coagulation initiator) is elevated in a septic patient, due to additional expression via monocytes and endothelial cells (ECs). The coagulation cascade is activated by the extrinsic pathway. Factor X is activated by TF, and the common pathway of coagulation is initiated [15]. Additional discussion regarding coagulation will be presented in subsequent sections.

### **1.3.1 Advancements in mechanical ventilation**

Significant effort is being directed toward improving outcomes with mechanical ventilation. Settings for mechanical ventilation may be fine tuned to reduce further lung damage. Positive end expiratory pressure (PEEP) is controlled to increase lung volume and keep alveoli open. Controlling PEEP also avoids excess oxygen delivery, which may further damage the lung. If PEEP is applied in small increments of 3 to 5 cm water, up to 15 cm, acceptable arterial oxygen saturation ( $\geq 0.9$ ) may be achieved without further damage to the lungs [7]. PEEP has been documented to cause an increase in the functional residual capacity of the lung, which may be the result of the recruitment of collapsed alveoli [8]. Tidal volume controls the amount of air required to inflate the lungs [7]. Elevated tidal volumes may cause lung injury, including damage to the alveolar-endothelial barrier. The pulmonary capacity of ARDS patients is decreased, therefore tidal volumes as low as 6 ml/kg may be more appropriate than the conventional 12 to 15 ml/kg.

Techniques such as inverse-ratio ventilation and airway-pressure-release ventilation may also be employed for better patient outcomes. Inverse-ratio ventilation limits excessive airway pressures by increasing the inspiratory period to increase mean airway pressures. This process is most beneficial to portions of the lungs that are occupied by a non-homogeneous distribution of pulmonary infiltrates. However, inverse-ratio ventilation requires heavy sedation and/or paralysis. Additional randomized trials are necessary to demonstrate benefit prior to wide adoption of this method. This is also true for airway-pressure-release ventilation, which is designed to open and stabilize collapsed portions of the injured lung in patients that are capable of spontaneous breathing. Continuous positive airway pressure is applied in this technique.

### **1.3.2 Pharmacological therapies**

Other alternatives to patient care involve pharmacologic therapies. Exogenous surfactant may be administered to substitute for the body's own dysfunctional surfactants. Surfactants may improve air-space stability, and have antibacterial or immunologic properties [16]. Benefits from such treatment would include decreased airway pressures, improved ventilation and reduction of

nosocomial pneumonia. However, this treatment has not been proven effective to date [7, 8]. Corticosteroids were evaluated due to their ability to alter host inflammatory responses, but provided no benefit [7, 17]. Acetylcysteine, a thiol-containing compound, has the ability to scavenge oxygen free radicals, making it an attractive antioxidant for investigation. Trials revealed no increase in gas transfer or survival rate [7, 18]. Ketoconazole inhibits thromboxane synthesis and leukotriene biosynthesis. It may prevent patients suffering from sepsis or multiple traumas from developing ARDS, but further investigation is needed [7, 19]. Alprostadil is another promising, but unproven option, which acts by blocking platelet aggregation, modulating inflammation and inducing vasodilatation [7]. Other vasoactive drugs, such as sodium nitroprusside, are used to enhance cardiovascular performance. Their ability to enhance vasoconstriction may improve gas exchange for ARDS patients, but current data are insufficient to draw conclusions [7, 20]. Pentoxifylline inhibits chemotaxis and activation of neutrophils in the animal model of sepsis. This phosphodiesterase inhibitor may prove beneficial in the future [7, 21]. The above mentioned drugs each display an element of possible therapy for ARDS patients, but further investigation and coupling of such drugs must first be accomplished.

### **1.3.3 Nitric oxide**

Inhaled nitric oxide (NO) is a promising adjunctive treatment for ARDS. This gas acts as a selective pulmonary vasodilator at concentrations of 2 ppm to 40 ppm, and actively binds to hemoglobin for quick inactivation [22-24]. Inhaled NO has been shown to have negligible toxic effects when administered at 50 ppm for less than 7 hours. At high concentrations of greater than 80 ppm, inhaled NO displays pro-inflammatory and pro-oxidant effects [25]. Continuous administration of NO consistently reduces pulmonary-artery pressure, but long term effects of such treatment have proven to be inadequate [7]. Patients that acquired ARDS from direct lung injury have responded more favorably to inhalation of NO than patients with indirect lung injury resulting in ARDS [25]. However, correct dosing of NO remains unclear.

Gerlach et al. suggest that NO may be more beneficial if the dose is reduced over time, or administered intermittently [26]. Low doses of exogenous NO may be most beneficial in the early stage ARDS for short durations [27]. Anti-inflammatory benefits have been reported after exposure to low levels of ambient NO within hospitals, ranging from 2 ppb to 550 ppb [24].

Respiratory repair is promoted through a reduction of leukocyte accumulation within the lungs. Inducible nitric oxide synthase (iNOS) and endothelial nitric oxide synthase (eNOS) are both often upregulated in response to hyperoxic conditions. iNOS-derived NO is believed to be anti-inflammatory in hyperoxic lung injury [28]. NO is synthesized by the conversion of L-arginine to L-citrulline by nitric oxide synthase (NOS) [29]. However, Potter et al. found no pathologic benefit from this activity, in mouse pup lungs [30]. There are notable benefits of inhaled NO therapy, yet correct administration remains unclear.

#### **1.4 EXTRACORPOREAL MEMBRANE OXYGENATION**

In the advanced disease state, ventilators become inadequate, which leads to the addition of Extracorporeal Membrane Oxygenation (ECMO) in many cases. ECMO, using blood oxygenators designed for acute open-heart procedures, offers an alternative method for gas exchange [2]. ECMO is achieved by pumping patient blood through an extracorporeal circuit, which transfers oxygen and carbon dioxide to and from the blood and gives the natural lungs time to heal. The patient is often cannulated at the femoral vein. Blood travels through the circuit with the help of a peristaltic or centrifugal pump, and is forced through an oxygenator. At this point, carbon dioxide is removed and oxygen is added. The blood is subsequently exposed to a heat exchanger to elevate the temperature before re-entry through the femoral vein [6].

Oxygenators currently utilized for ECMO are often composed of microporous hollow fibers (MHFs). Oxygen flows through the lumen of the fiber and blood flows around the outside of the fiber. Gas passes through pores of the MHFs, rather than the membrane material, making membrane resistance to gas transfer negligible [31]. Such oxygenators are designed for short-term use of 6 to 12 hours, in applications such as coronary artery bypass grafting surgery. Sustained use for ARDS patients leads to additional complications through blood-surface interactions, which can make the treatment no more favorable than mechanical ventilation. These fibers are functionally limited by plasma weeping, and biocompatibility issues associated with thrombogenesis. Plasma weeping is the penetration of liquid into the fiber pores, which inhibits gas exchange. Platelets deposit on the fiber surfaces and aggregate, also inhibiting gas exchange.

High levels of heparinization are required to reduce the risk of thrombus formation and the potential for thromboembolic events. Unfortunately, aggressive anticoagulation also leads to an increased risk of bleeding and further complications [32].

#### **1.4.1 Microporous hollow fiber membranes**

Oxygenators utilizing MHF technology are overwhelmingly made from polypropylene (PP) MHFs. PP has a higher gas permeability through pores than other relevant polymers, such as silicone or silicone coated membranes, it has high strength relative to microporous silicone and other polymers, and it is easily sterilized by ethylene oxide gas [33]. PP fibers are produced by leading companies such as, AKZO-NOBEL (Netherlands), Mitsubishi Rayon (Japan), Celgard (Charlotte, NC), and Terumo (Japan), and will vary in physical characteristics based upon the manufacturer [2, 33].

The structure of MHFs somewhat imitates the structure of capillaries found in the lung *in vivo*. Both a MHF and a glomerular capillary exhibit cylindrical cross-sections, and have similar wall thickness to cross-sectional diameter ratios. The cylindrical shape minimizes perimembrane boundary layers to increase transport efficiency [34]. Membrane pores allow gas exchange to occur through diffusion [2]. As mentioned, respiratory gases pass through the membrane pores rather than the membrane material [31]. The membranes are hydrophobic to discourage blood from entering into the pores [35].

Ideal membrane characteristics have been projected as follows: an effective permeability for oxygen and carbon dioxide should be present, water should not be passed in its liquid form by the membrane, and blood components should not be damaged by the membrane surface (i.e. possess thromboresistance and minimal chemical reactivity) [36].

**1.4.1.1 Microporous hollow fiber membrane permeance** Diffusion across the MHF membrane is dependent on the area and thickness of the membrane [37]. Pore diffusion for MHFs can be described by Knudsen diffusion of gases in cylindrical pores. Gas molecules will collide more frequently with each other if the pore diameter ( $d_{\text{pore}}$ ) is less than the mean free path length of the diffusing species ( $\lambda$ ), and the density of the gas is low [38]. The Knudsen number ( $K_n$ ) is given in Equation 1 [38].

**Equation 1** Knudsen Number

$$K_n = \lambda/d_{\text{pore}}$$

The gas exchange permeance ( $K$ ) is a measure of the rate of gas exchange for  $O_2$  or  $CO_2$ .  $K_m$  is the diffusional resistance of the MHF membrane, and is given in Equation 2, when Knudsen diffusion is assumed.  $K_m$  is a function of porosity ( $\epsilon$ ), pore diameter ( $d_p$ ), pore tortuosity ( $\tau$ ), fiber wall thickness ( $h$ ), molecular weight of the given gas ( $M$ ), the gas constant ( $R$ ) and absolute temperature ( $T$ ) [2].

**Equation 2** MHF membrane permeance for Knudsen diffusion

$$K_m = \epsilon \frac{2d_p}{\tau h} \sqrt{\frac{2}{\pi MRT}}$$

A membrane permeability of  $K_m \sim 10^{-2}$  mL/cm<sup>2</sup>/s/cmHg should provide efficient gas exchange capacity. Mitsubishi KPF fibers have been measured at  $K_m = 6.7 \times 10^{-2}$  mL/cm<sup>2</sup>/s/cmHg in a gas-gas environment, where gas is forced through an individual MHF of known surface area, causing the gas to permeate through the membrane [35, 39]. Celgard X30-240 polypropylene fibers have been measured in gas-gas tests at  $K_m = 1.72 \times 10^{-2}$  mL/cm<sup>2</sup>/s/cmHg and  $K_m = 1.4710^{-2}$  mL/cm<sup>2</sup>/s/cmHg for  $O_2$  and  $CO_2$ , respectively [35]. As a result of *in vivo* effects, this is not the case.

The permeance is inversely related to the resistance. The overall transfer resistance for a blood oxygenator is given in Equation 3 as  $1/K$  [2, 39].

**Equation 3** Gas transfer resistance

$$1/K = 1/K_m + 1/K_l$$

The inverse of  $K_l$  is the liquid-side transfer resistance from diffusional boundary layers.  $K_l$  is a function of the effective solubility coefficient of the diffusing gas ( $\alpha$ ), the diffusion coefficient of the diffusing gas ( $D$ ) and the average boundary layer thickness ( $\delta$ ) for blood (Equation 4) [2].

**Equation 4** Liquid side permeance

$$K_l = \frac{\alpha_l D_l}{\delta_{bl}}$$

For PP MHFs  $K_m$  is much greater than  $K_l$ , causing  $K_m$  to be negligible, and reducing the gas transfer resistance to essentially  $1/K_l$ . If composite or coated hollow fibers are employed,  $K_m$  may play a significant role in overall transfer resistance. Composite and coated hollow fibers require the gas to diffuse through the polymer (p) material instead of micropores.  $K_m$  for composite fibers is given in Equation 5 [2].

**Equation 5** Composite hollow fiber permeance

$$K_l = \frac{\alpha_p D_p}{\delta_p}$$

**1.4.1.2 Microporous hollow fiber membrane failure** The main chronic failure mode for MHFs used for ECMO is plasma wetting. Phospholipids, lipoproteins and/or proteins from blood adsorb onto the blood-contacting surface of the MHF [2]. The hydrophobic barrier, used to minimize plasma wetting, becomes hydrophilic as a result. In the absence of the hydrophobic barriers, plasma penetrates the fiber pores, because diffusion of gas species through a liquid is orders of magnitude lower than in gas. Diffusion of oxygen and carbon dioxide molecules is hindered by this hydrophilic membrane alteration [31, 35]. Overall gas exchange rates will ultimately decay, and the oxygenator will require replacement in as little as 4 to 12 hours following blood contact [35] [2]. Membrane permeance for liquid filled pores of MHFs is given in Equation 6 [2].

**Equation 6** Membrane permeance for liquid filled pores of MHFs

$$K_m = \varepsilon \frac{\alpha D_l}{\tau h}$$

The hemostatic mechanism designed to stop bleeding in an injured blood vessel is also employed in response to a foreign body, such as the large blood contacting surface area of MHFs [40]. The meniscus, formed on the membrane pore at the blood/gas interface, is site susceptible to protein adsorption, leading to thrombotic deposition and poor biocompatibility [34]. When blood contacts the membrane, coagulation factors and proteins, such as factor XII, factor VII, vWF, fibrinogen, albumin, hemoglobin, and gamma globulin, deposit [41]. Protein adhesion varies depending on the surface properties. Free energy, surface roughness and/or chemical composition can influence quantity or type of protein adsorption.

Platelet adhesive receptors, glycoprotein IIb/IIIa and glycoprotein Ib, interact with absorbed proteins to mediate platelet adhesion [40]. Platelets are non-nucleated disc shaped cells designed to arrest bleeding through formation of platelet plugs and catalyze coagulation reactions which lead to fibrin formation. Upon activation, platelets change in morphology to spiny spheres and extrude granule contents. Release of dense granule ADP, formation of thrombin, and biochemical activation of platelets leading to the generation of thromboxane A<sub>2</sub> occurs following platelet adhesion [42]. Additional platelets are recruited to the site of activation to form a platelet aggregate through calcium dependent binding of adjacent platelets by fibrinogen molecules, and thrombin binding to membrane receptors. Platelet aggregation leads to platelet procoagulant activity, such as expression of membrane phospholipids. Membrane phospholipids accelerate factor X activation and the conversion of prothrombin to thrombin, two critical processes in blood coagulation. Thrombin forms rapidly on the surface of aggregated platelets, activates more platelets and generates polymerizing fibrin[15]. The large surface area of ECMO circuits on which platelet deposition occurs, and heparin therapy can lead to thrombocytopenia [43-45].

The function of leukocytes and erythrocytes in thrombus formation is less explicit than that of platelets. Activated platelets expressing p-selectin will attract leukocytes through rolling interactions. Leukocytes will also adhere to platelet-bound fibrinogen in a haemostatic plug, or thrombus [46]. An association between leukocytosis and thrombotic complications has been shown in several clinical studies [46]. Erythrocytes will add to thrombus mass, but are generally

thought to play a passive role [15, 42]. However, *in vitro* work by Hellem et al. and Siniabiadi et al. has shown that erythrocytes enhance platelet aggregation by their tumbling nature in blood flow which generates a radial platelet gradient, increasing the platelet concentration at the boundary wall. In addition, high hematocrit results in higher blood viscosity and a higher residence time for circulating platelet factors and coagulation factors near the thrombotic site [47]. Research is ongoing to clearly define the roles of leukocytes and erythrocytes in thrombus formation associated with foreign body response.

Thrombus formed from a combination of interactions between the surface, platelets and coagulation proteins may be enzymatically degraded by fibrinolysis [15, 48]. The fibrinolytic system is designed to facilitate healing following inflammation by removing fibrin deposits. Tissue plasminogen activator is released from ECs in the blood vessels following stimulation by thrombin, or may be introduced therapeutically through pharmaceutical agents [15, 49]. The fibrinolytic enzyme, plasmin, is found bound to fibrin/fibrinogen, or circulates in the inactive form as a protein plasminogen. Plasminogen is activated by plasminogen activators to digest fibrin clots, in the bound form, or impair platelet binding and aggregation, in the circulating form [41]. Upon digestion, soluble fibrin/fibrinogen digestion products, such as fibrin degradation products and D-dimer, are released into circulating blood [15, 41]. Studies have found decreases in the activation of the fibrinolytic and inflammatory systems following the administration of antifibrinolytic compounds, such as the serine protease inhibitor aprotinin, during cardiopulmonary bypass procedures employing oxygenators primarily composed of MHF membranes [48, 50].

Anticoagulants are given prior to cardiopulmonary bypass surgery, or during ECMO, to attempt to minimize thrombus formation associated with blood contact to a foreign surface. Heparin is most commonly used for anticoagulation, since the effects of the drug can be neutralized with the administration of protamine. Heparin binds antithrombin III and amplifies its potency by a factor of 1000 to effectively inhibit thrombin and factors IXa, Xa, XIa, and XIIa. However, post-operative bleeding is of concern following oxygenator withdrawal [41, 48]. A balance in the management of therapeutic agents, such as heparin, protamine and aprotinin, and the coagulation and fibrinolytic pathways must be maintained to limit complications associated with hemostasis, particularly when ECMO is employed.

### 1.4.2 Standard blood oxygenators and microporous hollow fibers

As mentioned above, the natural lung basal carbon dioxide removal is 240 mL/min and oxygen consumption is 270 mL/min. Oxygenators generally provide approximately 40% of the basal needs. A well-developed design may provide 135 mL/min oxygen and 120 mL/min of carbon dioxide transfer, acting at 50% efficiency [2]. Current oxygenators can perform consistently for six hours during cardiopulmonary bypass. Oxygenators are generally limited to one-day use, but can possibly last for several weeks before failure due to poor gas exchange and noticeable thrombus formation occur [15].

Table 1 presents a list of commercially available oxygenators with PP membranes, the most commonly used MHF membrane for adult respiratory support [37]. Surface area varies between each model, ranging from 1.7 m<sup>2</sup> to 2.5 m<sup>2</sup> [37].

**Table 1** Nine MHF oxygenators  
Comparison of surface area and priming volume [37]

	Membrane		Heat exchanger		Priming volume (ml)
	Fibre	Area (m <sup>2</sup> )	Material	Area (m <sup>2</sup> )	
Maxima PRF	Polypropylene	2.3	Aluminium	0.11	480
Forté	Polypropylene	2.4	Polyolefin	0.55	295
Affinity	Polypropylene	2.5	Rvs	0.16	270
Affinity NT	Polypropylene	2.5	Rvs	0.168	270
Quantum	Polypropylene	1.9	Rvs	0.1194	274
Optima	Polypropylene	1.7	Rvs	0.1374	260
Capiox 1.8	Polypropylene	1.8	Rvs	0.22	270
Quadrox	Polypropylene	1.8	Polyethylene	0.6	250
Hilite	Polypropylene	1.9	Polyurethane	0.55	275

The Affinity NT (Medtronic, USA) and Quantum (Bard Inc., Haverhill, MA, USA) oxygenators were found to produce the best oxygen transfer of these nine, based on clinical findings in patients undergoing coronary bypass surgery, with statistically significant differences of  $p < 0.01$  and  $p < 0.05$ , respectively [37]. **Table 2** compares the percent hemoglobin and platelet numbers between the above mentioned nine oxygenators. Oxygenators were evaluated during patient support in cardiopulmonary bypass procedures for 1-1.5 hrs. Hemoglobin and platelet numbers were taken pre- and post-operatively, hence % decrease is shown in the table in comparison to pre-operative values. The data are notable in that little difference is observed across various models.

**Table 2** Hemoglobin and platelet levels in nine MHF oxygenators

Shows a decrease in hemoglobin and platelets in the first postoperative samples compared to preoperative values [37]

	HB (% decrease)	Platelets (% decrease)
Maxima	70 ± 9	65 ± 21
Forte	74 ± 13	67 ± 16
Affinity	78 ± 12	57 ± 11
Affinity NT	72 ± 7	65 ± 15
Quantum	70 ± 10	65 ± 12
Capiox	75 ± 6	71 ± 10
Optima	72 ± 7	70 ± 7
Quadrox	71 ± 7	64 ± 11
Hilite	71 ± 6	64 ± 13

Gas exchange capability is dependent on multiple factors, including fiber bundling, fiber structure, winding of the fibers and flow pattern through the fiber bundles [37]. Many adaptations to fibers or fiber configurations have been presented to optimize flow and gas transfer characteristics. AKZO NOBEL (Germany) produces the MHFs, OXYRAY, made of polyethylene, and OXYPHAN, made of PP. Both have nearly identical properties to other PP MHFs, but processing techniques are different. OXYPHAN, a hydrophobic, microporous PP membrane is produced through a technique created by AKZO NOBEL. A thermally induced phase separation process homogeneously mixes the polymer with two natural seed oils. The product is then spun and cooled, resulting in a porous structure with consistent and uniform pore distribution (oil is removed). TERUMO (Tokyo, Japan) uses a similar process to AKZO NOBEL, using mineral oils. This produces less consistent pore size and distribution, and leaves the fiber more susceptible to plasma/blood leakage. Mechanical strength of this PP membrane is very low [33].

Mitsubishi and Hoechst use a "drawing" process to create a net like structure of dense, unexpanded regions alternating with small ruptures (or pores) on polypropylene fibers. However, this process allows pores to penetrate the full depth of the membrane wall, allowing the possibility of plasma breakthrough or leakage to occur. Optima uses a microporous membrane from AKZO NOBEL, which it claims to exhibit high gas permeability, high resistance to plasma

breakthrough, and high tensile strength obtained from a cross-wound mat configuration [33]. These are all key aspects in membrane performance.

Surface modified MHF membranes are also clinically available and commonly used. Heparin-coatings, surface modifying additives (SMA) and poly-2-methoxyethylacrylate (PMEA) are examples of surface treatments applied to MHF membranes [51, 52]. Medtronic's AFFINITY<sup>®</sup> NT oxygenator is available with covalently bonded heparin coatings of either Carmeda<sup>®</sup> (proprietary anticoagulant active sequence) or Trillium<sup>®</sup> (incorporates proprietary anticoagulant active sequence, sulphate and sulfonate groups to mimic the negative charge of endothelium, and hydrated polyethylene oxide polymer chains) (Medtronic, Minneapolis, USA) [53]. Baxter offers the Duraflow-II coating (Baxter Corporation, Irvine, CA), a heparin coating which uses an ionic process to attach heparin to the surface [54, 55]. SMAR<sub>x</sub>T (COBE Cardiovascular Inc, Arvada, CO) is an example of an oxygenator utilizing the SMA copolymer [51]. The CAPIOX<sup>®</sup> RX (Terumo, Tokyo, Japan) is an example of an oxygenator utilizing PMEA [52]. SMA- and PMEA- coated circuits are more commonly used in cardiopulmonary bypass procedures than heparin-coated circuits, which are commonly employed in ECMO procedures. SMA and PMEA coatings aim to reduce contact activation during cardiopulmonary bypass, but the effectiveness of the surface modification is unclear. Some studies show clinical benefits, such as elevation of plasma anti-inflammatory IL-10 and urinary alpha-1-microglobulin 48 hours postoperatively [56]. Other studies conclude that SMA- and PMEA-coated circuits do not improve platelet consumption or decrease blood product use for patients undergoing cardiopulmonary bypass procedures, but may still have some clinical benefit [52].

When heparin function is preserved on the surface of cardiopulmonary bypass or ECMO circuits, heparin coatings hold several advantages over non-coated surfaces. These heparin-coated surfaces attenuate the system inflammatory response, and present a hydrophilic, protein resistant barrier to improve surface biocompatibility [57]. Contact activation, coagulation activation, complement activation and platelet and leukocyte activation (directly or indirectly) are attenuated [57-59]. Niimi et al. concluded that heparin coating of PP oxygenator fibers decreased platelet adhesion without affecting adsorption of major adhesive proteins [40, 44]. Studies involving use of Duraflow-coated cardiopulmonary bypass circuits concluded that lower activated clotting times (ACT) (e.g. ACTs of 300 instead of ACTs of 400) could be maintained with lower levels of systemic heparinization, and fibrinogen consumption was reduced [54, 60].

Spiess et al. observed a reduction in tissue plasminogen activator (TPA) in patients undergoing coronary artery bypass graft procedures when a Carmeda (Medtronic Inc, Anaheim, CA) coated cardiopulmonary bypass circuit was employed [61]. Nonetheless, mortality rates still remain high in ECMO for ARDS patients, even though heparin-coated oxygenators are commonly employed. This provides motivation for the development of more biocompatible oxygenating devices.

### 1.4.3 Mass transfer augmenting blood oxygenators

Mass transfer augmentation is being explored in devices such as the chronic artificial lung (CAL), the paracorporeal respiratory assist lung (PRAL), and the pumping artificial lung (PAL). The CAL (formerly known as the Active Mixing Membrane Oxygenator, or AMMO) was developed at Ension, Inc. as an oxygenator and cardiac pump. It utilizes a spinning disc of PP fibers to oxygenate blood at a targeted blood flow rate of 4 L/min. The paracorporeal device is designed for up to 21 days of use with a targeted O<sub>2</sub> efficiency of 500 mL/min/m<sup>2</sup> and a targeted surface area of 0.5 m<sup>2</sup> [62]. Currently, the prototype has a CO<sub>2</sub> exchange efficiency of 370 mL/min/m<sup>2</sup> [63].

The PRAL is under development at the University of Pittsburgh, under Dr. William J. Federspiel, as an aid for acute lung failure. The prototype is composed of a bundle of PP MHF membranes with gas exchange area of 0.25 m<sup>2</sup>. At test speeds of 1500 RPM the device could generate 750 mL/min fluid flow against 52 mmHg pressure, remove CO<sub>2</sub> at a rate of 256 ± 16 mL/min/m<sup>2</sup>, and provide O<sub>2</sub> at a rate of 206 ± 11 mL/min/m<sup>2</sup>. Minimal erythrocyte damage was shown, but an increase in plasma free hemoglobin was noted [64].

The PAL, manufactured by Makarewicz and Mockros, also employs annular rotation of a MHF bundle. A modified Biomedicus BMP-50 pump head houses the MHFs to give a surface area of 0.6 m<sup>2</sup>. CO<sub>2</sub> can be removed at a rate of 125 mL/min/m<sup>2</sup> and O<sub>2</sub> can be provided at a rate of 119 mL/min/m<sup>2</sup> for *in vitro* testing using saline at flow rates of 7 LPM. However, gas exchange was independent of rate of fiber bundle rotation [65, 66].

All three of these devices are in pre-clinical phases, but provide innovative designs that may lead to significant improvements in oxygenation for acute lung failure patients. This

ongoing research reflects an effort to improve blood biocompatibility, O<sub>2</sub> delivery and CO<sub>2</sub> removal.

#### **1.4.4 Ongoing research for improved oxygenator biocompatibility**

Ongoing research for improved blood biocompatibility, O<sub>2</sub> delivery and CO<sub>2</sub> removal is not limited to overall oxygenator design. The use of coated and alternative hollow fiber membranes is also being explored. Groups are using siloxane coatings and/or heparin surface treatments in designs for possible device improvement. Niimi et al. coated a capillary membrane oxygenator with less than 2µm of silicone. This design resulted in less trauma to blood components and reduced thrombogenicity than in PP fibers, which was attributed to surface smoothness [67]. Iida et al. found their coating of less than 2µm silicone to be better for long-term cardiac support, in addition to cardiopulmonary bypass surgery applications [68]. The silicone film also prevents plasma infiltration of the pores, which contributes to a longer *in vivo* life span in comparison to PP fibers. PP fibers have more adverse effects on blood elements than silicone coated membranes, resulting in higher plasma free hemoglobin content in the blood. Yet, plasma free hemoglobin levels have been shown to be very low for non-coated fibers in general [37, 67]. Niimi et al. also found platelet adhesion was reduced without affecting adsorption of major proteins, by covalent attachment of heparin to the fiber surface. They concluded that heparin coating combined with low dose heparinization can reduce platelet adhesion and activation to potentially reduce the inflammatory response, thrombosis and fibrinolysis [40, 44].

Other groups have investigated alternative hollow fibers for use in oxygenators. Maeda et al. developed a silicone membrane hollow fiber oxygenator and compared it to the commercially available Kolobow (Avecor 1500, Medtronic Inc., Minneapolis, MN) silicone oxygenator, finding superior efficiency and less blood trauma [69]. Nonporous membranes of silicone, like that found in the Kolobow, have advantages such as less damage to blood and longer clinical life span [36]. Toomasian et al. provided extracorporeal life support to sheep on a long term gas exchange device made of polymethylpentene (PMP) fibers for 72 hours without plasma leakage [70]. PMP fibers have an asymmetric pore structure and dense outer skin that inhibits direct contact of blood and gas across a micropore [70]. Niwa et al. has developed a membrane oxygenator composed of novel asymmetric polyimide hollow fibers [71]. Often a compromise is

made between gas exchange capabilities and blood-surface biocompatibility with these new technologies.

Additionally, endothelialization of MHFs is being investigated. The addition of ECs could be very useful since they may reduce anticoagulation therapy, limit fiber wet out, provide an additional diffusion barrier, and produce nitric oxide and surface heparin. Negative factors may include risk of inflammation state causing coagulation, interaction with the immune system and surface retention difficulties [44]. Takagi M et al. have endothelialized PP MHFs to create a hybrid artificial lung. MHFs were covalently bonded with fibronectin to maintain a high EC density, even in the presence of a shear force of  $1.15 \text{ N/m}^2$ . A cardiopulmonary bypass system was made from 150 endothelialized MHFs of 8 cm length to support *in vivo* extracorporeal support of Sprague-Dawley rats for 60 minutes. In comparison to blood bypassed over untreated, non-endothelialized polypropylene MHFs, concentrations of IL-10 (an inflammatory inhibitor) increased and TNF- $\alpha$  (proinflammatory factor) decreased [72].

The need remains to provide adequate gas transfer and limit adverse affects associated with oxygenators. Although silicone and heparin coatings may provide some advantages over current models, more work needs to be done to address biological, chemical and mechanical requirements associated with artificial oxygenation. Use of lower levels of anticoagulants would likely benefit the patient's overall hemostasis, which may be achieved with certain MHF coatings. Even if reduction of anticoagulation therapy can be accomplished safely, a profound need for chronic respiratory support remains. Issues associated with high levels of anticoagulation, bleeding, fiber wet out and thrombosis persist as critical limitations for patients requiring chronic respiratory support.

## **1.5 EC CONSIDERATIONS**

### **1.5.1 EC inflammatory phenotype**

A hemocompatible, non-inflammatory EC phenotype contributes to maintaining the proper balance between thrombosis and fibrinolysis [41]. There are multiple EC products that regulate hemostasis. Prostacyclin is a vasodilator and inhibitor of platelet aggregation. Nitric oxide is also

secreted as an inhibitor of platelet aggregation and adhesion, and acts as a vasodilator. Ectonucleotidases are surface enzymes that regulate the breakdown of platelet-active and vasoactive nucleotides. Thrombomodulin is expressed on the surface of ECs to act as an anticoagulant. Tissue factor pathway inhibitor is synthesized by ECs to inhibit tissue factor, a procoagulant. Type I plasminogen activator inhibitor (PAI-I) is a secreted, circulating and matrix-bound inhibitor of tissue plasminogen activator, a fibrinolysis initiator [73]. ECs express heparin sulfate on their surface, which can remove potential agonists and reduce the possibility of focal platelet activation [74].

Avoiding entrance into an inflammatory EC phenotype is crucial for maintaining an antithrombogenic endothelialized MHF surface. Activation of the endothelium results in recruitment of platelets and leukocytes to the activated site [74, 75]. The membrane of an EC contains multiple adhesion receptors, such as integrins, cadherins, cellular adhesion molecules (CAMs) of the immunoglobulin superfamily and selectins. ECs expressing p-selectin support transient interactions with platelets [76]. And secretion of von Willebrand factor (vWF) from ECs can lead to adhesive interactions of platelets [74, 77]. E-selectin is associated with tethering and rolling interactions leading to adhesion of leukocytes [76, 78]. Platelet EC adhesion molecule-1 (PECAM-1, CD31) is related to inflammation through its involvement in extravasation of leukocytes and has also been shown to increase thrombosis in the vasculature when upregulated [79]. Intracellular adhesion molecule-1 (ICAM-1, CD54) is expressed on the membrane of ECs and binds to integrins (CD11 a & b) present on neutrophils and macrophages when upregulated. Vascular cell adhesion molecule-1 (VCAM-1, CD106) is also expressed by ECs and regulates the adhesion of monocytes, basophils and eosinophils through integrin (CD49d/CD29) binding [80]. Tissue factor (thromboplastin) is expressed as a procoagulant on activated endothelium. Platelet-activating factor is platelet and leukocyte agonist, which is both surface-expressed and secreted by ECs [73].

### **1.5.2 Coatings for EC attachment**

Cell retention may be improved on artificial surfaces by implementing engineered approaches, or adding biologically adhesive proteins to the substrate [81, 82]. Arg-Gly-Asp (RGD, amino acid synthetic peptide for cell attachment-promoting activity), Arg-Gly-Asp-Ser (RGDS, amino acid

synthetic peptide for cell attachment-promoting activity), Fn-like (a fibronectin-like engineered peptide containing binding sequences), biotin (a water-soluble vitamin), a combination of biotin-avidin (the combination increases thermal stability of binding and promotes structural order), 1,4-diisocyanate butane (BDI, provides a chemical link to improve protein binding stability), polyethylene glycol (PEG, provides a chemical link to improve protein binding stability), pronectin (an adhesion peptide with multiple copies of the human fibronectin RGD attachment domain), etc. are examples of spacers or cell adhesive peptides that have been used to enhance protein adsorption and EC attachment [83-87]. Collagen, matrigel, gelatin, and fibronectin are commonly applied proteins to aid in EC attachment. These proteins can be found in the extracellular matrix below the monolayer of ECs lining blood vessels *in vivo*, and therefore make desirable candidates for *in vitro* EC attachment as well [72, 88].

Engineered approaches, or protein adsorption approaches to cell adhesion have been shown to promote cell-surface growth and compatibility. Wang et al. found gelatin- and RGD-modified polyurethane surfaces promoted human umbilical vein EC (HUVEC) growth [89]. Numerous groups have also shown increased cell attachment to polymer surfaces when combined engineered and/or protein adsorption methods are used. Chung et al. showed an increase of 8.5 times for HUVEC growth on a poly(epsilon-caprolactone)-PEG-RGD surface in comparison to a poly(epsilon-caprolactone) surface without modification [90]. Zhu et al. modified polyurethane surface with diamine and covalently grafted it with gelatin to promote HUVEC growth [91].

Plasma glow discharge may be applied to surfaces to enhance protein adsorption and EC attachment as well [92]. Pratt et al. showed a synergistic effect between fibronectin and plasma discharge treated polyethylene terephthalate films that greatly enhanced EC attachment [93]. To perform plasma discharge, the material is placed in a chamber, a gas source is pulled through the chamber under vacuum and plasma is discharged with an electrical current onto the material surface [94]. Air, oxygen, water and ammonia are common sources for plasma discharge. If ammonia gas is selected as the source, for example, amine groups will attach to the surface. With ammonia plasma discharge, surface hydrophilicity will increase [95].

### 1.5.3 Shear stress exposure

Numerous studies have been conducted for laminar flow across endothelialized cover slips, or in other 2-D models. Far fewer studies have been conducted in 3-D models. However, both types of experiments have observed EC alignment under the influence of shear through cytoskeletal rearrangement [96]. EC alignment has been shown to occur at 10 dynes/cm<sup>2</sup> under unidirectional steady laminar flow within 7-9 hours by Davies et al. [97]. Davie et al. also showed that ECs subjected to laminar shear stresses from 8-15 dynes/cm<sup>2</sup> over 24 hours aligned in the direction of flow without entering the cell cycle [98]. However, with turbulent shear stresses at 1.5 dynes/cm<sup>2</sup> for 3 hours, EC DNA synthesis in the absence of cell alignment, cell retraction and/or cell loss were observed [98]. The EC response to shear is both magnitude and flow pattern dependent [99]. In addition, cell function, morphology and gene expression is altered with exposure to fluid shear stress [100]. Under chronic shear stress, ECs flatten, structurally remodel to spread the shear stress over greater surface area and therefore increase adherence to the substratum through focal contacts [101]. Increased stress fiber formation was shown in flow preconditioned HUVECs [81].

The well defined flow environments of parallel plate chambers and cone-plate viscometers do not provide exact replicas of the shear stress environment that ECs may encounter in an active mixing oxygenator. Blood may be assumed to be a Newtonian fluid as long as moderate to high shear stresses are maintained. In areas of low shear stress, or potential stagnant areas of an oxygenator, blood may behave as a non-Newtonian fluid [102]. ECs *in vivo* are exposed to secondary flow patterns, depending on location in the blood vessel [102]. Active mixing oxygenators may provide secondary flow patterns as well due to the nature of the mixing, yet insufficient characterization of the influence of flows has been performed to elucidate the potential adverse effects on ECs.

It has been demonstrated that levels of VCAM1, ICAM-1, PECAM-1, e-selectin, p-selectin, and TF can increase with fluid flow [77-80, 102-105]. It has also been observed that laminar shear stress appears to protect ECs from inflammatory responses, by inhibiting tumor necrosis factor (TNF)- $\alpha$ , and EC proliferation, and by inducing growth arrest proteins such as GADD45 and p21 [99, 106, 107]. Lack of cell proliferation with increased shear stress is attributed to the inability of the cell to enter into the S-phase, which affects the overall cell

cycle[102]. The behavior of ECs will be observed within the scope of this project, to determine if CAMs and selectins are upregulated in response to shear stress, or protected by it.

#### 1.5.4 Hyperoxia and ECs

Hyperoxia has been shown to have deleterious effects on ECs. Patients receiving mechanical ventilation as treatment for ARDS may be exposed to 100% oxygen at times. Such high levels of oxygen have an adverse effect on inflammation and coagulation. Capillary ECs are susceptible to oxygen toxicity, which leads to structural alterations. Platelets accumulate within the microvasculature of the lungs, followed by neutrophil accumulation. Upregulation of CAMs is observed in early stages of oxygen toxicity damage. PECAM-1 is a signal transducer expressed at junctions between ECs, and is necessary for transendothelial migration of leukocytes [108]. Multiple isoforms of PECAM-1 may be presented by ECs. These isoforms elicit different roles, including an early role in the inflammation cascade [108, 109]. Piedboeuf et al. found significant increases in PECAM-1 mRNA within 48 hours of exposure to 100% oxygen, in mice. This coincided with the appearance of leukocytes in the lung tissue. Additionally, the PECAM-1 expression was found mostly on ECs, and less abundantly on platelets and leukocytes [108].

ICAM-1 mRNA levels were significantly elevated within 48 hours of exposure to oxygen at levels of 95% or greater as well, in mice *in vivo*. Alveolar epithelial cells were the primary site of ICAM-1 production [108, 110]. Welty et al. reported increased neutrophil adhesion and transmigration following increased expression of ICAM-1 expression on ECs stimulated by inflammatory cytokines in mice *in vivo* [13]. But, DeLisser et al. suggests that neutrophil recruitment may occur independently of ICAM-1, based on *in vivo* experiments with mice [109]. Nonetheless, it is believed that multiple CAMs are involved in leukocyte and neutrophil recruitment in the above mentioned hyperoxic mouse models [108].

Barazzone et al. showed how a combination of changes in CAMs and cytokine levels can lead to platelet sequestration, detectable in mouse lungs following 72 hours of 100% O<sub>2</sub> exposure. ICAM-1 and TNF- $\alpha$  levels increased significantly, as shown by Northern blots of mRNA followed by the platelet entrapment. Platelet deposition decreased in response to TNF antagonist and anti-CD11a monoclonal antibody [110].

Hyperoxia affects other factors in addition to CAMs. Inflammatory cytokines, such as TNF- $\alpha$  and interleukin-6 (IL-6) are upregulated [13]. Overproduction of PAI-1, which impairs fibrinolytic activity, has been demonstrated in mice lungs [111]. Perkowski et al found an increase in p21 expression (relevant to inhibition of cell cycle progression), an increase in Bcl-X<sub>L</sub> (an anti-apoptotic gene), an increase in reactive oxygen species (ROS), a decrease in BAX (a pro-apoptotic gene), and a decrease in thrombomodulin, following 48 hour exposure to greater than 95% O<sub>2</sub> [112]. Downregulation of thrombomodulin may contribute to activation of the inflammatory and coagulation cascades. Inflammatory reactions have been shown to cause oxidative damage as well, more specifically, activated leukocytes release ROS such as H<sub>2</sub>O<sub>2</sub>, NO, O<sub>2</sub><sup>-</sup>, OH and HOCl [113]. An increase in ROS can lead to an increase in cytokines (e.g. TNF- $\alpha$ ), chemokines (e.g. IL-8) and CAMs (e.g. ICAM-1). Increased ROS expression also causes DNA fragmentation, changes in EC metabolism and permeance, crosslinking of membrane proteins, and peroxidation of lipids and inhibition of cellular phosphates. In essence, increased ROS can cause direct EC damage [112, 114, 115].

## **1.6 THE BIOHYBRID LUNG APPROACH**

### **1.6.1 Significance of the biohybrid lung**

Current oxygenation devices lack suitable long term support capabilities. Such devices fail to incorporate a vital biocompatible surface that could rectify biocompatibility issues associated with long term support. The following chapters will describe the development of a biohybrid lung prototype. The biohybrid lung prototype seeks to provide a biocompatible surface for long term ECMO support for ARDS patients. By endothelializing MHFs that constitute the major blood contacting surface area of the device, the biohybrid lung prototype seeks to greatly reduce or eliminate the need for chronic anticoagulation or anti-platelet agents. The attached endothelial layer provides a naturally occurring biocompatible surface for blood interaction if the cells are maintained in a non-inflammatory, anti-thrombotic phenotype.

Oxygenator (in reality, gas exchange device, oxygenator is a misnomer) exchange is a common complication associated with ECMO support, and leads to blood product consumption

and further complications. Oxygenator change-out is required after plasma weeping and platelet deposition have significantly degraded gas transfer within the device. Providing a biocompatible surface to reduce or eliminate the need to perform oxygenator exchange would offer considerable benefit to ECMO patients. The endothelial layer should act as a protective barrier to decrease plasma weeping and platelet deposition. The enhanced biocompatibility offered by the biohybrid lung may provide a solution to ARDS patients that would otherwise be unable to tolerate aggressive mechanical ventilation or traditional ECMO therapy. In addition, it may provide an improved quality of life to patients who may successfully undergo traditional therapies.

The MHF bundle will rotate up to 1500 RPM to facilitate active mixing of the blood. Shear stresses fall in the physiologic range of less than 35 dynes/cm<sup>2</sup>. Active mixing may act to reduce the required surface area for adequate gas transfer and lower the burden of biocompatibility associated with a larger device. Although the EC layer may slightly decrease the gas transfer efficiency of the device, by increasing the diffusion length, this tradeoff is acceptable for the potential to substantially reduce thrombotic and plasma weepage complications. Oxygen levels will be elevated above normoxia (21% O<sub>2</sub>) to enhance oxygen delivery to the blood further reducing the required device surface area.

The main focus of this research was to study the interaction of ECs within the fluid environment of the biohybrid lung for improved biocompatibility. Key questions of permissible shear stress, oxygen tolerance and platelet deposition were addressed. Some other important questions were not explored in the scope of this project. These issues include in depth evaluation of active mixing, CO<sub>2</sub> removal and developing a practical cell harvesting protocol. Active mixing may minimize boundary layer effects, and could also lead to a decrease in the surface area requirements and overall size of the device. Relationships were not developed between active mixing experimentation and boundary layer effect reduction or device size. Oxygen transfer and accumulation data were collected experimentally to look at oxygen delivery with increased fiber bundle rotation rates.

While one aspect of this project was focused on oxygen toxicity, CO<sub>2</sub> removal was not investigated. Accumulation of CO<sub>2</sub> may ultimately lead to cell death and long term device complications. Elevated levels of CO<sub>2</sub> may cause changes in pH that are detrimental to cellular integrity. Therefore, CO<sub>2</sub> removal is not a trivial issue. Passive diffusion may, or may not

provide a suitable means for CO<sub>2</sub> removal. Sufficient alternatives for CO<sub>2</sub> removal will not be addressed in this dissertation, but it is important to be aware of the impact that CO<sub>2</sub> accumulation may have on this system. CO<sub>2</sub> removal will need to be addressed at some point in the overall development of a biohybrid lung prototype before it can reach clinical trials.

Another key issue not tackled in the scope of this project is EC harvest and expansion. It is envisioned that ECs will be harvested from a patient's own peripheral source. This process may include venous sources or microvasculature in adipose tissue. The cells would be plated in culture, stimulated with EC specific growth factors and expanded to an appropriate cell seeding density. However, at this point in time there is value in first understanding the basic endothelial response to hyperoxia and elevated shear stresses in the context of a rotating MHF bundle.

### **1.6.2 Surface modification of microporous hollow fiber membranes**

MHFs have been designed to limit cell adhesion, and thus, require surface modification to support EC adherence. Several surface modification techniques were evaluated to determine the appropriate treatment methodology. In order to compare surface treatments, patches of modified MHFs were evaluated for EC adhesion. Consideration was also given to possible consequences associated with blood contact onto areas of exposed surface treatment, should ECs not achieve confluence for all fibers or if cells were lost to detachment by shear forces or other phenomena. MHFs were anticipated to have subconfluent EC coverage.

### **1.6.3 Specific aim #1: bioreactor development**

The model biohybrid lung, expected simulating conditions to occur in devices sufficient in size to provide adequate gas exchange for an adult, provided an appropriate environment to answer basic questions concerning EC retention and function without the financial and spatial demands of a full scale prototype. The biohybrid lung prototype is more of an overall concept, and the term bioreactor is used to describe the physical housing that centers round a removable, rotating MHF module, allowing for fluid and gas sampling. The bioreactor was designed to incorporate both fiber bundle rotation, and gas flow through the fiber lumen, while minimizing the use of cell culture supplies over a test period of up to 7 days.

Non-MHF module material interactions within the bioreactor were a key concern due to their possible negative influence on EC retention and device biocompatibility. Debris from seal or shaft wear or other material interactions can have a toxic effect on cells. Sufficient levels of debris may kill ECs or induce an inflammatory phenotype [15]. Material selection was therefore evaluated to avoid cytotoxicity. Metallic corrosion or wear could also lead to mechanical failure, which could result in loss of active mixing or loss of separation between gas and liquid pathways, for example. Maintaining system sterility was an additional challenge. Development of appropriate assembly techniques was crucial for maintaining sterility within the system.

#### **1.6.4 Specific aim #2: ECs conditioned to shear stress**

Endothelialized MHF bundles were conditioned to rotational shear stress in a normo-physiological range and evaluated. A shear-conditioning regimen was developed to combat cell loss. It was hypothesized that ECs would have an upper bound for shear tolerance, that when exceeded would lead to cell dislodgement. It was also thought that a shear-training regimen would be needed to retain cells initially. Immediate exposure of ECs to shear stress has been shown to cause cell loss [21]. An initial period of static cell culture provides cells with an opportunity to firmly adhere to the surface.

Some cell loss may occur while the module is being conditioned to shear and transferred to the bioreactor. This loss will be difficult to compensate for once rotational shear begins. From preliminary experiments, cells cease to proliferate following continuous exposure to shear stress. Therefore, it is important to reach nearly confluent levels prior to introducing the module into the bioreactor. It is believed that cell retention will decrease with increased rotational shear. This may not be apparent in the designated rotational range of up to 1500 RPM.

It was also thought that ECs would be able to sustain physiologic rates of shear stress without detaching from the MHF bundle. Vascular ECs experience a range of shear stresses depending on location *in vivo*. The physiologic range of shear stress on vascular endothelium has been reported as 1 to 40 dynes/cm<sup>2</sup> [20]. It is reasonable to use this range of shear stress as a guide for *in vitro* experimentation. However, it is also possible that ECs will respond differently to lower or higher shear stresses *in vitro* than they would *in vivo*.

In order to evaluate endothelial response, e-selectin (CD62E), p-selectin (CD62P) and PECAM-1 expression was evaluated, as well as cell retention. ECs expressing an inflammatory phenotype often over express CAMs and selectins [77-79, 104, 105]. Jankowski et al. used flow cytometric techniques to measure expression of ICAM-1 and TF. They found an increase in TF on endothelialized grafts exposed to 2.5 dynes/cm<sup>2</sup> for 6 hours, versus the static control. EC retention was not affected by shear exposure [35]. It was anticipated that there is a maximum shear level that may be achieved without losing cells or inducing inflammation. If an inflammatory phenotype is present, more conservative operating conditions may need to be established, which could involve less oxygen and/or shear to make the biohybrid lung feasible.

### **1.6.5 Specific aim #3: thrombotic deposition and inflammation in the biohybrid lung prototype**

This aim sought to assess platelet deposition and EC inflammatory response to bovine blood introduced within the biohybrid lung prototype. Whole bovine blood was mixed in the biohybrid lung prototype for 2 hrs with non-surface modified, non-endothelialized MHF bundles or endothelialized, surface modified MHF bundles. Thrombotic deposition was subsequently evaluated under light microscopy or with SEMs. EC phenotype was evaluated for upregulation of e-selectin or p-selectin. It was hypothesized that an endothelialized surface would greatly reduce platelet attachment and thrombotic deposition on MHFs. The endothelial layer should provide a naturally occurring barrier that discourages thrombosis if a non-inflammatory EC phenotype was retained. Non-endothelialized, uncoated MHFs, found in commercial oxygenators, do not discourage thrombus formation, and were therefore expected to show more thrombotic deposition than endothelialized MHF bundles [116].

There was additional concern that subconfluent areas of MHFs may promote platelet deposition for two reasons. One reason is that the amount of platelet deposition could be dependent on the applied surface treatment. For example, collagen has been shown to promote EC attachment, but it is also known to directly facilitate platelet deposition [117]. Fibronectin has also been shown to promote EC attachment, but the protein is not pro-thrombotic [93]. Thrombotic deposition would be anticipated on subconfluent areas of collagen treated MHFs, but not fibronectin treated MHFs. The second reason is that ECs *in vivo* present a continuous,

semipermeable barrier. ECs communicate through intracellular junctions to regulate permeability and maintain homeostasis [118]. Disruption of cell to cell contact could disrupt homeostasis. ECs that do not contact one another on MHFs may express an inflammatory phenotype that could be pro-thrombotic [104]. Several surface treatments were applied to MHF patches and varying levels of confluence were achieved. Thrombotic deposition, following whole blood incubation, was quantified to address concerns related to subconfluence.

It was hypothesized that thrombotic deposition on subconfluent MHFs should not be statistically significantly higher than platelet deposition on confluent MHFs. If anticoagulation is required, the heparin concentration will likely be much less than that required for non-endothelialized MHFs. Ideally, the device will not require any anticoagulation. However, minimal heparinization offers an acceptable alternative if this goal cannot be achieved.

#### **1.6.6 Specific aim #4: hyperoxia in the biohybrid lung prototype**

In light of all the undesirable effects associated with hyperoxia, endothelial response to high oxygen partial pressures in the MHF lumen was examined. ECs were evaluated for phenotype alteration under hyperoxic conditions within the biohybrid lung model. A rotating fiber bundle had oxygen perfused through the lumen of each fiber within the bioreactor. Gas transfer across the membrane exposed the EC monolayer to hyperoxic conditions. The EC phenotype was then assessed.

It was expected that ECs would exhibit a certain level of tolerance to hyperoxia. There may be an upper limit to the oxygen partial pressures that are reasonable to utilize within the device. Barry et al. showed far less effect of oxygen toxicity for mouse lungs exposed to 85% oxygen, compared to 100% oxygen [36]. Many researchers have shown deleterious effects of hyperoxia on lung tissue and endothelium; however there appears to be a range of hyperoxia that will be tolerated for longer periods of time. ECs exposed to hyperoxia *in vitro* in tissue culture experiments did not show the same deleterious affects as ECs exposed to hyperoxia in the whole organ or *in vivo* [119, 120].

It was also thought that oxygen delivery to the biohybrid lung might be limited by the presence of an EC layer. The rationale was that coatings can present an added barrier for gas

transfer across the MHF membrane. The addition of an EC layer might potentially increase the permeance of the composite synthetic and biological membranes.

## **2.0 SURFACE MODIFICATION OF MICROPOROUS HOLLOW FIBER MEMBRANES**

### **2.1 INTRODUCTION**

*In vivo*, the endothelial lining of blood vessels presents an anti-thrombotic surface to circulating platelets and leukocytes [121]. The biohybrid lung discussed herein aims to replicate this surface on MHFs to promote biocompatibility of the device and potentially reduce anticoagulation requirements. As discussed in section 1.5.1, ECs expressing a non-inflammatory phenotype are capable of regulating hemostasis by expressing and/or secreting thrombomodulin, prostacyclin, nitric oxide, ectonucleotidases, tissue factor pathway inhibitor, heparin sulfate and type I plasminogen activator inhibitor.

In order to achieve endothelialization of MHFs, surface modification was performed to promote cellular attachment. Surface treatment and endothelialization of MHFs is desirable since it creates a barrier to plasma weeping into the MHF pores. MHFs are inherently non-conductive to cell adhesion; therefore several surface modifications were evaluated to determine the appropriate treatment to encourage EC attachment. Additional criteria included maintaining ECs in culture, and obtaining near-confluent EC coverage with minimal incubation periods.

Proteins commonly found in the extracellular matrix secreted by ECs, particularly that of the arterial wall, were considered to promote EC attachment. This lists includes collagen, fibronectin, laminin and elastin [88, 122]. Specifically collagen, gelatin and fibronectin were evaluated as potential surface modification proteins for the biohybrid lung prototype. Gelatin was chosen since it is less thrombogenic in comparison to collagen, but provides the desirable adhesive properties associated with collagen. Fibronectin was selected since it has shown an ability to encourage EC growth and proliferation [88].

Initial cell adhesion and viability tests were performed with HUVECs on PP, siloxane coated polypropylene fibers (polydimethyl-siloxane PDMS) and PMP fibers. As the biohybrid lung prototype evolved, it was found to be advantageous to use BAECs so that blood-surface biocompatibility testing could be performed with bovine blood. Polymethylpentene fibers were selected as the appropriate MHF for the biohybrid lung due to their asymmetric porosity design, which limits plasma leakage in comparison to polypropylene fibers, and ready availability in comparison to siloxane-coated polypropylene fibers. Therefore, methods and results will be separated into HUVEC and BAEC sections to avoid confusion.

## **2.2 METHODS**

### **2.2.1 Surface modification of MHFs to support HUVEC growth**

MHF mats of PP fibers (Celgard Inc., Charlotte, NC), PDMS (Senko, Japan), or PMP (Oxyplus/Membrana, Celgard Inc., Charlotte, NC), were cut into patches of 30 fibers, measuring 2.5 cm in length. Six MHF patches were glued (60% Polycin, 40% Vorite by mass, 2 part polyurethane adhesive, Cas Chem, Bayonne, NJ) into a 50 ml conical tube, in an alternated pattern, per surface modification. One drop of glue was applied to both edges of the MHF patch. One tube was left unmodified to serve as a control.

Select groups of fiber patches underwent radio frequency glow discharge (RFGD) (Super Plasmod, March Plasma, Concord, CA), while glued into a 50 ml conical tube, with the cap removed. The pressure in the RFGD chamber reduced to 0.3 Torr. Ammonium gas was pulled under vacuum into the energized chamber (current of 100 Watts) for 60 seconds.

Following optional RFGD treatment, all fiber groups were sterilized with ethylene oxide gas (ETO) at 48°C (EO Gas™). Protein adsorption was applied following ETO sterilization. Select groups received additional surface treatment with coatings of fibronectin (Sigma, St. Louis, MO), type-I collagen (Sigma), Matrigel (BD Biosciences), BDI (Sigma), and BDI with RGDS (Sigma). Fibronectin was applied at 5 µg/mL. Collagen and Matrigel were applied to fully coat samples in a 6-well plate with a dilution of 1:5 (matrigel: PBS or collagen:PBS).

Protein adsorption with fibronectin, collagen or matrigel was performed in an incubator at 37°C and 5% CO<sub>2</sub> for 45 minutes to 1 hour. BDI was applied, as provided by the manufacturer, in enough volume (0.5 mL) to cover the sample for 10 minutes, with minimal air contact to the BDI. RGDS was applied as a solvent at a concentration of 100 µg/mL. Some samples received the surface treatment following RFGD pre-treatment, while other samples did not receive treatment or only received RFGD treatment.

After surface modification, HUVECs (Cambrex, CC-2519) were added to 50 mL conical tubes to give a total cell seeding density of roughly  $4 \times 10^5$  cells. The tubes were placed on a hematology mixer (one set speed) overnight in an incubator at 37°C and 5% CO<sub>2</sub>. The following day, seeded patches were removed and placed into a static culture environment in six-well plates. HUVECs were cultured in endothelial growth medium (EGM™-2MV-Microvascular EC Medium-2, Cambrex, CC-3202) in an incubator at 37°C with 5% CO<sub>2</sub>.

Mitochondrial activity was measured by the methylthiazolyl diphenyl-tetrazolium (MTT) (Sigma, M 5655) assay at days 1, 4 and 7. MTT is water soluble tetrazolium salt that can be converted to an insoluble purple formazan by cleavage of the tetrazolium ring by dehydrogenase enzymes, such as active mitochondrial dehydrogenases of living cells [123]. This conversion will not occur with dead cells. The insoluble formazan is solubilized with isopropanol, and measured spectrophotometrically at a wavelength of 570 nm to obtain an absorbance [123]. MTT was diluted with PBS (1:10) and added at a concentration of 5 µg/mL to cell culture medium on endothelialized MHFs. After a 3-5 hour incubation period, endothelialized MHFs were transferred to a new 6-well plate, where a 0.04 M HCl/isopropanol solution was added to replace the original volume of cell culture medium. Absorbency measurements were read the following day. MTT calibration curves were made by plotting the cell number (x-axis) against the absorbency corresponding to the cell number (y-axis).

Cellular adhesion is expressed as either absorbance or cells/cm<sup>2</sup>. Data expressed as absorbance do not have relative calibration curves, so the data cannot be converted to cells/cm<sup>2</sup> or % cell coverage. Data for polypropylene fibers are shown in shades of green, data for PDMS fibers are shown in shades of blue, and data for PMP fibers are shown in shades of purple.

### **2.2.2 Surface modification of PMP MHFs to support BAEC growth**

Mats of PMP MHFs (a gift from Celgard) were cut into patches of 30 fibers, measuring 2.5 cm in length. Six MHF patches were glued (60% Polycin, 40% Vorite by mass, 2 part polyurethane adhesive, Cas Chem) into a 50 mL conical tube per surface modification. One tube was left unmodified to serve as a control. Select groups of fiber patches received RFGD (March Plasma Systems) treatment as described in section 1.2.1. The MHF surface became more hydrophilic, as verified by a decrease in the water in air contact angle.

All fiber groups were sterilized with ETO gas at 48°C (Cellomics, EO Gas™). Select groups received additional surface treatment with type I collagen (Sigma, C9791), gelatin (Sigma, G1393) or fibronectin (Sigma, F1141). Type I collagen was applied at 10 µg/mL, gelatin was applied at 0.2% (1 µL/cm<sup>2</sup>, as provided by the manufacturer) and fibronectin was applied at 5 µg/mL.

Bovine aortic ECs (BAECs) (Cambrex, BW-6002) were cultured in endothelial growth medium (EGM™MV-Microvascular EC Medium, Cambrex, CC-3125) in an incubator at 37°C with 5% CO<sub>2</sub> until confluence before being seeded onto MHFs. After surface modification, BAECs were added to 50 mL conical tubes to give a total cell seeding density of approximately 4 x 10<sup>5</sup> cells. The tubes were placed on a hematology mixer overnight. The following day, seeded patches were removed and placed in six-well plates for a period of static culture. Mitochondrial activity was measured by the MTT assay at days 1, 2, 3, 5 and 7. Cellular adhesion is expressed as % cell coverage, based on absorbency readings. Refer to Appendix B for % cell coverage calculations.

### **2.2.3 Statistics for MHFs to support HUVEC growth**

Results are displayed as ± standard deviation (± SE). Repeated measures ANOVA testing was used to compare HUVEC coverage. Post-hoc Newman Keul tests were used to compare surface modification data at selected time points, or to compare selected time points for specific surface modifications. Significance was considered to exist at p<0.05.

#### **2.2.4 Statistics for PMP MHFs to support BAEC growth**

Results are displayed as  $\pm$  standard error of the mean ( $\pm$  SE). Repeated measures ANOVA testing was used to compare BAEC coverage. Post-hoc Newman Keul tests were used to compare surface modification data at each time point, and comparison of time points for specific surface modifications. Significance was considered to exist if  $p < 0.05$ .

### **2.3 RESULTS**

#### **2.3.1 Surface modification of MHFs to support HUVEC growth**

RFGD with ammonium gas was implemented to provide attachment of amine groups to the surface of the polymer. MHF samples modified with RFGD were evaluated with x-ray photoelectron spectroscopy (XPS, at NESAC/BIO, University of Washington) to quantify amine attachment. Nitrogen groups were not detected on these samples, and therefore amine attachment was shown to be unsuccessful. However, the MHF surface did become more hydrophilic, as verified by contact angle on polypropylene films treated with RFGD. The hydrophilic RFGD modification did promote EC attachment, as shown below.

A combination of RFGD and fibronectin treatment provided a statistically significant increase ( $p < 0.05$ ) in mitochondrial activity attributed to HUVEC fiber coverage by day 7, as compared to untreated, RFGD treated or fibronectin treated MHFs. This occurred on both polypropylene and PDMS MHFs and is shown in Figure 2-1.

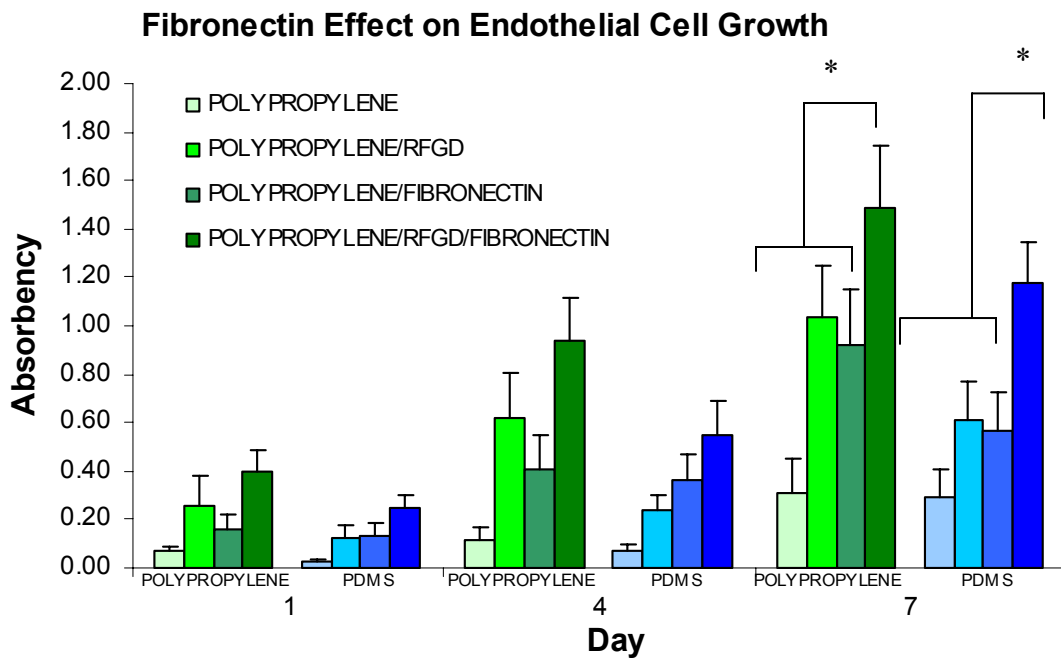


**Figure 2-1** Fibronectin effect on HUVEC growth on PP and PDMS MHFs

Comparison of EC growth on polypropylene and PDMS fibers treated with RFGD, fibronectin, or a combination. At day 7 RFGD and fibronectin treated MHFs had significantly ( $p < 0.05$ ) more HUVEC activity than all other surface treatment groups, for both polypropylene and PDMS fibers ( $n=6$ ).

There was no statistically significant difference by day 7 of HUVEC growth on PDMS fibers that were collagen coated, matrigel coated, RFGD modified, or RFGD modified with collagen adsorption, shown in Figure 2-2.

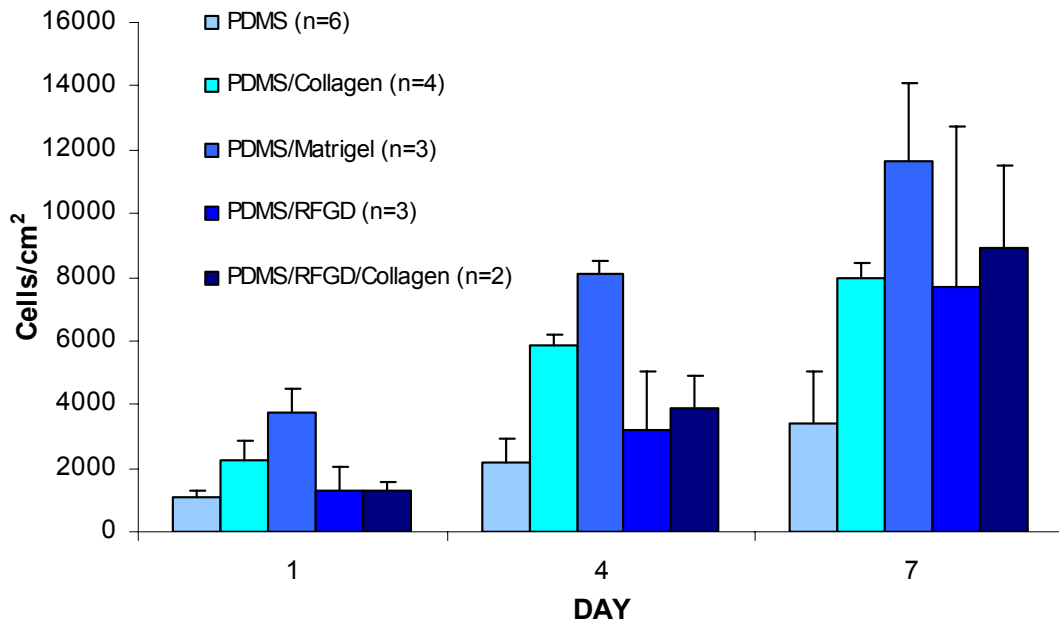


**Figure 2-2** Collagen and matrigel effect on HUVEC growth on PDMS MHFs

Comparison of HUVEC growth on PDMS fibers treated with RFGD, collagen, collagen with RFGD, matrigel coatings, and a control (n varies from 2 to 6)

Figure 2-3 shows HUVEC growth on PDMS fibers treated with RFGD alone, BDI alone, RFGD and BDI, BDI and RGDS, or RFGD with BDI and RGDS. At day 7 of HUVEC growth there were no statistically significant differences between the more important surface treatment groups of RFGD, RFGD with BDI, or RFGD with BDI and RGDS. Morphological changes were observed on PDMS fibers treated with BDI. The fibers appeared to reduce in size and become more brittle.

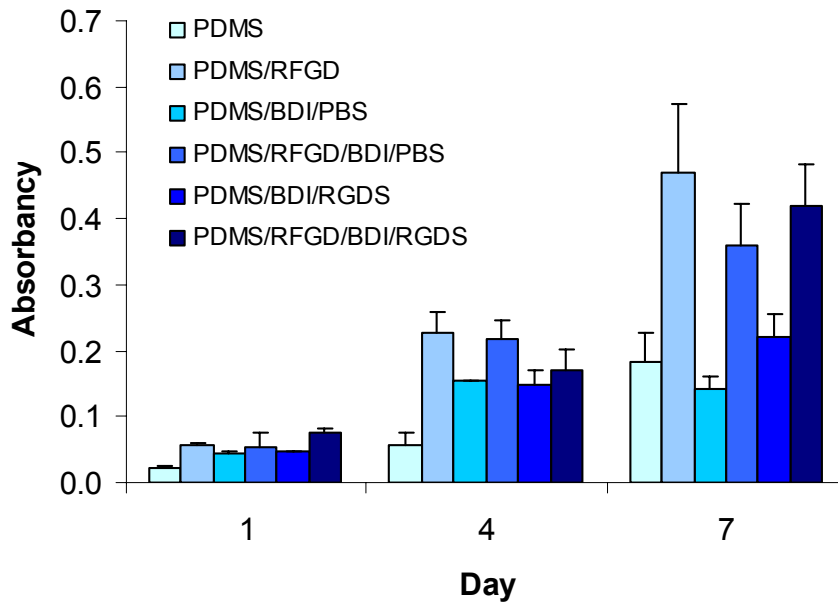


**Figure 2-3** RGDS effect on HUVEC growth on PDMS MHFs

Comparison of EC growth on PDMS control fibers and PDMS fibers treated with RFGD or RFGD, BDI and RGDS (n=5)

### 2.3.2 Surface modification of PMP MHFs to support BAEC growth

To encourage BAEC attachment, various surface modification techniques were investigated. Evaluated surface types consisted of control PMP MHFs, PMP MHFs modified with RFGD and PMP MHFs modified with RFGD and protein adsorption (collagen, gelatin or fibronectin). BAEC coverage increased significantly with the RFGD treatment of PMP MHFs within the first day of culture ( $p < 0.05$ ). Coverage increased even more with protein adsorption. RFGD modification in combination with fibronectin adsorption resulted in the greatest amount of BAEC coverage onto MHF patches in the shortest period of time. By day 5 of culture PMP MHFs treated with RFGD and fibronectin had significantly more BAEC coverage than any other surface treatment ( $p < 0.05$ ). By day 7 of culture near BAEC confluence was achieved on PMP MHFs treated with RFGD and gelatin or Fn. This coverage was statistically greater in comparison to other surface treatments ( $p < 0.05$ ). Figure 2-4 shows difference in BAEC growth on five surface types.

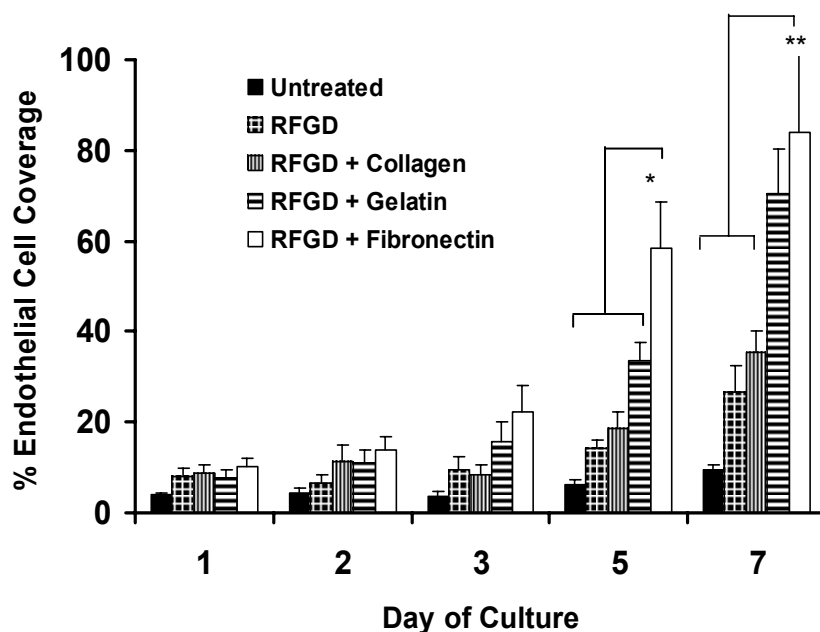


**Figure 2-4** BAEC coverage on PMP MHF patches of varying surface modification

\* indicates BAEC coverage was statistically significantly greater on PMP fibers treated with RFGD and fibronectin adsorption than all other groups at day 5 ( $p < 0.05$ ). \*\* indicates BAEC coverage was statistically significantly greater on PMP fibers treated with RFGD and fibronectin adsorption than all other groups except PMP fibers treated with RFGD and gelatin adsorption at day 7 ( $p < 0.05$ ). Error bars represent SEM.

## 2.4 DISCUSSION

With modification of MHF patches, EC attachment and confluent coverage was obtained for both HUVECs and BAECs. Surface modification with RFGD followed by fibronectin adsorption consistently showed favorable cell attachment and proliferation results on all three fiber types (PP, PDMS, PMP). The BDI and RGDS treatment was eliminated, due to morphological changes of the fibers attributed to the BDI. Full endothelialization of MHFs was quickly obtained with treatment of RFGD followed by either gelatin adsorption or fibronectin adsorption in studies utilizing BAECs. These surface treatments provide effective ways to quickly enhance cell attachment and growth on MHFs, and have been shown to heighten cell retention [81] [72, 82]. Takagi et al. showed increased cell attachment on PP MHFs with adsorbed or covalently bonded

pronectin, gelatin and fibronectin, compared to control, unmodified PP MHFs. EC coverage was greatest on PP MHFs treated with fibronectin [72].

BAECs also grew well on MHFs treated with RFGD and collagen, however this may not be an ideal surface treatment since collagen is a pro-thrombotic protein. Thrombotic deposition might be more likely to form on a collagen coated surface if full endothelialization were not achieved. Therefore, it is imperative to select a surface modification that will maintain an anti-thrombotic surface for the biohybrid lung prototype. Work has been done by others to combat thrombotic deposition by modifying MHFs with coatings of heparin or siloxane. Such modified fibers reduce plasma filling of the micropores by presenting a thin coating, however gas diffusion is limited by the coating [124].

PMP fibers are desirable for deterrence of plasma leaking due to a non-symmetric design that consists of non-uniform porosity which is higher at the inner fiber lumen. RFGD treatment of MHFs showed an increase in hydrophilicity on the fiber surface that could promote protein adsorption at the open pore meniscus, the gas-blood interface of PP fibers. PMP fibers already present a thin skin to inhibit plasma leakage, so increased hydrophilicity is less of a concern in respect to plasma leakage for these fibers. ECs prefer to attach to hydrophilic surfaces, making the RFGD treatment favorable for PMP fibers.

ECs also preferred to attach to the nylon weft fibers of MHFs. ECs would adhere and initially grow on wefts in larger numbers than on the actual MHF surface. MHFs without surface treatment had highest EC coverage on the wefts with little coverage on the MHF. Wefts may present a more thrombogenic surface than the MHF, therefore confluent EC coverage of this area may be desirable.

EC growth and coverage were followed over a 7 day period to more accurately compare surface modifications using low initial seeding densities. If higher cell seeding densities were used, EC confluence could be achieved on PMP MHFs modified with RFGD and gelatin adsorption, or RFGD and fibronectin adsorption, in 1 to 2 days. This information is relevant to obtain EC coverage more rapidly, but it was also valuable to distinguish which surface treatment would encourage more EC growth over a longer period of time. If a less than desirable quantity of cells is available for use in the biohybrid lung, figure 2-4 shows that higher cell coverage will be obtained with RFGD surface modification and fibronectin adsorption for MHFs in less time than with the other surface modifications shown.

## **3.0 BIOREACTOR DEVELOPMENT**

### **3.1 INTRODUCTION**

The biohybrid lung provides a system to study EC phenotype and shear response. It also incorporates oxygenation into an active mixing device with a biological component, ECs. Material components selected for use in the biohybrid lung prototype were evaluated for their potential cytotoxicity and overall impact on device performance. Careful thought was given to the design of separate gas and liquid pathways within the device. A bearing and seal configuration was selected to facilitate active mixing within the device through the use of a rotating center piece. The center piece has a shaft that fits into the bearing and seal housing. The nature of this design can be very demanding on torque requirements from the motor. High torque requires careful seal selection for the intended application. When the constraints of a 37°C, high humidity, high salinity environment are included, along with extended use of up to 7 days, and rotational speed of 1500 RPM, seal selection becomes even more crucial. Seals can degrade, which can cause leaking and formation of debris. Heat generation is also a common complication associated with rotating seal/bearing designs.

Multiple factors were taken into consideration for design of the biohybrid lung prototype. In addition to cell cytotoxicity, active mixing, and oxygen delivery, the biohybrid lung prototype was designed to minimize the use of expensive resources such as cell culture medium and blood, as well as maintain sterility. This chapter will discuss the development of a biohybrid lung prototype used to facilitate active mixing of endothelialized MHFs in cell culture medium or blood at rotational speeds of up to 1500 RPM.

## 3.2 METHODS

### 3.2.1 Biohybrid lung prototype design and development

The main design objectives of the biohybrid lung prototype specified that oxygen flow through the lumens of the MHF bundle under rotation, sterility be maintained and components be able to withstand elevated levels of humidity and temperatures of 37°C for the duration of each experiment. Bioreactor components must be able to undergo sterilization and remain sterile upon device assembly. In addition, fluid transfer should be conducted with ease. Medium may be changed with disposable syringes through luer ports, or it may be circulated with a perfusion system. Either way, it is important that rotation of the MHF bundle not be stopped during an experiment.

Oxygen and carbon dioxide probes were used to access medium. Final raw materials consisted of cast acrylic for the housing, Teflon for removable housing caps, titanium shafts treated with diamond-like carbon coating (Anatech LTD), titanium screws and a titanium module base. Bioreactor parts, including titanium, end caps and housing, were machined by Daniel T. McKeel at the McGowan Institute for Regenerative Medicine. Shafts were initially made from medical grade stainless steel (316L), but this led to corrosion and pitting. Bearings were stainless steel. The final seals were Teflon (ES Dygert Co.). Earlier seals were made from nitril or vyton (Chicago Rawhide, 711803 & 721526), but leaking and debris resulted. A continuous duty servo-brushless motor and power supply (Parker Hannifin Corp.) with the ability to vary speeds in small increments from 1 RPM to greater than 1500 RPM was selected. The controller interface was located outside of the incubator. A schematic of the final version of the biohybrid lung incorporating the desired characteristics is shown below (Figure 3-1).

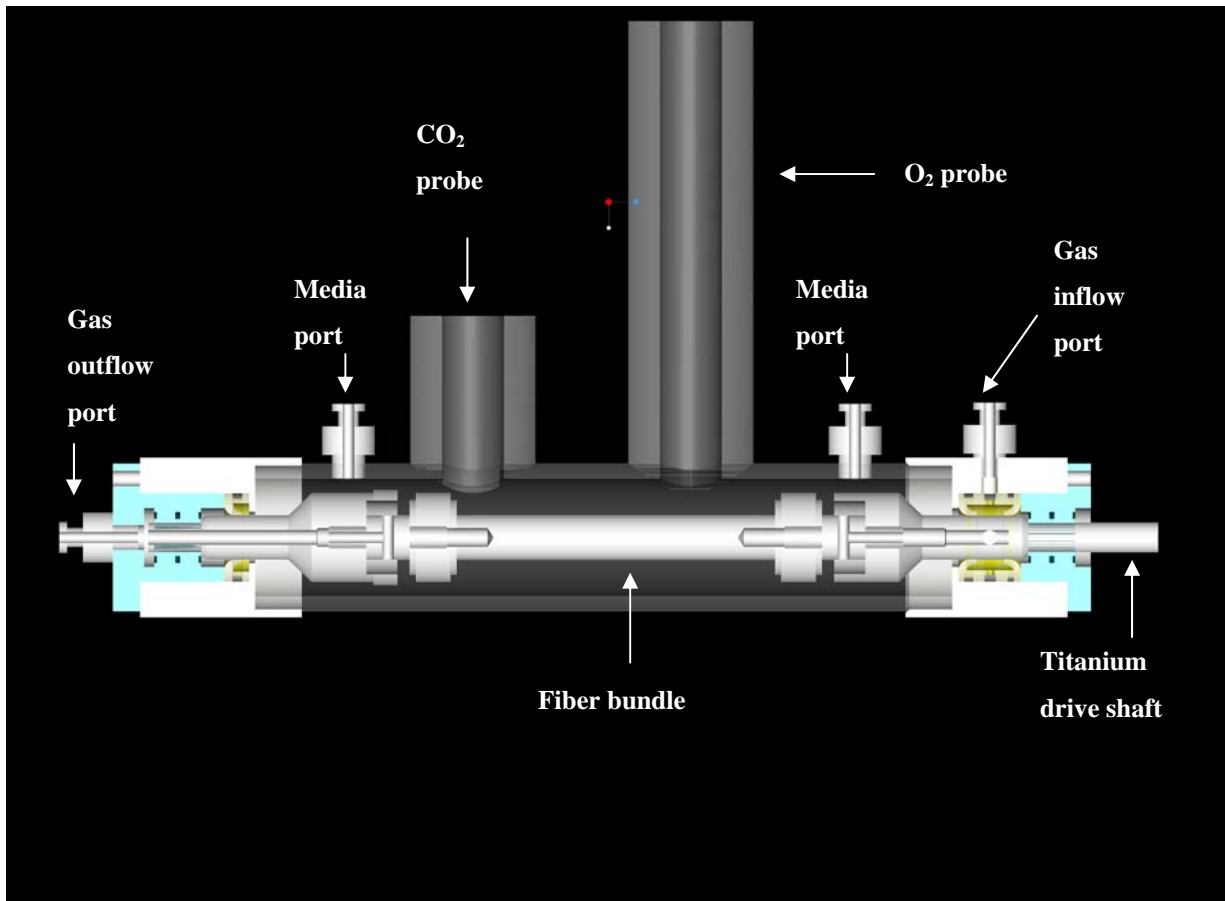


**Figure 3-1** Schematic of biohybrid lung prototype

In order to best determine materials appropriate for use in the biohybrid lung prototype, components were tested individually and as a unit. Individual components such as stainless steel, titanium, nitril seals, vyton seals, and Teflon seals were soaked in EGM-MV medium for up to 7 days. The medium and components were viewed under the microscope for signs of debris, degradation and corrosion. Cell viability was assayed for endothelialized wells that were incubated with materials from the biohybrid lung prototype versus a control of seeded wells, for up to 7 days. Alamar Blue (Biosource, cat# DAL1100), a non-destructive cell viability assay, or MTT (Sigma M 5655), a destructive cell viability assay was used [123, 125]. The MTT assay was described in section 2.2.1. Alamar Blue is soluble and non-toxic, therefore cell growth and proliferation can be monitored while the cells are in use. A dilution of 1:10 (Alamar Blue: cell culture medium) was applied directly to cell culture medium from the stock solution supplied by the manufacturer. Alamar Blue reduction was measured on a spectrofluorometer at 570 nm and 600 nm, following 5 hours of incubation with ECs and bioreactor components. The percent

reduction of Alamar Blue was calculated and compared to a calibration curve to estimate the number of viable cells present in the sample [125, 126].

The complete system ran in water, medium and with HUVECs for several days. Visual assessment was applied to detect any accumulation or floating debris. Medium and components were microscopically evaluated for signs of corrosion and degradation.

### **3.2.2 Bioreactor Sterility and Assembly**

Much attention was given to assembly of the device to maintain sterility. MHF bundles were sterilized with ETO gas before BAECs were seeded on to them. Seeding tubes were sterilized with ETO gas as well, to maintain sterility before the bundle was placed in the bioreactor. Bioreactor parts and assembly equipment was ETO gas sterilized prior to setup with sterile procedure in a cell culture hood. The following pieces were ETO gas sterilized for every bioreactor setup: vice, plastic guide tube (cut cast acrylic of ½” inner diameter), 2 open conical tubes of thread, tweezers, razors, thermocouple, silicone tubing, tubing connectors (luer locks, luer locks with barbs, etc.), bioreactor shaft guide (a custom made titanium cylinder of 3” length open on one end with an inner diameter of 3/8”), 8 strips of parafilm, bioreactor housing, 2 end caps, 2 screws to hold the MHF bundle, 2 titanium shafts, seals in holders, bearing in holders, 4 custom made Teflon gaskets, 6 screws to hold the end caps, 1 rubber stopper, and one custom made air outflow gasket. Two sterile 3-way stopcocks and one T-75 tissue culture flask cap were also used during assembly.

All sterile pieces were laid out on open sterile ETO packages for assembly. The endothelialized MHF bundle was taken from the seeding tube with tweezers and shafts were screwed into the ends. Thread was wrapped, with the aid of the mini-vice and plastic tube, around balloon seals covering the shafts to separate the gas and liquid pathways. The shaft guide was used for assembly of the MHF bundle into the distal end seal and bearing holders. An outer layer of MHFs was cut off of the MHF bundle. This layer served as a protective barrier during cell seeding, cell growth and initial device assembly. It was originally wrapped on top of balloon seals covering the MHF bundle. The MHF bundle was then inserted into the bioreactor housing and the proximal end seals and bearings were secured into place with assistance of the shaft guide. Silicone tubing and stopcocks were attached to the medium sampling ports. 50 mL of cell

culture medium was added to the device. The thermocouple was inserted through the rubber stopper and placed in one of the two probe holder positions. The tissue culture flask cap was placed on top of the other probe holder. Both were secured with parafilm. Following assembly, the bioreactor was immediately placed in the incubator.

### 3.2.3 Shear Stress Calculations for Rotation of a MHF Bundle

The Navier-Stokes motion equations for rotation of an inner cylinder in a stationary cylinder were applied for constant  $\rho$  (density) and  $\mu$  (dynamic viscosity). The governing equation is given below (Equation 7) [127].

**Equation 7** Navier-Stokes equation for cylindrical coordinates (r-component), constant  $\rho$  and  $\mu$

$$\rho \left( \frac{\partial v_\theta}{\partial t} + v_r \frac{\partial v_\theta}{\partial r} + \frac{v_\theta}{r} \frac{\partial v_\theta}{\partial \theta} + v_z \frac{\partial v_\theta}{\partial z} + \frac{v_r v_\theta}{r} \right) = -\frac{1}{r} \frac{\partial p}{\partial \theta} + \mu \left[ \frac{\partial}{\partial r} \left( \frac{1}{r} \frac{\partial}{\partial r} (r v_\theta) \right) + \frac{1}{r^2} \frac{\partial^2 v_\theta}{\partial \theta^2} + \frac{\partial^2 v_\theta}{\partial z^2} + \frac{2}{r^2} \frac{\partial v_r}{\partial \theta} \right] + \rho g_\theta$$

The equation was evaluated in one-dimension, in the theta direction with respect to r. The following assumptions were made. Fluid flow is in the  $\theta$ -direction (Equation 8).

**Equation 8** Fluid flow in  $\theta$ -direction

$$v_\theta \neq 0, v_r = 0$$

Fluid velocity is only a function of r (Equation 9).

**Equation 9** Fluid velocity is only a function of r

$$v_\theta = f(r)$$

Gravity and pressure effects are negligible (Equation 10).

**Equation 10** Gravity and pressure effects are negligible

$$g_\theta = 0, p=p(r,z)=0$$

Fluid flow is assumed to be at steady state (Equation 11).

**Equation 11** Steady State Flow

$$\frac{\partial}{\partial t} = 0$$

The Navier-Stokes equation was simplified with the above assumptions (Equation 12).

**Equation 12** Simplified Navier-Stokes equation

$$0 = \frac{d}{dr} \left( \frac{1}{r} \frac{d}{dr} (rv_{\theta}) \right)$$

Equation 12 was solved to obtain  $v_{\theta}$  (Equation 13).

**Equation 13** Equation for  $v_{\theta}$

$$v_{\theta} = C_1 r/2 + C_2/r$$

Boundary conditions were chosen (Equation 14)

**Equation 14** Boundary conditions

$$@ r = R_i, v_{\theta} = \Omega R_i$$

$$@ r = R_o, v_{\theta} = 0$$

The boundary condition for a given radius is  $r$ .  $R_i$  is the radius of the titanium module with MHFs and  $R_o$  is the radius of the inner wall of the bioreactor housing.  $\Omega$  is the angular velocity. The equation for  $v_{\theta}$  with the given boundary conditions substituted in is shown (Equation 15).

**Equation 15** Boundary conditions substituted into the equation for velocity in the  $\theta$  direction

$$v_{\theta} = -\frac{r\Omega R_i^2}{(R_o^2 - R_i^2)} + \frac{\Omega R_i^2 R_o^2}{r(R_o^2 - R_i^2)}$$

The angular velocity,  $\Omega$ , is found from RPM multiplied by circumference. The dynamic viscosity is given as  $\mu$ . The shear rate is given below with units of  $[s^{-1}]$  (Equation 16).

**Equation 16** Shear rate

$$\frac{\tau}{\mu} = -\frac{dv_{\theta}}{dr} = \frac{\Omega R_i^2 (r^2 + R_o^2)}{r^2 (R_o^2 - R_i^2)}$$

The shear stress, with units of  $[dynes/cm^2]$ , is found by multiplying the shear rate with the dynamic viscosity (times a factor of 10 for unit conversion). The dynamic viscosity of blood is 3 cp, or  $0.003 \text{ Ns/m}^2$ .

### 3.3 RESULTS

#### 3.3.1 Biohybrid lung prototype design and development

The first biohybrid lung prototype is shown below with the addition of Alamar Blue in the cell culture medium (Figure 3-2).



**Figure 3-2** Original biohybrid lung prototype

Alamar Blue was originally used to assess live cell number within the device, and is shown in Figure 3-2. However, control experiments showed that Alamar Blue was not accurate

in predicting cell number above  $4 \times 10^5$  to  $5 \times 10^5$  cells. Original materials of stainless steel 316L resulted in corrosion and pitting, and debris formation by the vyton (or nitril, not shown) seals, as shown (Figure 3-3 & Figure 3-4).

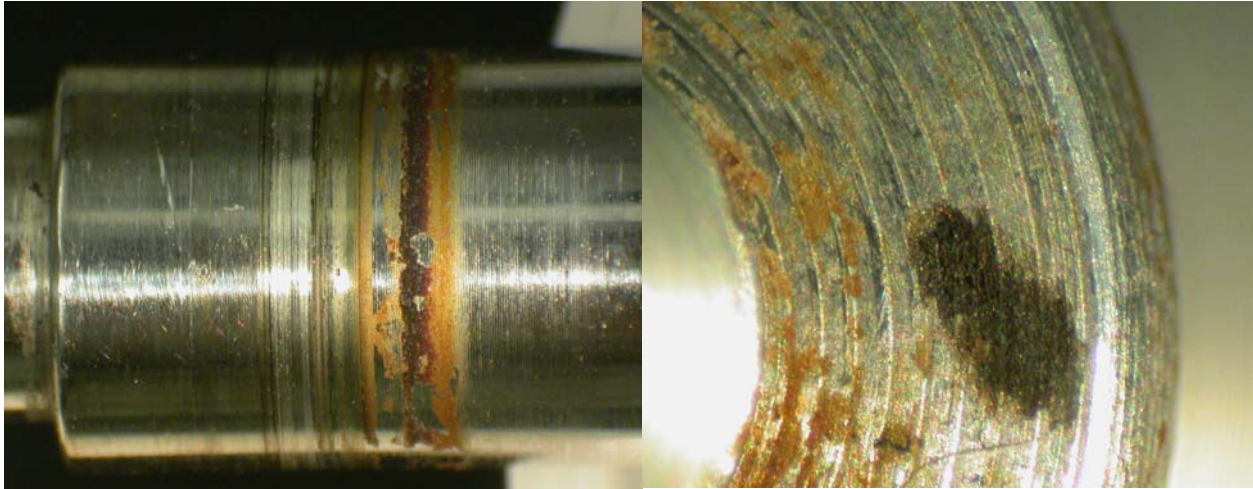


**Figure 3-3** Original biohybrid lung prototype stainless steel components  
Corrosion and pitting occurred with original stainless steel bearings and shafts



**Figure 3-4** Vytan seal exhibited debris in the original biohybrid lung prototype

The final prototype of the biohybrid lung is shown below (Figure 3-4).



**Figure 3-5** Finalized biohybrid lung prototype

An exchangeable MHF bundle and seeding tube are shown below (Figure 3-6). The inner, outer and middle fiber layers are exposed when looking down the cylinder.

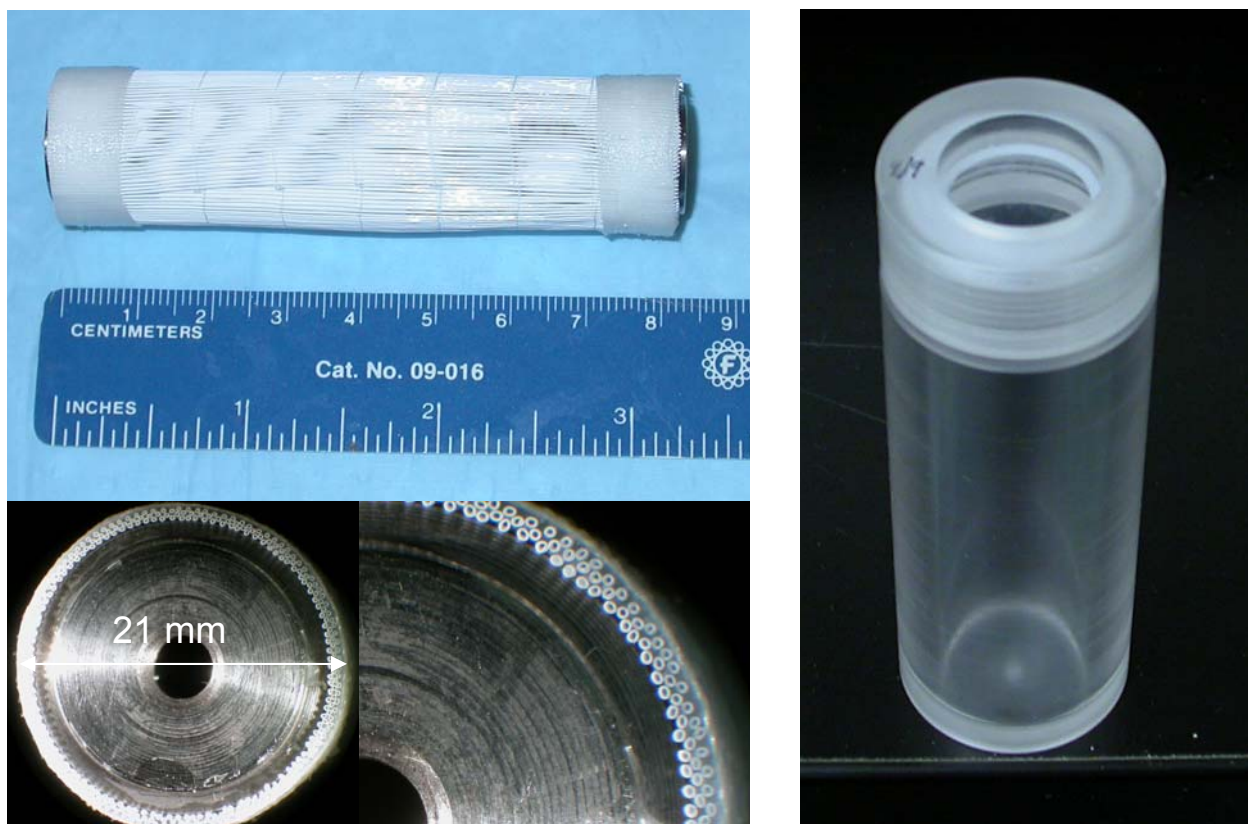


**Figure 3-6** Microporous hollow fiber bundle and seeding tube

Microporous hollow fiber matt potted around a titanium core: (a) side view, (b) looking down the core, (c) custom made seeding tube with a permeable membrane end cap.

The prototype allows for gas flow through the lumen of MHFs during rotation through an entry and exit pathway. Rotation was increased gradually up to a tested speed of 1500 RPM. Custom made Teflon seals supported high levels of torque required for steady rotation of the MHF bundle. DLC coating on the titanium shafts provided a smoother finish that reduced friction between the shaft and bearing. However, as speed increased within the biohybrid lung prototype, heat production also increased. To compensate for heat generation, the incubator temperature was dropped incrementally with speed increases to an end temperature of 32°C. At speeds of 100 RPM or greater a fan was positioned along the housing of the biohybrid lung prototype to dissipate heat. At speeds of 500 RPM or greater, room temperature air was directed onto the exterior of the biohybrid lung prototype housing.

The system allowed for media exchange during continuous rotation. Oxygen and carbon dioxide levels could be monitored within the medium in the system through two separate ports.

Temperature was monitored with the addition of a thermocouple. BAECs remained viable under rotation in the biohybrid lung prototype throughout the testing period of 7 days or greater.

### 3.3.2 Shear Stress Calculations

After simplifying the Navier-Stokes equation, shear rates and shear stresses were calculated for the given RPM (Table 3).

**Table 3 Shear stress calculations**

RPM	Wall Shear Rate ( $s^{-1}$ )	Wall Shear Stress (dynes/cm <sup>2</sup> )
50	32.93	1.0
100	65.87	2.0
150	98.81	3.0
200	131.75	4.0
250	164.68	4.9
300	197.62	5.9
350	230.56	6.9
400	263.49	7.9
450	296.43	8.9
500	329.37	9.9
550	362.30	10.9
600	395.24	11.9
650	428.18	12.8
700	461.11	13.8
750	494.05	14.8
800	526.99	15.8
850	559.92	16.8
900	592.86	17.8
950	625.80	18.8
1000	658.73	19.8
1050	691.67	20.8
1100	724.61	21.7
1150	757.54	22.7
1200	790.48	23.7
1250	823.42	24.7
1300	856.35	25.7
1350	889.29	26.7
1400	922.23	27.7
1450	955.16	28.7
1500	988.10	29.6

### 3.4 DISCUSSION

A biohybrid lung prototype was successfully designed and constructed to rotate endothelialized MHF bundles. The final prototype was an evolution of several different prototypes to promote cellular retention. The final prototype differed from earlier prototypes by the use of titanium instead of medical grade stainless steel, and custom made Teflon seals instead of commercially available nitril and vyton seals. Inclusion of a servo-brushless motor was also crucial for achieving torque requirements. It was necessary to include cooling mechanisms, such as fans, lowered incubator temperature and a stream of room air, to maintain a physiologic temperature range. Experiments were easily lost to overheating or under heating without the use of a thermocouple and constant adjustment to cooling mechanisms. There were four copies of the prototype available for use. Two of the four units produced more heat generation than the others, even though they were “identical”. Heat production would also vary from experiment to experiment. Heat generation is common with rotating devices that have a shaft contacting bearings and seals. Bearings purged with a cooling fluid are sometimes implemented to address this problem. Many new rotational medical devices are switching to magnetically levitated impellers to reduce heat generation. However, with the biohybrid lung it was very difficult to implement such technologies due to the necessity of separating gas and liquid pathways.

The final biohybrid lung prototype was EC compatible at speeds accelerated up to 1500 RPM over a test period of 7 days or greater. Key features of this design included exchangeable MHF bundles, controlled rotation of MHF bundles, separation of the gas-liquid interface within the prototype, and ability to sample and exchange medium. It was critical to design a device that would not negatively impact cell retention so that EC response to shear stress and/or hyperoxia could be evaluated without confounding variables associated with device performance. Developing methods to maintain sterility within the device was also a major challenge. This was also a crucial aspect of the project due to the length of individual experiments. From the time BAECs were seeded onto the MHF bundle, to the time endothelialized MHF bundles were assembled into the biohybrid lung, to the time that the biohybrid lung experiment was terminated, approximately 3 weeks had passed. In those 3 weeks, numerous opportunities for contamination arose. Medium was changed daily, which required removal of the MHF bundle from the seeding tube during the first 1.5-2 weeks. A 20 minute assembly process was

implemented for bioreactor setup in the cell culture hood. Medium was exchanged via syringes through medium ports in the incubator. These ports were briefly open to air during medium exchanges. This technique of medium exchange was actually much more successful for avoiding contamination than medium exchanges through a perfusion system. When perfusion systems were implemented, they remained closed to air at all times. However, the abundance of surface area from tubing and connectors were likely factors leading to much more frequent device contamination.

Separation of the gas-liquid pathway presented a design challenge for sterile, efficient assembly. If the device was not assembled, filled with cell culture medium and placed within the incubator within approximately 30 minutes, BAECs would die and the experiment would be lost. Initially, o-rings were intended to slip over the titanium shaft and balloon to seal and separate the gas-liquid pathway. An adequate seal could not be obtained with o-rings. Ultimately sterile thread was wrapped tightly around the balloon seals with sterile technique. This added additional time and complexity to the assembly process, but provided adequate separation of the gas-liquid pathway.

The biohybrid lung prototype provides an ideal controlled system for studying ECs exposed to shear stress on MHFs. Sterility is maintainable within the system. With proper material selection it was shown that BAEC viability was also maintained. This prototype was designed to efficiently test EC function under shear stress *in vitro*. Maximum shear stresses were calculated for rotation rates up to 1500 RPM, which corresponded to a shear stress of 29.6 dynes/cm<sup>2</sup>. Shear stresses were estimated for the outer fiber of the 3 layer fiber bundle. Middle and inner fiber layers would experience lower shear stresses, since they are protected by the outer fiber layer. Shear stresses calculated for the biohybrid lung fall within the physiologic range.

Shear stresses on ECs and MHFs may be higher than predicted using the Navier-Stokes equations. Taylor vortices have been reported to form in the gap between two concentric cylinders when the inner cylinder is rotated [128, 129]. Batten et al. have reported Taylor vortices at Reynolds numbers of  $5 \times 10^3$  and  $8 \times 10^3$  based on the gap width between two cylinders [128]. Refer to Appendix D for estimated Taylor numbers in the biohybrid lung prototype. High Taylor numbers are an indication of turbulent flow and higher fluid velocities around the MHFs and ECs, which may require that ECs form stronger adhesions to the MHFs and flatten more to

distribute more surface area. The function of adherent ECs may also change in response to Taylor vortices. A higher fluid velocity scheme may improve oxygen accumulation in the biohybrid lung by reducing boundary layer effects.

Limitations still exist in the final biohybrid lung prototype, described herein. The system requires nearly continuous user attention to maintain a temperature of  $37 \pm 2^\circ\text{C}$  and viable cell culture medium. There are numerous variables that can lead to contamination of the system, or complete cell loss. The device has not been entirely optimized to promote blood-surface biocompatibility. A large portion of the blood contacting part of the device is composed of materials other than endothelialized MHFs. This includes the cast acrylic housing, Teflon seals, string, balloon seals between the gas and liquid pathways, end caps and fluid ports.

## **4.0 ENDOTHELIALIZATION AND ROTATION OF MHF BUNDLES**

### **4.1 INTRODUCTION**

Mixing within the biohybrid lung may reduce gas diffusion losses from blood boundary layers near individual MHFs. As discussed in section 1.4.3, active mixing in some devices, such as the PRAL, can increase gas transfer. However, little is known about the consequences of shear stress on ECs under rotational mixing. It is hypothesized that ECs in the biohybrid lung will be able to sustain physiologic rates of shear stress without detaching from the MHFs. In order to achieve endothelialization of MHFs, surface modification was performed to promote cellular attachment on MHF bundles. Surface treatment and endothelialization of MHFs creates a barrier to reduce plasma leakage, but in turn may limit gas diffusion.

This chapter will discuss behavior and functionality of ECs observed within the biohybrid lung prototype. The biohybrid lung provides a system to study EC phenotype and shear response. BAECs were selected so that subsequent biocompatibility studies could be conducted with bovine blood. BAEC phenotype was evaluated with an antibody against p-selectin to quantify cellular expression of this inflammatory marker. Retention of BAECs on MHFs under rotation and expression of a non-inflammatory phenotype for BAECs exposed to shear stress under rotation are demonstrated.

## 4.2 METHODS

### 4.2.1 Endothelialization of MHF bundles

MHF mats were wrapped in three layers around a titanium core and potted to form a bundle (Figure 3-6). MHF bundles were surface modified by RFGD treatment. Following ETO gas sterilization, fibronectin adsorption was applied at 10 µg/mL and bundles were seeded with BAECs at a seeding density of approximately  $15 \times 10^6$  cells. Cast acrylic seeding tubes were developed with a threaded removable cap outfitted with a permeable fluoro-ethylene based polymer membrane (Kimberly-Clark, self-seal plus sterilization pouch) to allow for improved gas transfer (Figure 3-6). Seeding tubes containing BAECs and MHF bundles were placed on a hematology mixer and rotated for 12-24 hours in an incubator at 37°C at 5% CO<sub>2</sub> before being placed in static culture. Near confluent cell growth was achieved within one to two weeks of seeding. Daily media exchange was performed.

### 4.2.2 Rotation of endothelialized MHF bundles

Following static culture, endothelialized modified MHF bundles were transferred with sterile techniques to the biohybrid lung prototype and left in static culture for several hours. Fiber bundle rotation began at 20 RPM and was increased in increments of 30-50 RPM every 2-3 hours until the desired speed was reached. Media was exchanged daily through media ports of the system. Final speeds of rotation ranged from 250 RPM to 1500 RPM. Figure 4-1 illustrates RPM ramping to a speed of 750 RPM over 7 days.

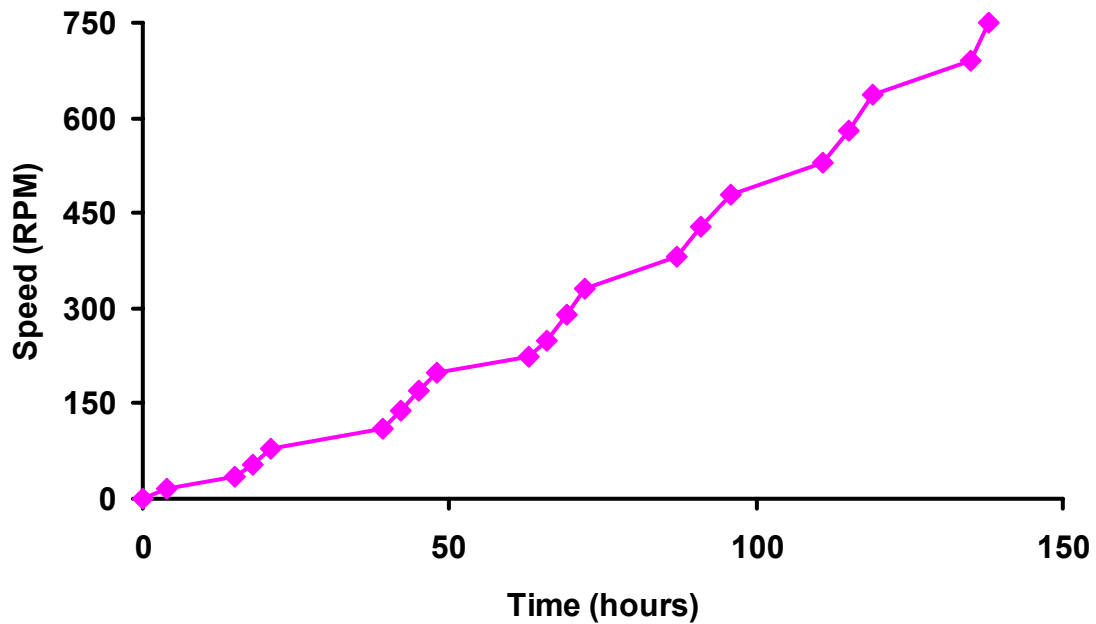


**Figure 4-1** Protocol for acceleration of an endothelialized MHF bundle in the biohybrid lung prototype

After the target speed was achieved in the biohybrid lung prototype and maintained for  $\geq$  12 hrs, speed was decelerated over 2 hours. After deceleration the biohybrid lung prototype was disassembled and the MHF bundle was removed. Half of the bundle was rinsed in PBS two times for two minutes, fixed in 2% paraformaldehyde and rinsed in PBS for two minutes. The MHFs were subsequently labeled with Rhodamine-Phalloidin (Molecular Probes, R415) and DRAQ5 (Biostatus Limited) for confocal imaging of BAEC F-actin filaments and nuclei, respectively. The other half of the bundle was treated with HEPES buffered saline solution, trypsin/EDTA and trypsin neutralizing solution to remove BAECs from the MHFs. BAECs were centrifuged at 220 x g for 5 minutes and resuspended in PBS with calcium and magnesium to produce two 0.5 mL samples. One sample was incubated in the dark for 20 minutes with 5  $\mu$ L of 0.1 mg/100 $\mu$ L of a monoclonal antibody against human P-selectin (Takara Mirus Bio, Madison, WI). The other sample was incubated in the dark for 20 minutes with 100  $\mu$ L of mouse IgG1 isotype control monoclonal antibody (Caltag Laboratories, MG115). Both samples were centrifuged at 220 x g for 5 minutes. Samples were incubated with 20  $\mu$ L of 1.5 mg/mL antimouse IgG(H+L)(cross-adsorbed against bovine, human and equine serum proteins) goat FITC in the dark for 20 minutes (Pierce Biotechnology Inc, Rockford, IL). Samples were then centrifuged at 220 x g for 5

minutes. Samples were resuspended in 2% paraformaldehyde and evaluated with flow cytometry. A Becton-Dickinson FACScan was used to quantify percent of cells positive for binding of the antibody against p-selectin to the isotype control.

## **4.3 RESULTS**

### **4.3.1 Endothelialization of MHF bundles**

BAEC confluence on MHF bundles was achieved within 1-2 weeks. Dynamic culture of 12-24 hours, followed by static culture, was required for cell adherence and growth. Confluence could not be achieved without a static period of culture. The permeable membrane of the seeding tube supported adequate oxygenation during static culture. Without this membrane incorporated into the seeding tube, BAECs died within a few days. BAEC coverage is shown on MHFs prior to rotation (Figure 4-2) using an MTT assay.

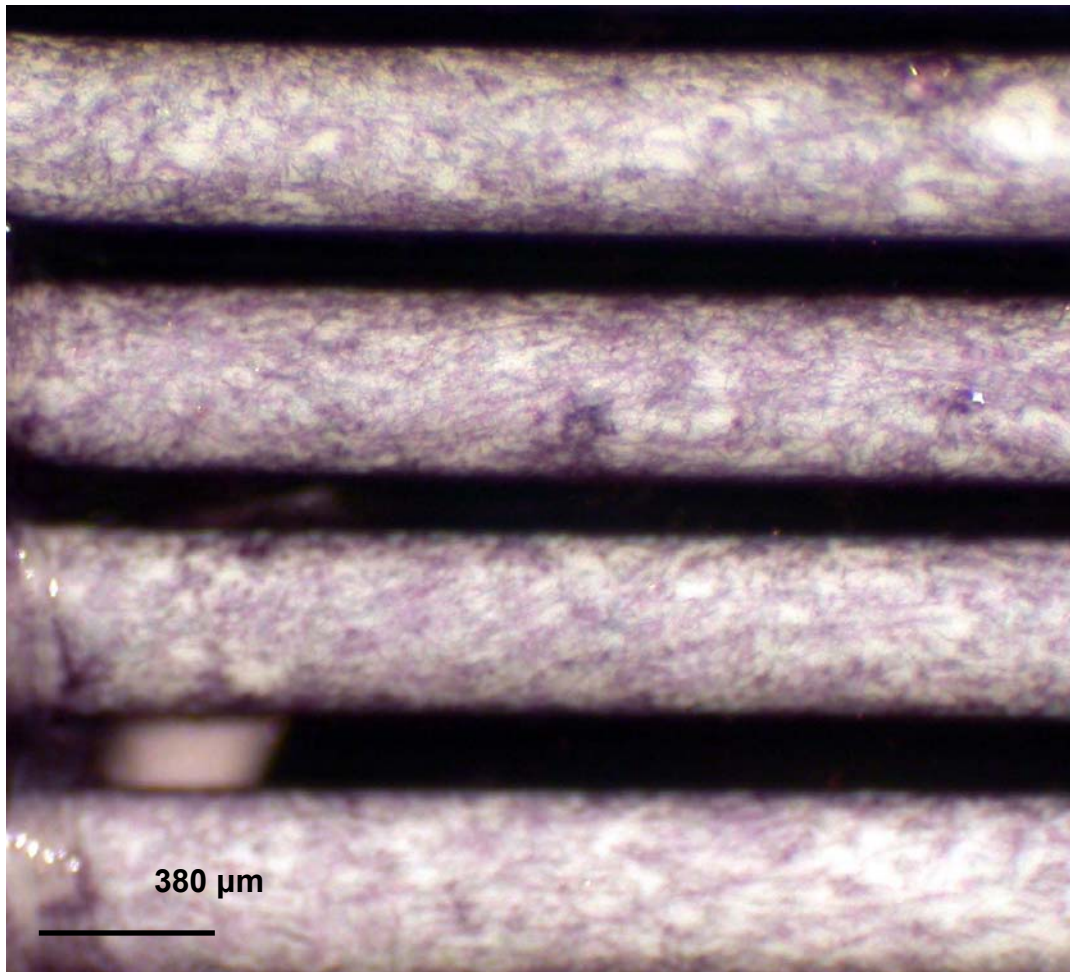
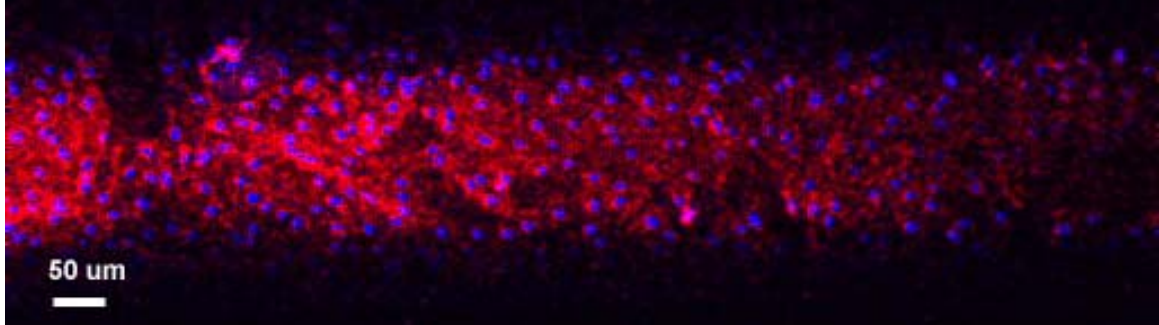


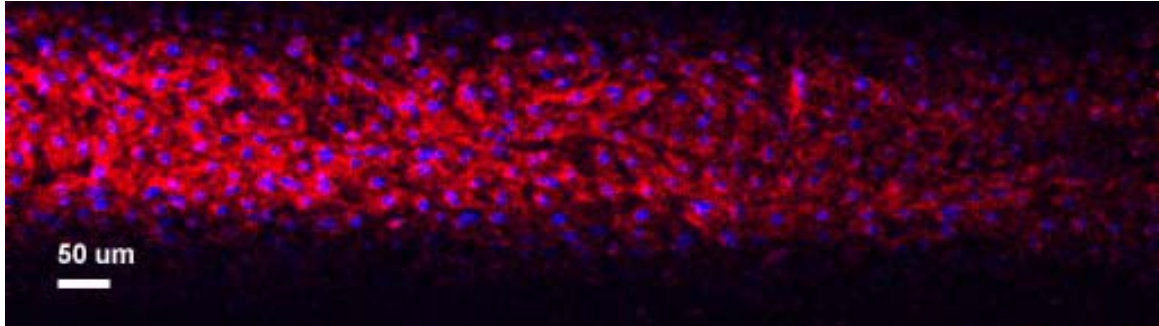
**Figure 4-2** Endothelialized microporous hollow fiber bundle, without rotation  
MHFs stained with MTT

BAEC coverage is also shown with confocal imaging using fluorescent labeling with rhodamine-phalloidin and DRAQ5 (Figure 4-3).

a)



b)



c)

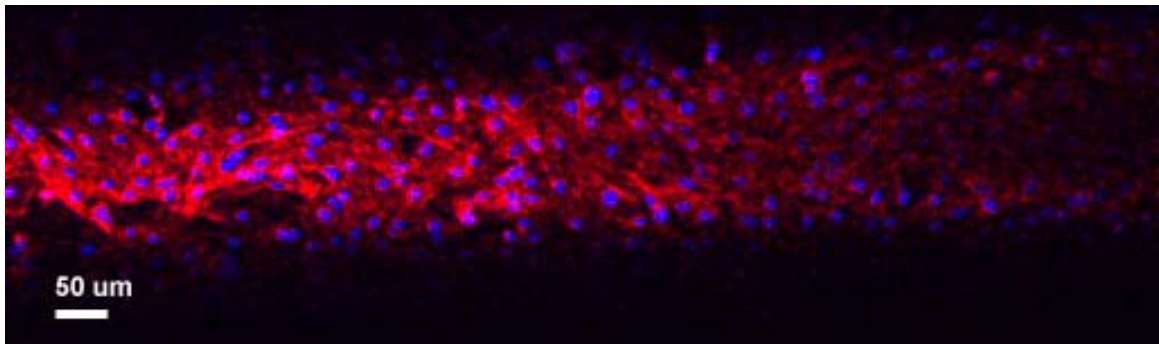


**Figure 4-3** Endothelialized microporous hollow fiber bundle without rotation

MHF are labeled with DRAQ5 and rhodamine-phalloidin: (a) inner fiber layer (b) middle fiber layer (c) outer fiber layer

#### **4.3.2 Rotation of endothelialized MHF bundles**

After near BAEC confluence was achieved in static culture, MHF bundles were placed in the biohybrid lung prototype. Methods were perfected to transfer endothelialized MHF bundles into the prototype under sterile conditions. Rotation began at 20 RPM several hours after assembly, and was increased to 40 RPM 2 hours later. Rotation was then increased in increments of 30-50 RPM approximately every 2 hours, except over-night, until the desired RPM was achieved. This strategy resulted in BAEC adherence at physiologic shear rates tested up to 29.6 dynes/cm<sup>2</sup>,

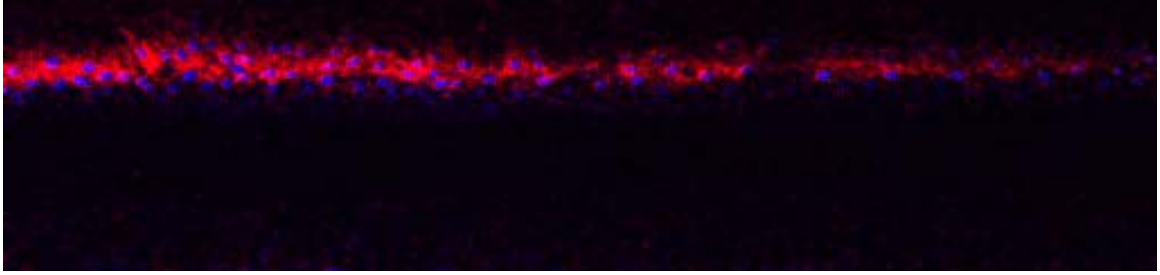
which corresponded to a rotation at 1500 RPM. BAECs frequently aligned perpendicular to fluid flow. More parallel BAEC alignment occurred at 750 RPM than 250 RPM.

The initial seeding strategy involved seeding cells directly into the bioreactor. HUVECs (used before the switch to BAECs for blood biocompatibility studies) were seeded onto MHF modules in the bioreactor and had shear stress continually applied with the intention of growing cells under shear stress. Immediately following cell deposition, the bioreactor was transferred to the incubator, attached to the motor and rotation began at 20 RPM. This approach did not result in cell attachment and retention. Cell viability was shown at day 1 in the bioreactor using Alamar Blue. Day 2 evaluation with Alamar Blue indicated a large reduction in viable cells. By day 3 no response was indicated via Alamar Blue. MTT staining and adsorption supported the conclusion.

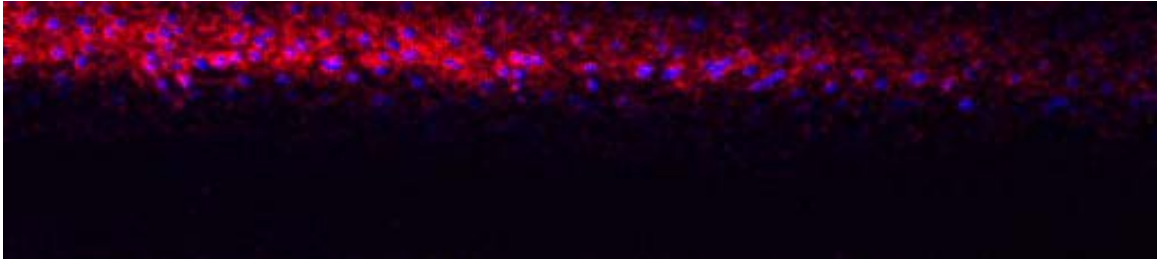
The majority of BAECs from MHF bundles had levels of inflammation slightly elevated from base line, post-rotation. In tissue culture flasks BAECs stimulated with IL-1 $\beta$  or TNF- $\alpha$  expressed 20% and 26% P-selectin, respectively. BAECs taken from MHF bundles routinely expressed 4-8% p-selectin. Isotype controls were set to 2% binding levels to account for non-specific binding of IgG isotype antibodies and cell autofluorescence. However, similar elevated levels of P-selectin expression were found on MHF bundles prior to rotation. There was not a significant difference for p-selectin expression between BAECs from isotype control groups (sample size of 7) and BAECs from rotated MHF bundles (sample size of 7), but there was a significant difference between BAECs from rotated MHF bundles and positive control groups of BAECs stimulated with TNF- $\alpha$  or IL-1 $\beta$  (sample size of 4), when evaluated with one-way ANOVA with post-hoc comparison using Tukey's test for significance of  $p < 0.05$ .

Uniform BAEC coverage was frequently found throughout the top, middle and bottom layers of MHF bundles at 250 RPM (Figure 4-4).

a)



b)



c)

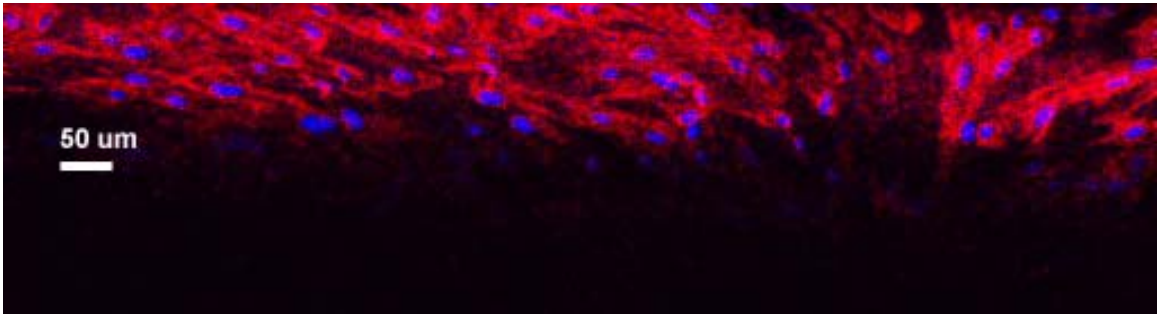


**Figure 4-4** Endothelialized microporous hollow fiber bundles with rotation

MHFs are labeled with DRAQ5 and rhodamine-phalloidin, rotated at 250 RPM: (a) inner fiber layer (b) middle fiber layer (c) outer fiber layer

Preferred BAEC coverage on the outer MHF layer at speeds ranging from 500-1500 RPM is shown below (Figure 4-5). Rhodamine-Phalloidin is shown in red and DRAQ5 is shown in blue. The degree of BAEC coverage did vary across the MHF bundle, but did not appear to be related to speed of bundle rotation.

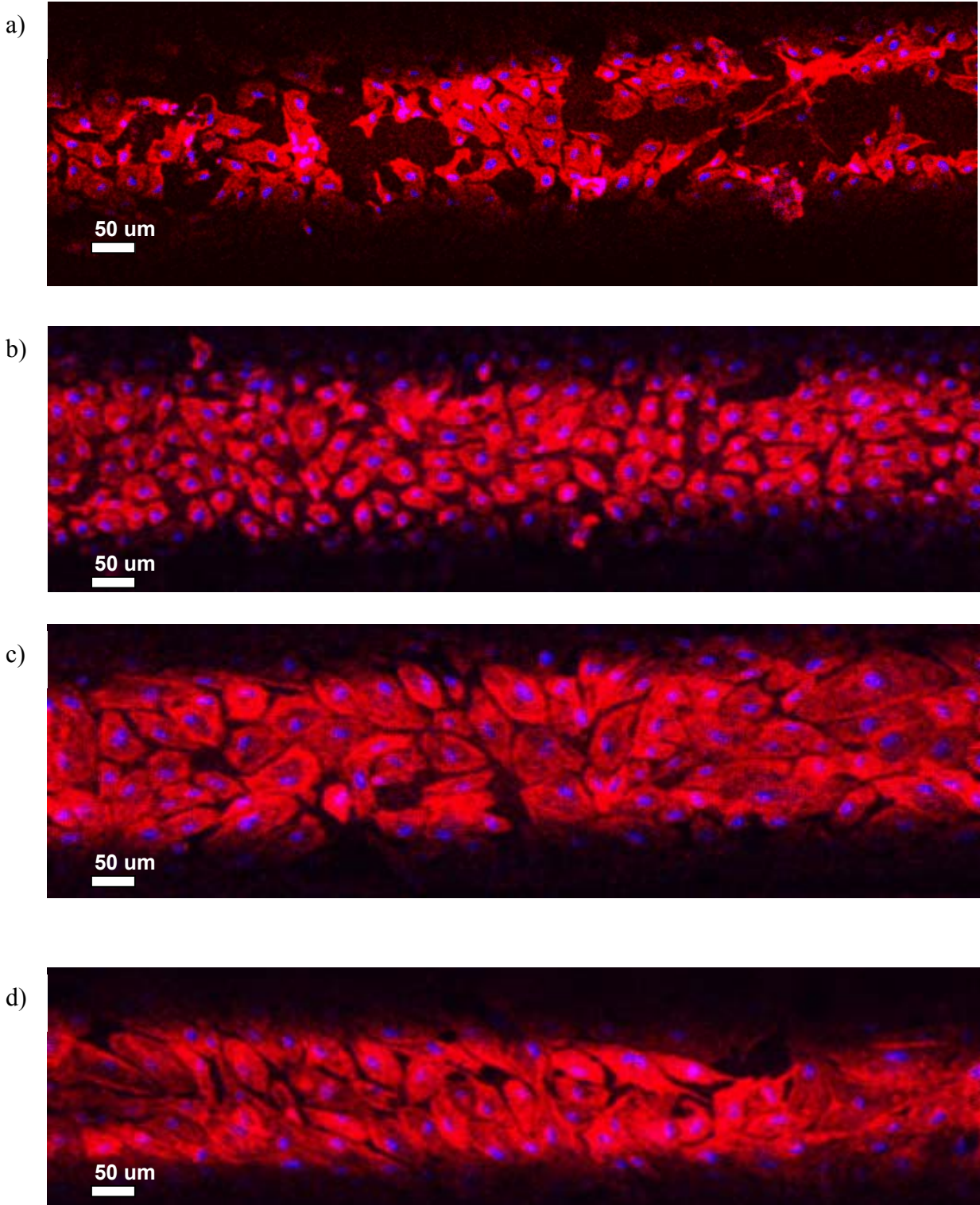


**Figure 4-5** Outer layer of endothelialized microporous hollow fiber bundles, with rotation  
MHFs are labeled with DRAQ5 and rhodamine-phalloidin: (a) 500 RPM (b) 750 RPM (c) 1000 RPM (d) 1500 RPM

## 4.4 DISCUSSION

Near confluent BAEC coverage was obtained on MHF bundles modified by RFGD treatment and fibronectin adsorption, as seen with MHF patches. A key factor toward reaching confluence on the MHF bundles was not only the surface modification, but also the seeding technique. EC coverage could not be achieved when MHFs were seeded under continuous dynamic culture. MHF bundles seeded in seeding tubes and continuously rolled on a hematology mixer and MHF bundles seeded directly in the biohybrid lung prototype under rotation did not show any EC adherence after several days.

The shear stress magnitude that BAECs may tolerate while maintaining a non-inflammatory phenotype was examined in this biohybrid lung prototype. Near confluence was achieved at each shear stress tested, however dead cells consistently appeared in cell culture medium as it was replaced. BAECs appeared to flatten and spread out more at higher rotational speeds. BAECs did not appear to grow under rotational shear stress, as described earlier with observations made during the seeding process. Others have noted a quiescent state of endothelium, or lower proliferation of ECs in the presence of fluid flow exerting high shear stress [102, 107]. This may support the observation that near confluence was maintained while ECs were shed from the MHF bundles.

In the biohybrid lung, cell alignment was observed in some instances, but the degree of alignment varied across the fiber surface. Alignment frequently appeared perpendicular to fluid flow, but sometimes alignment occurred in parallel to fluid flow. More parallel alignment was seen at 750 RPM than 250 RPM. However, fluid flow around MHFs is more complex than fluid flow in parallel plate experiments, and alignment may also be more complex. BAECs were observed to flatten and spread out with increased time and shear stress as well. Samet et al. reported that ECs seeded in a ventricle shaped perfusion chamber did not align with flow after 20 hours of pulsatile flow at  $1.5 \text{ dynes/cm}^2$ , but cell morphology did change [130]. Frame et al. found that flow-induced rearrangement of EC F-actin are dependent on the shape of the surface which ECs are grown on [131]. The shape of the underlying surface has more impact on EC response than the origin of the EC type, and may cause an altered response to flow. Significantly less EC alignment in the direction of laminar flow was observed for ECs grown on curved surfaces than ECs grown on flat surfaces, in the findings from Frame et al. [131].

It has also been observed that laminar shear stress appears to protect ECs from inflammatory responses, by inhibiting tumor necrosis factor, and endothelial proliferation, and by inducing growth arrest proteins [99, 106]. Minimal levels of inflammation occurred with BAECs grown on MHF bundles whether or not these ECs were exposed to shear stress in the biohybrid lung prototype. Inflammation was evaluated using flow cytometric techniques to quantify expression of p-selectin. Ideally, other markers would be evaluated in combination with p-selectin. Antibodies against tissue factor, ICAM-1, e-selectin, VCAM-1 and PECAM-1 were evaluated with flow cytometric techniques for BAECs, but did not show upregulation in the presence of TNF- $\alpha$  or IL-1 $\beta$  in tissue culture flasks. However, some of these antibodies, antibodies against e-selectin, VCAM-1 and PECAM-1, did show expression using immunofluorescence and will be used to further evaluate BAEC phenotype. In addition, BAEC phenotype is evaluated further in subsequent chapters by exposing endothelialized MHFs to bovine blood to determine if thrombotic deposition is reduced in comparison to non-endothelialized MHFs. A low level of inflammation may be tolerable if surface thrombogenicity is reduced related to a non-endothelialized MHF control.

Rotation of endothelialized MHF bundles was evaluated up to 1500 RPM. EC near-confluence was maintained at 1500 RPM. The shear rate for the outer layer of fibers in a MHF bundle rotating at 1500 RPM was calculated to be 29.6 dynes/cm<sup>2</sup>. More work is necessary to determine if mixing improves gas transfer within the biohybrid lung prototype, and to what extent. Fiber spacing and layout, as well as overall device design will most likely have a considerable influence on improving gas transfer. A device such as the Paracorporeal Respiratory Assist Lung (PRAL), developed by Federspiel et al. could be endothelialized and used to optimize gas transfer [64]. The PRAL has been designed to augment gas exchange by increasing fiber bundle rotation at a set fluid flow rate. Blood flow rate can be maintained at low levels and still provide clinically significant CO<sub>2</sub> removal.

## **5.0 THROMBOTIC DEPOSITION AND INFLAMMATION IN THE BIOHYBRID LUNG PROTOTYPE**

### **5.1 INTRODUCTION**

Artificial oxygenation in the intensive care setting is commonly conducted with two modalities, mechanical ventilation and ECMO. This type of support is often required for acute lung injuries, such as ARDS, chronic lung conditions, such as chronic obstructive pulmonary disease (COPD), and other conditions that may compromise pulmonary function [132]. For short-term applications, such as coronary bypass surgery, some concerns regarding blood oxygenator biocompatibility can be reduced with the use of heavy anticoagulation regimens [133]. When artificial oxygenation with blood oxygenators is required for extended periods of times, i.e. days instead of hours, issues concerning biocompatibility come to the forefront. In the case of mechanical ventilation, extended support cannot be maintained without the risk of mechanically induced tissue damage from high airway pressures, as well as biologically-induced tissue damage from hyperoxia [7, 8, 11-13]. In the case of ECMO, high levels of anticoagulation cannot be maintained without the serious risk of bleeding [40, 44].

The biohybrid lung prototype has been developed to address two of the primary blood biocompatibility issues associated with current ECMO systems. The oxygenators in ECMO units commonly use MHF bundles that are subject to plasma infiltration into the open pores of the fiber wall over time. This phenomenon, also referred to as plasma weeping, markedly reduces gas exchange rates [35]. In addition, platelets may adhere and become activated by the artificial surfaces of the oxygenator, particularly the high surface area of the MHFs [134-136]. Adherent platelets can become activated, form aggregates and support the blood coagulation cascade. To reduce the risk of thrombus formation, which can reduce gas transfer rates and lead to thromboembolism, high levels of heparin anticoagulation are required. High levels of

anticoagulation together with the depletion of platelets and coagulation factors due to surface activation lead to increased risk of bleeding and further complications [32].

Endothelialization of the surfaces of MHFs is intended to present a more biocompatible surface, one that is actively anti-thrombotic. Ideally, circulating blood will interact with autologous ECs on MHFs as it would with autologous ECs lining blood vessels. This chapter investigates to what degree this may be true, at least acutely, using *in vitro* experiments with BAECs and bovine blood. Issues of sub-confluent EC coverage, inflammation of ECs and different surface modifications are also addressed.

Blood-surface biocompatibility was evaluated by quantifying thrombotic deposition on MHF patches. These studies were used to compare surface modifications, non-endothelialized MHFs to endothelialized MHFs, and sub-confluent endothelialized MHFs to confluent endothelialized MHFs. From these data the optimal surface modification was selected and applied to MHF bundles for the biohybrid lung prototype. Thrombotic deposition and EC phenotype were then evaluated for MHF bundles rotated at target speeds of 250 RPM or 750 RPM. This chapter explores the effect of endothelialization on biocompatibility in the biohybrid lung prototype.

## 5.2 METHODS

### 5.2.1 Bovine blood collection and preparation

Blood was collected via jugular venipuncture of adult female Holsteins with an 18 gauge, 1½" needle, and mixed into collection bags with 10% acid citrate dextrose (ACD) (10 mL of Solution A ACD to 90 mL of bovine blood). Collection bags were then transferred in coolers back to the University of Pittsburgh McGowan animal facility for re-calcification. Blood was first heparinized with 0.5 U/mL, then subsequently re-calcified with 1M  $\text{CaCl}_2^{2+}$  to a final concentration of 2-3 mM calcium and balanced to a pH of 7.4 with 1M NaOH on an ABL (blood gas analyzer) (700 series, Radiometer Copenhagen). All blood was used within 24 hours of collection and stored at 2-8°C prior to use.

Heparinization levels appropriate for comparison of different surface modified MHF patches were determined by a control experiment with non-modified MHF patches exposed to varying heparin concentrations ranging from 0.5-0.8 U/mL. Heparinized blood was warmed in an incubator at 37°C for 15 minutes prior to use. Patches were placed in 6 mL siliconized Vacutainer® tubes containing no additives (BD Biosciences) with 5 mL of heparinized blood. Tubes were placed on a hematology mixer (Medmark Technologies LLC.) in an incubator at 37°C and 5% CO<sub>2</sub> for 2 hours. Visual inspection of tubes was made at 30, 60, 90 and 120 minutes. Two samples were evaluated at each heparinization level. Heparin concentrations desirable for experiments were determined based on the control, untreated MHFs exhibiting a level of thrombotic deposition that was visually apparent. A concentration of 0.6 U/mL heparin was commonly chosen.

### **5.2.2 MHF patches exposed to bovine blood**

Once an appropriate level of anticoagulation was selected, surface modified, endothelialized MHF patches were evaluated. The heparin concentration was adjusted to the desired level, and blood was warmed for 15 minutes prior to use. 5 mL of blood was added to each Vacutainer® tube. One surface modified, endothelialized patch was placed in each tube and incubated on the hematology mixer for 2 hours. Following incubation, fiber patches were removed and placed in a heparin/saline rinse solution of 10 U/mL heparin. Images of thrombotic deposition were taken with a digital camera (Nikon Coolpix 4500) on a dissecting scope (Nikon SMZ660, 10x eyepiece magnification with a 0.6x objective, yielding 6x magnification). Twenty samples were tested for each surface modification technique at each time point, with the exception of a few samples lost during the experimental process for a variety of reasons. Total sample number was 493. Five independent blood collections were performed to test 100 samples per blood draw.

### 5.2.3 MHF bundles exposed to bovine blood

Non-endothelialized, non-surface modified PMP MHF bundles were setup in the biohybrid lung prototype and spun at the target speed of 250 RPM or 750 RPM to serve as controls. 120 mL of heparinized bovine blood (0.8 U/mL heparin) was passed through the system through the medium perfusion ports, with 50 mL of the blood left in the biohybrid lung prototype for 2 hrs of incubation. For surface modified, endothelialized MHF bundles, heparinized bovine blood (0.8 U/mL heparin) was introduced and incubated for 2 hrs after the target speed was achieved within the biohybrid lung prototype and maintained for  $\geq 12$  hrs.

Following incubation, the biohybrid lung prototype was disassembled and the MHF bundle was removed. Control MHF bundles were cut in half for light microscopy imaging and SEM preparation. Endothelialized MHF bundles were cut in quarters for light microscopy imaging, SEM imaging, confocal imaging and flow cytometric evaluation. Bundle portions designated for light microscopy were rinsed and stored in 10 U/mL heparin/saline rinse solution. Bundle portions designated for SEM imaging were rinsed in 10 U/mL heparin rinse solution, rinsed in PBS, soaked in 2.5% glutaraldehyde at room temperature for one hour, rinsed in PBS three times and stored in PBS. Bundle portions designated for confocal imaging were rinsed in 10 U/mL heparin rinse solution, rinsed in PBS, fixed in 2% paraformaldehyde and rinsed in PBS for two minutes. The MHFs were subsequently labeled with antibodies against PECAM-1 (monoclonal mouse anti-ovine CD31, Serotec) or E-selectin (polyclonal CD62E/Endothelial Leukocyte Adhesion Molecule, Labvision) (dilution of 10  $\mu$ L antibody to 500 mL PBS). Following primary antibody incubation, samples were incubated with secondary antibodies (4  $\mu$ L per 500 mL PBS), Rhodamine-Phalloidin (dilution 2:1000, F-actin stain) (Molecular Probes, R415) and DRAQ5 (dilution 1:1000, nuclear stain) (Biostatus Limited). Alexa fluor 488 goat anti-mouse IgG (H+L) (highly cross adsorbed) and alexa fluor 488 goat anti-rabbit IgG (H+L) (highly cross adsorbed) (Molecular Probes) served as secondary antibodies for primary antibodies against PECAM-1 and E-selectin for samples at 750 RPM, respectively.

The MHF bundle section designated for flow cytometric evaluation of p-selectin expression by adherent ECs was rinsed with 10 U/mL heparin/saline, rinsed in PBS, and treated with HEPES buffered saline solution, trypsin/EDTA and trypsin neutralizing solution to remove BAECs from the MHFs (Cambrex, CC-5034). BAECs were centrifuged at 220 x g for 5 minutes

and resuspended in PBS with calcium and magnesium to make two 0.5 mL samples. One sample was incubated in the dark for 20 minutes with 5  $\mu$ L of 0.1mg/100 $\mu$ L of a monoclonal antibody against human p-selectin, as described in section 4.2.2, and flow cytometry was performed on all samples.

#### **5.2.4 Statistics**

Results are displayed as  $\pm$  standard error of the mean (SE). One-way ANOVA testing was used to compare BAEC coverage and thrombotic deposition. Bonferroni and Tukey's multiple comparison tests were used to compare surface modification data at each time point, and comparison of time points for specific surface modifications ( $p < 0.05$ ). A Student's t-test was used to compare p-selectin expression between different rotations for MHF bundles.

### **5.3 RESULTS**

#### **5.3.1 Bovine blood collection and preparation**

Heparin levels of 0.6 U/mL were commonly chosen for experiments involving MHF patches and bovine blood exposure. Heparin levels of 0.8 U/mL heparin were selected for experiments that exposed rotating MHF bundles to bovine blood. This was based on thrombotic deposition obtained on control, unmodified PMP MHF patches incubated in varying heparin concentrations and rotated for 2 hours on a hematology mixer. Higher levels of thrombotic deposition, therefore lower levels of heparinization, were desirable for experiments involving thrombotic on surface modified, endothelialized MHF patches, since thrombotic deposition was being evaluated via light microscopy only. Lower levels of thrombotic deposition, therefore higher levels of heparinization, were desirable on endothelialized MHF bundles, since SEM and confocal imaging were used to evaluate thrombotic deposition and EC phenotype, respectively. Enough

thrombotic deposition to compare MHF bundles with and without endothelialization was desired, however, it was valuable to view the underlying EC.

### 5.3.2 MHF patches exposed to bovine blood

Both percent of EC coverage and type of surface modification greatly influenced thrombotic deposition on MHF patches. Thrombotic deposition was compared via light microscopy on a non-endothelialized, non-modified MHF patch compared to an endothelialized MHF patch surface modified with RFGD and fibronectin adsorption (Figure 5-1).

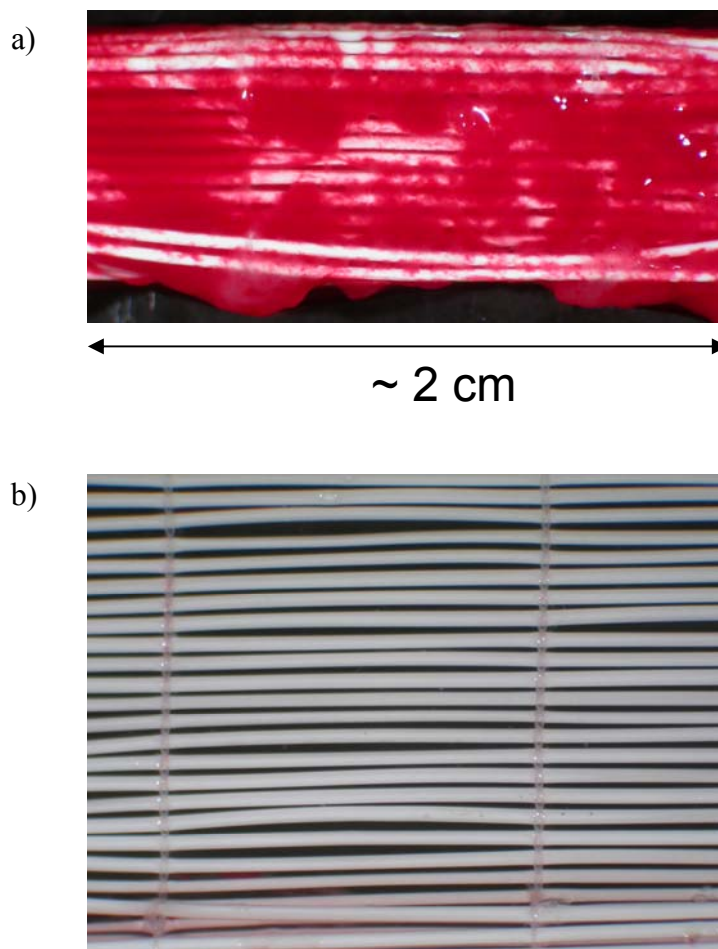


**Figure 5-1** Thrombotic deposition shown on MHF patches with light microscopy  
Thrombotic deposition is shown with light microscopy a) non-modified, endothelialized MHF patch, b) endothelialized MHF patch surface modified with RFGD treatment and fibronectin adsorption

Thrombotic deposition can be compared in electron micrographs on an endothelialized, non-modified MHF patch relative to an endothelialized MHF patch modified with RFGD and fibronectin adsorption (Figure 5-2). Figure 5-2a shows thrombotic deposition in the lower left hand corner, including platelets and erythrocytes. Figure 5-2b shows confluent EC coverage without thrombotic deposition.

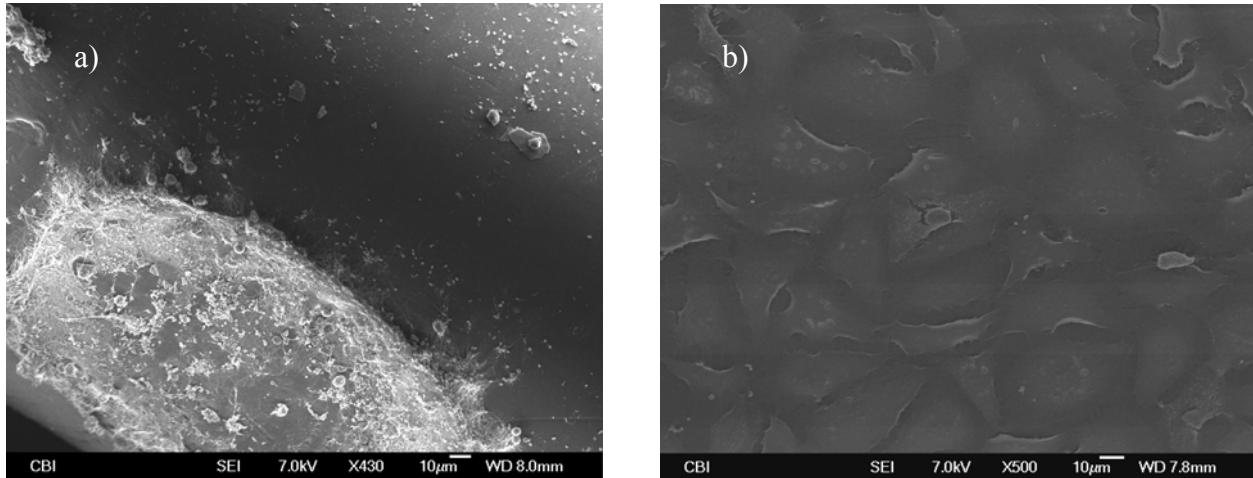


**Figure 5-2** Thrombotic deposition on MHF patches shown by SEM

a) non-modified, non-endothelialized, b) endothelialized MHF patch surface modified with RFGD treatment and fibronectin adsorption

In general, higher BAEC coverage resulted in lower thrombotic deposition (Figure 5-3).

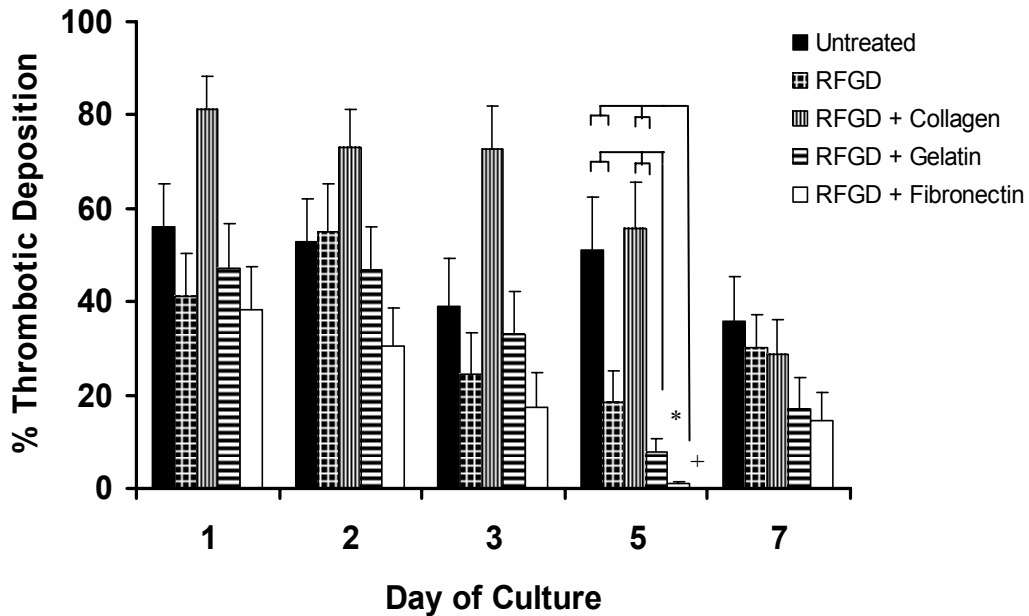


**Figure 5-3** Thrombotic deposition on endothelialized PMP MHF patches

Varying surface modifications are shown for day 1-7 of BAEC growth. By day 5 of BAEC growth, MHFs treated with RFGD and gelatin (indicated by \*) or fibronectin (indicated by +) adsorption had significantly ( $p < 0.05$ ) less thrombotic deposition than untreated MHFs or MHFs treated with RFGD and collagen adsorption. Error bars represent SE.

MHF patches treated with RFGD and collagen adsorption were the exception. By day 7 of BAEC growth, a critical point of endothelialization appeared to be achieved which resulted in non-significant differences in thrombotic deposition levels between surface types. This critical level of endothelialization was different for each surface type. Only MHF patches treated with RFGD and gelatin or fibronectin adsorption reached near confluence by day 7 of BAEC growth.

MHF patches without surface modification had the lowest EC coverage compared to surface modified MHF patches at all days. Thrombotic deposition on non-modified patches did not show a significant difference from other groups until day 5, when thrombotic deposition on non-modified patches was shown to be statistically higher than all groups except RFGD with collagen (Figure 5-3). Untreated MHFs reached a maximum of 10% ( $\pm 1.2\%$  SE) BAEC coverage within the 7 day growth period.

MHF patches treated with RFGD alone had significantly less thrombotic deposition than MHF patches treated with RFGD and collagen by day 1 ( $p < 0.05$ ). By day 5 thrombotic deposition was also significantly less on RFGD modified MHFs than untreated MHFs ( $p < 0.05$ ). MHFs treated with RFGD reached a maximum of 27% ( $\pm 5.8\%$  SE) BAEC coverage within the 7 day growth period.

MHF patches treated with RFGD and collagen adsorption had significantly more thrombotic deposition than RFGD or RFGD and fibronectin treated MHF patches by day 1 ( $p < 0.05$ ). By day 3 of BAEC growth RFGD and collagen treated MHFs had significantly more thrombotic deposition than all groups except untreated MHFs, which was observed again on day 5 of BAEC growth ( $p < 0.05$ ). A significant difference in thrombotic deposition was not shown between untreated and RFGD plus collagen treated MHFs at any of the days. Maximum BAEC coverage for RFGD plus collagen treated fibers reached 36% ( $\pm 4.6\%$  SEM) within 7 days.

MHF patches treated with RFGD and gelatin adsorption performed equivalently to RFGD and fibronectin treated MHF patches in relation to thrombotic deposition by day 3. Both groups had significantly less thrombotic deposition than RFGD and collagen treated MHF patches by day 3 of BAEC growth ( $p < 0.05$ ). At day 5 of BAEC growth both groups had significantly less thrombotic deposition than untreated and RFGD with collagen treated MHF patches ( $p < 0.05$ ). At no time was there a significant difference in thrombotic deposition between MHF patches treated with RFGD and gelatin or RFGD and fibronectin ( $p < 0.05$ ). MHF patches treated with RFGD and gelatin adsorption had a maximum BAEC coverage of 70% ( $\pm 9.8\%$  SE) within the 7 day growth period. MHFs treated with RFGD and fibronectin adsorption reached a maximum of 84% ( $\pm 18\%$  SE) BAEC coverage within the 7 day growth period.

Amongst groups it can be seen in Figure 5-3 on what day of BAEC growth significant differences in thrombotic deposition occurred. Untreated MHFs did not show statistically significant differences in thrombotic deposition at any day. MHFs treated with RFGD alone only showed a significant difference between day 2 and 5 ( $p < 0.05$ ). Thrombotic deposition was not different between days 3, 5 and 7. BAEC coverage in the range of 8% ( $\pm 1.8\%$  SE) to 27% ( $\pm 5.8\%$  SE) did not result in significantly lower levels of thrombotic deposition for RFGD treated fibers. MHFs treated with RFGD and collagen adsorption showed a significant difference only at day 7, indicating lower thrombotic deposition than all other days ( $p < 0.05$ ). MHFs treated with RFGD and gelatin adsorption showed a significant difference at day 5 compared to day 1 and 2

( $p < 0.05$ ). Significant differences in thrombotic deposition did not occur for fibers with 16% ( $\pm 4.6\%$  SE) to 70% ( $\pm 9.8\%$  SE) BAEC coverage for this group. For MHFs modified with RFGD and fibronectin adsorption, there was not a significant difference between days 3, 5 or 7. BAEC coverage ranged from 22% ( $\pm 5.9\%$  SE) to 84% ( $\pm 18\%$  SE).

### **5.3.3 MHF bundles exposed to bovine blood**

MHF bundles were rotated at 250 RPM ( $n=4$ ) or 750 RPM ( $n=3$ ) in bovine blood for 2 hours. Electron micrographs show comparable thrombotic deposition between control untreated and non-endothelialized MHF bundles and MHF bundles that were endothelialized and surface modified at each fiber layer (Figure 5-4 and Figure 5-5). High levels of thrombotic deposition were found on the inner layer of both the control (Figure 5-4 a) and the endothelialized fiber (Figure 5-4d). Moderate deposition is shown on the middle and outer fiber layers of control and endothelialized bundles (Figure 5-4 b,c,e,f). Moderate to heavy levels of thrombotic deposition are shown on the control MHF bundle after rotation at 750 RPM (Figure 5-5 a,b,c). Mild deposition is shown on the inner and outer fiber layers of the endothelialized bundle (Figure 5-5 d,e). Mild to moderate coverage is shown on the middle fiber layer of the endothelialized fiber bundle (Figure 5-5f). Electron micrographs shown are representative of multiple images that were taken.

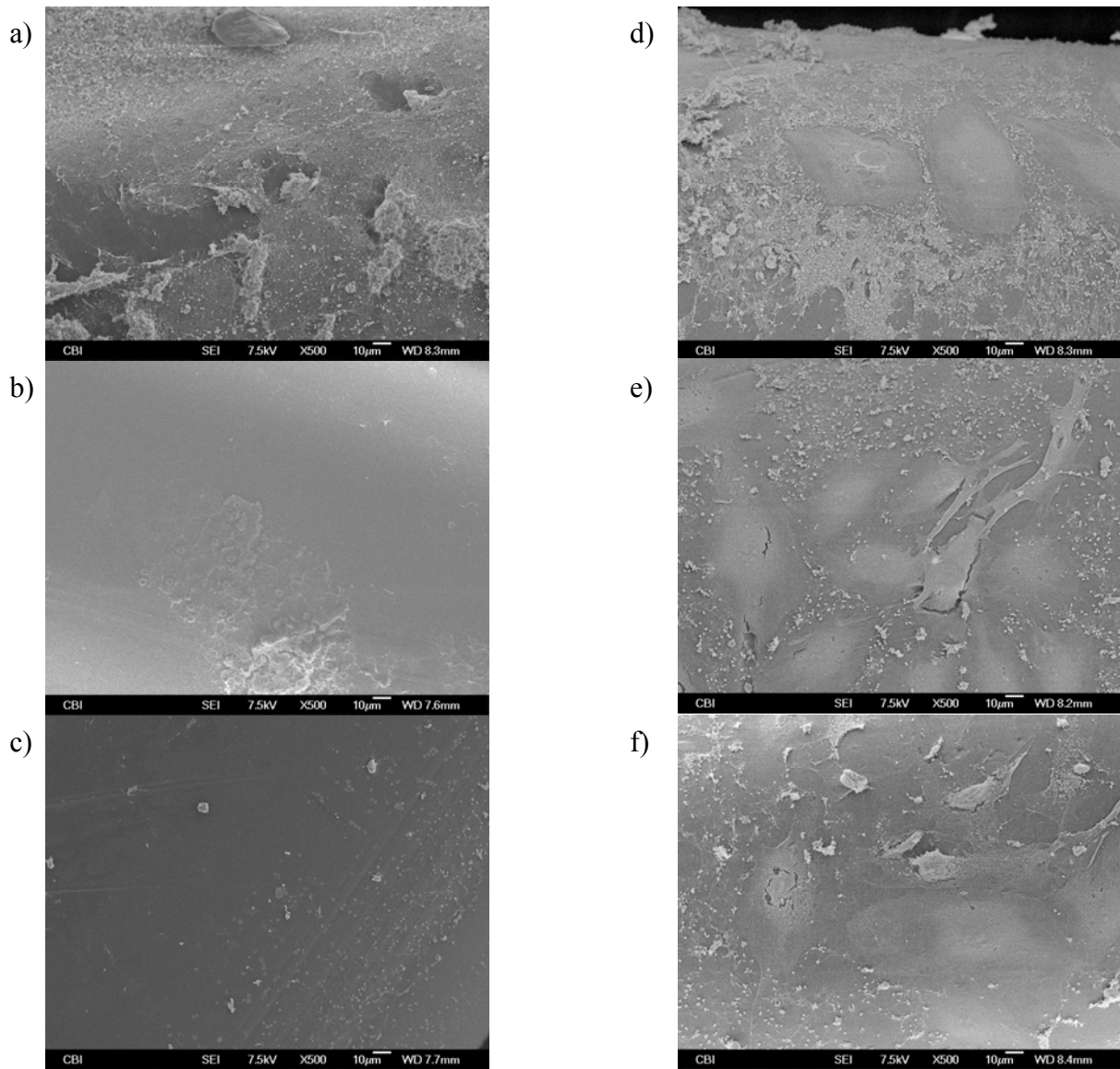


**Figure 5-4** Electron micrographs of MHF bundles following rotation at 250 RPM and bovine blood exposure

a) inner layer: control without surface modification or endothelialization, b) middle layer: control without surface modification or endothelialization, c) outer layer: control without surface modification or endothelialization, d) inner layer: surface modified with Radio Frequency Glow Discharge and fibronectin adsorption, and endothelialization, e) middle layer: surface modified with Radio Frequency Glow Discharge and fibronectin adsorption, and endothelialization, f) outer layer: surface modified with Radio Frequency Glow Discharge and fibronectin adsorption, and endothelialization

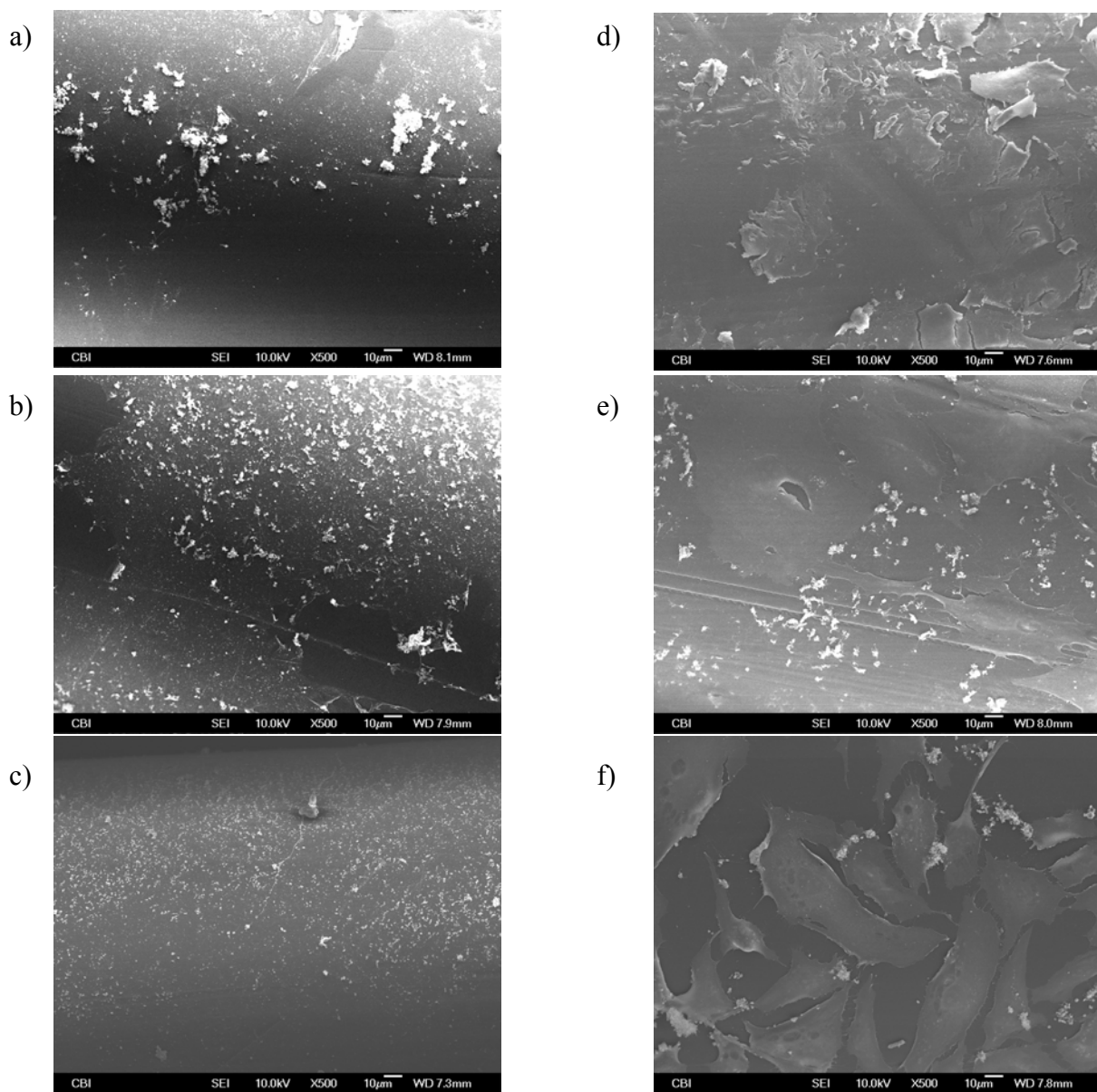


**Figure 5-5** Electron micrographs of MHF bundles following rotation at 750 RPM and bovine blood exposure

a) inner layer: control without surface modification or endothelialization, b) middle layer: control without surface modification or endothelialization, c) outer layer: control without surface modification or endothelialization, d) inner layer: surface modified with Radio Frequency Glow Discharge and fibronectin adsorption, and endothelialization, e) middle layer: surface modified with Radio Frequency Glow Discharge and fibronectin adsorption, and endothelialization, f) outer layer: surface modified with Radio Frequency Glow Discharge and fibronectin adsorption, and endothelialization

P-selectin expression by BAECs as measured by flow cytometry is shown in Figure 5-6. BAECs from tissue culture flasks were stimulated with TNF- $\alpha$  or IL-1 $\beta$ , to serve as positive controls (Figure 5-6). Incubation of cells with the secondary antibody alone is indicated by 2 $^{\circ}$ .

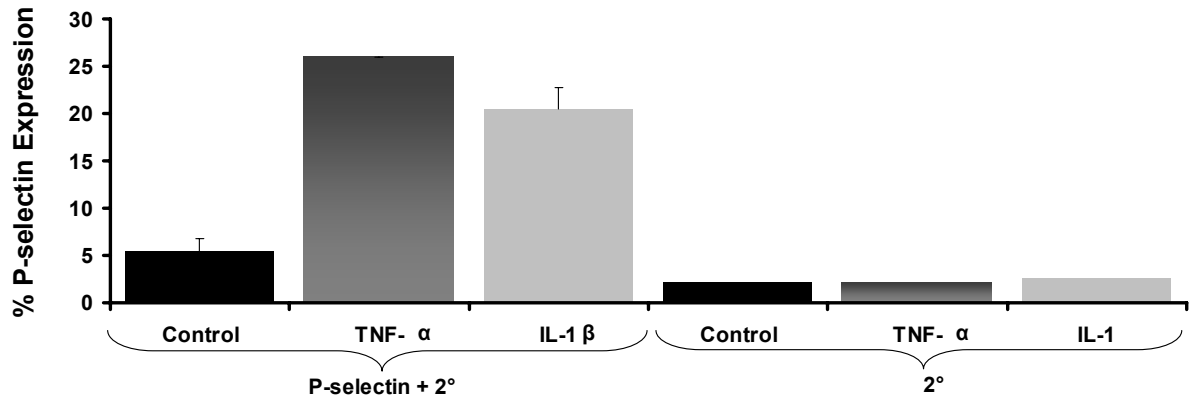


**Figure 5-6** P-selectin expression for control BAECs from tissue culture flasks

BAECs were non-stimulated control, stimulated with TNF- $\alpha$  or stimulated with IL-1 $\beta$ . Incubation with the secondary antibody alone is indicated by 2 $^{\circ}$ .

Average values of p-selectin expression ( $\pm$  SE) by BAECs taken from surface modified MHF bundles rotated in bovine blood for 2 hours are shown (Figure 5-7).

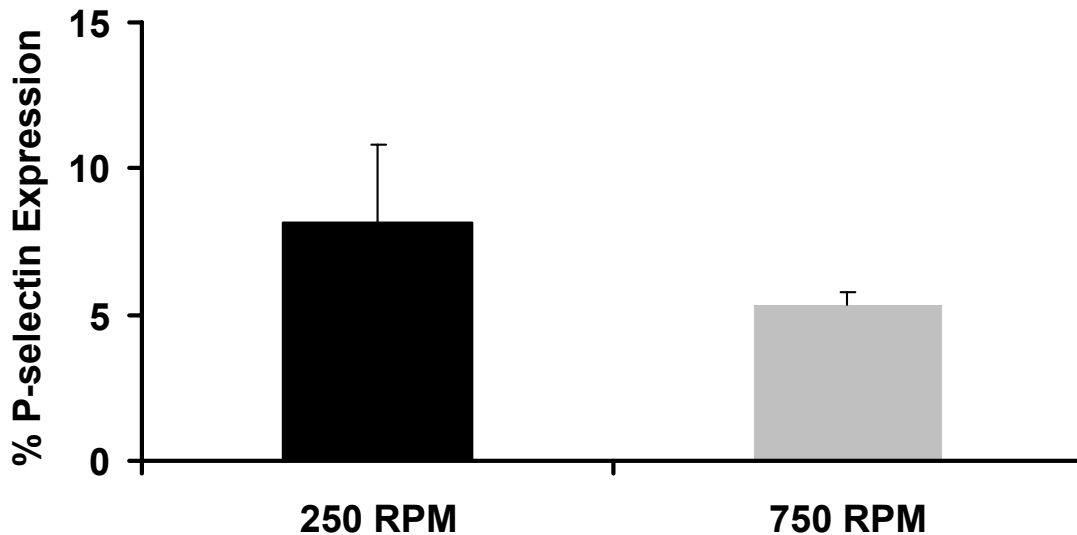


**Figure 5-7** P-selectin expression by BAECs from endothelialized MHF bundles

MHF bundles were surface modified with RFGD treatment and fibronectin adsorption, following rotation

P-selectin expression on MHF bundles spun at 250 RPM and on MHF bundles spun at 750 RPM, were not significantly different, although a trend towards higher expression at lower RPM was seen. Low levels of PECAM-1 expression and moderate levels of e-selectin expression were observed with confocal imaging. Refer to Appendix E for PECAM-1 images.

## 5.4 DISCUSSION

The focus of this chapter has been to explore the effect that endothelialization has on the blood biocompatibility in the biohybrid lung prototype. Data in Figure 5-3 show that both the type of surface modification and the amount of EC coverage directly influence thrombotic deposition on MHF patches. It was shown that with less than 100% BAEC coverage, equivalent levels of thrombotic deposition occurred, ranging from 22-84% BAEC coverage for MHF patches treated with RFGD and fibronectin adsorption in this experiment, for example. At low levels of BAEC

coverage, roughly 10% or less, thrombotic deposition was relatively high for all surface types. This is illustrated in figure 5-3 for days 1 and 2 in particular. Therefore, little difference was seen in comparison of thrombotic deposition for low BAEC coverage. MHFs treated with RFGD and collagen adsorption were the exception to this, resulting in statistically significantly higher thrombotic deposition than some groups, namely RFGD or RFGD with fibronectin adsorption, by day 1 ( $p < 0.05$ ). This finding was not unanticipated, considering that collagen is a pro-thrombotic protein [137]. Similar to the effect seen with low BAEC coverage being associated with high thrombotic deposition, by day 7 of BAEC growth EC coverage was high enough on all surface types that nearly equivalent levels of low thrombotic deposition were observed. An alternative control, such as irradiated ECs or a non-EC cell type, could have also been utilized for thrombotic deposition comparisons on MHFs to further address the question of whether or not the EC phenotype was responsible for decreased thrombotic deposition.

Day 5 of BAEC growth showed the most notable results (Figure 5-3). MHFs surface modified with RFGD and fibronectin, and MHFs surface modified with RFGD and gelatin had significantly less thrombotic deposition than untreated MHFs or MHFs treated with RFGD and collagen. Others have noted the importance of proteins such as fibronectin for cell attachment and retention [72, 81, 82]. Takagi et al. have also studied development of a hybrid artificial lung with endothelialized MHFs. Their experiments evaluated EC adherence and serum properties 24 hrs after seeding and 1 hr of *in vivo* bypass in a rat model. Rotation of endothelialized MHFs and evaluation of thrombotic deposition were not addressed. Instead, key endpoints were change in IL-10 (an inflammation inhibitor) and TNF- $\alpha$  (an inflammation inducer) levels in serum. Serum exposed to endothelialized bypass circuits resulted in an increase of IL-10 levels and decrease in TNF- $\alpha$  levels compared to non-endothelialized circuits. These findings support suppression of inflammation with the addition of ECs to MHFs oxygenation systems [72, 138].

Two major contributors to thrombotic deposition and experimental outcome were the level of heparin in the blood and ease of the blood draw. Heparin levels appropriate for comparison of surface modified MHF patches were determined by a control experiment utilizing non-modified patches exposed to varying heparin concentrations ranging from 0.5-0.8 U/mL. Patches that presented very low thrombotic deposition were not desirable since a good comparison could not be made between surface modifications. Likewise, complete thrombotic deposition occurring early in the incubation process was not desirable. Factors, such as air in the

collection bag and the quality of the blood draw also contributed to the amount of heparin needed. Efforts were made to eliminate as much air as possible from the collection system. Problems associated with the blood draw were more difficult to control. Younger bovines often had smaller jugular veins which frequently caused the needle to slip in and out of the vein with swallowing during collection. Some bovines would startle during the draw, causing the needle to slip out, requiring several repeat sticks. In general, older bovines had larger veins and were less likely to struggle. This resulted in fewer problems with the blood draw, and a need for lower anticoagulation. Control experiments were run with each blood collection to provide suitable comparisons.

The presence of an inflammatory phenotype for ECs was evaluated by increased expression of PECAM-1, p-selectin or e-selectin, known indicators of inflammation [77, 79, 139]. Expression ranged from low to moderate for all MHF bundles tested at 250 RPM and 750 RPM. Significant differences between levels of p-selectin expression were not found between endothelialized MHF bundles rotated at 250 RPM and 750 RPM. EC phenotype was also evaluated indirectly in terms of thrombotic deposition that was apparent in electron micrographs. Endothelialized MHF bundles surface modified with RFGD and fibronectin adsorption did not show an obvious reduction in thrombotic deposition in comparison to untreated MHF bundles without endothelialization at 250 RPM. These bundles did show very similar levels of deposition in comparison to controls of untreated bundles. At 750 RPM endothelialized MHF bundles surface modified with RFGD and fibronectin adsorption did appear to have less thrombotic deposition than control MHF bundles. Therefore, speed of rotation could have an impact on thrombotic deposition on MHFs coupled to type of surface modification and level of endothelialization. These experiments are somewhat limited by the nature of being *in vitro*, acute experiments, however the *in vitro* results displayed an encouraging trend.

## **6.0 HYPEROXIA IN THE BIOHYBRID LUNG PROTOTYPE**

### **6.1 INTRODUCTION**

Oxygenation of the biohybrid lung is described in relation to EC phenotype, limitation of oxygen transfer in the presence of an EC layer, and the relationship between bundle rotation rate and oxygen accumulation in the fluid phase of the device. This chapter seeks to determine if oxygen accumulation will be less in cell culture medium or blood for endothelialized MHF bundles compared to non-endothelialized MHF bundles in the biohybrid lung prototype. It addresses changes in oxygen accumulation associated with rotational speed. And, the EC phenotype is evaluated after exposure to hyperoxia at 95% oxygen.

As discussed in section 1.5.4, ECs exposed to hyperoxia may upregulate p-selectin, e-selectin and/or other indicators of an inflammatory phenotype. If an inflammatory phenotype is expressed, an increase in thrombotic deposition on endothelialized MHFs would be expected, in comparison to endothelialized MHFs exposed to blood under normoxic conditions. It was also noted in section 1.4.1.1, that coating MHFs can result in lower gas transfer in comparison to uncoated MHFs.

### **6.2 METHODS**

#### **6.2.1 Oxygen accumulation in cell culture medium in the biohybrid lung prototype**

12-24 hrs after the target speed was attained in the biohybrid lung prototype, a stream of 95% O<sub>2</sub> and 5% CO<sub>2</sub> was added through the lumen of the fiber bundle for 24 hrs. The gas mixture traveled from a gas tank (1.5 psi) through tygon tubing (approximately 15 feet in length) into the

gas pathway inlet of the biohybrid lung and exited through the gas pathway outlet. An outlet to air was instituted just before the gas inlet site to maintain desired pressure within the biohybrid lung prototype. The exiting gas stream was pulled by vacuum and maintained at a flow of 0.05 lpm (Fathom Technologies, model GR116-1-A-PV). Transducers were used to close the system to atmospheric pressure and maintain the desired flow rate.

Cell culture medium samples (0.4 mL) were taken from the distal medium port at 1, 3, 5, 10, 20, 30, 45 and 60 minutes following introduction of 95% O<sub>2</sub> and 5% CO<sub>2</sub>. Samples were collected in gas tight glass syringes (Hamilton Company, 81320) and immediately run on an ABL 520 or ABL 5 (Radiometer Copenhagen) to obtain pO<sub>2</sub> and pCO<sub>2</sub> levels (n=5 for each speed). Non-endothelialized, non-surface modified polymethylpentene (PMP) MHF bundles were setup in the biohybrid lung prototype and spun at the target speed of 250 RPM or 750 RPM in cell culture medium to serve as controls. pO<sub>2</sub> and pCO<sub>2</sub> levels were obtained at the same time points for controls (n=3 for each speed). If 95% O<sub>2</sub> and 5% CO<sub>2</sub> accumulated on the liquid side, pO<sub>2</sub> values of 722 mmHg would be expected, and pCO<sub>2</sub> values of 38 mmHg would be expected.

## **6.2.2 Bovine blood collection and preparation**

Blood was collected as described in section 5.3.1. Blood was first heparinized with 1 U/mL, then subsequently re-calcified with 1M CaCl<sup>2+</sup> to a final concentration of 2-3 mM calcium and balanced to a pH of 7.4 with 1M NaOH on an ABL (700 series, Radiometer Copenhagen). All blood was used within 24 hours of collection and stored at 2-8°C prior to use. Heparinized blood was warmed in an incubator at 37°C for 15 minutes prior to use.

## **6.2.3 Oxygen accumulation in bovine blood in the biohybrid lung prototype**

The O<sub>2</sub>/CO<sub>2</sub> gas mixture was briefly turned off as 120 mL of re-calcified, heparinized bovine blood (1 U/mL heparin) was introduced into the system. 50 mL of the blood was left in the biohybrid lung prototype for 1 hr of incubation. The gas flow was restored at the beginning of the incubation period and 0.4 mL samples of blood from the distal medium port were taken at 1,

3, 5, 10, 20, 30, 45 and 60 minutes. Samples were run on an ABL 520 or ABL5 (Radiometer Copenhagen) to obtain pO<sub>2</sub> and pCO<sub>2</sub> levels (n=3 for each speed).

Non-endothelialized, non-surface modified PMP MHF bundles were setup in the biohybrid lung prototype and spun at the target speed of 250 RPM or 750 RPM to serve as controls. 120 mL of re-calcified, heparinized bovine blood (1 U/mL heparin) was passed through the system, with 50 mL of the blood left in the biohybrid lung prototype for 1 hr of incubation. The blood was sampled with the above protocol to collect pO<sub>2</sub> and pCO<sub>2</sub> levels (n=3 for each speed).

#### **6.2.4 Evaluation of endothelialized MHF bundles following hyperoxia and bovine blood exposure**

Following incubation, the biohybrid lung prototype was disassembled and the MHF bundle was removed. Control MHF bundles were cut in half for light microscopy imaging and SEM preparation. Endothelialized MHF bundles were cut in quarters for light microscopy imaging, SEM imaging, confocal imaging and flow cytometry evaluation. Bundle portions designated for light microscopy were rinsed and stored in 10 U/mL heparin/saline rinse solution. Bundle portions designated for SEM imaging were rinsed in 10 U/mL heparin rinse solution, rinsed in PBS, soaked in 2.5% glutaraldehyde at room temperature for 1 hour, rinsed in PBS 3 times and stored in PBS. Bundle portions designated for confocal imaging were rinsed in 10 U/mL heparin rinse solution, rinsed in PBS, fixed in 2% paraformaldehyde and rinsed in PBS for two minutes. The MHFs were subsequently labeled with antibodies against PECAM-1 (mouse anti-ovine CD31, Serotec, MCA1097) or E-selectin (CD62E/Endothelial Leukocyte Adhesion Molecule, Labvision, RB-070-P) (dilution of 10 µL antibody to 500 mL PBS) as described in section 5.2.3. The bundle section designated for flow cytometry was prepared as described in section 4.2.2 for evaluation of p-selectin expression.

### **6.2.5 Statistics**

Results are displayed as  $\pm$  standard error of the mean (SE). One-way ANOVA testing was used to compare pO<sub>2</sub> levels. Tukey's multiple comparison and LSD comparison tests were used to compare data from different test conditions (speed of rotation or with or without BAEC) at each time point ( $p < 0.05$ ). The LSD comparison is a simple comparison test based on an overall F-test, with the disadvantage that it does not adequately control experimentwise error rates. Tukey's multiple comparison test is considered overly conservative in most cases, it is based on the studentized range statistic, and controls well for experimentwise error rate [140]. A t-test was used to compare p-selectin expression between different rotations for MHF bundles.

## **6.3 RESULTS**

### **6.3.1 Oxygen accumulation in cell culture medium in the biohybrid lung prototype**

A plot of oxygen accumulation data in cell culture medium for MHF bundles with or without BAECs rotated at 250 RPM and 750 RPM is shown below (Figure 6-1).

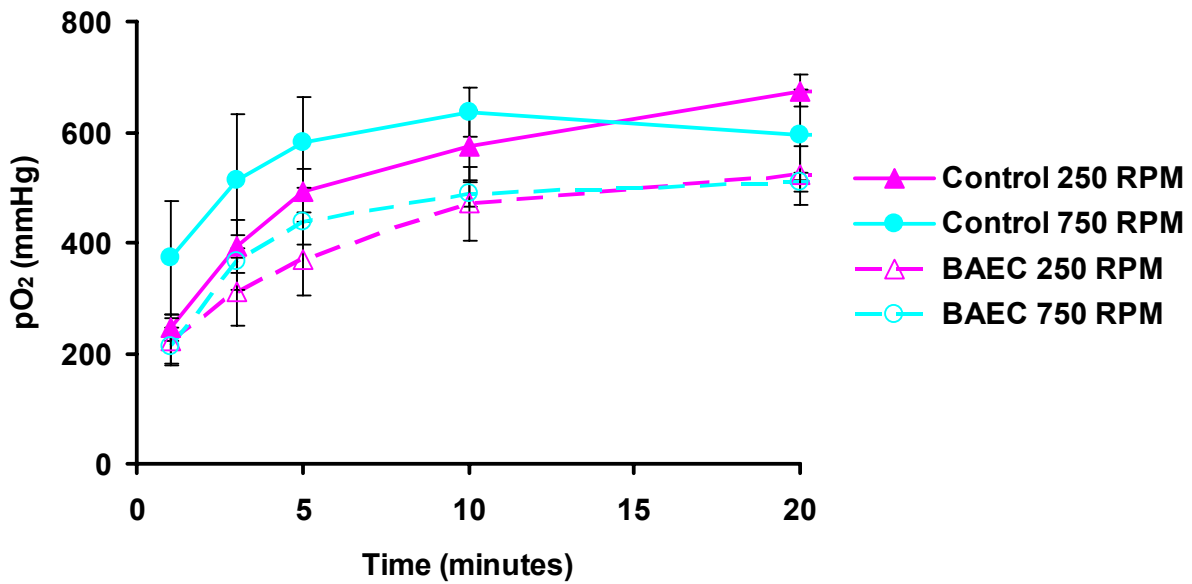


**Figure 6-1** Oxygen accumulation in the biohybrid lung prototype in cell culture medium

Oxygen levels appeared to reach a steady equilibrium state by 20 minutes, therefore data past 20 minutes are excluded. MHF bundles rotated at 750 RPM have a faster accumulation in oxygen than MHF bundles rotated at 250 RPM. However, significant differences between groups at each specific time were not found. Non-endothelialized, non-surface modified MHF bundles trended toward a faster accumulation in oxygen than surface modified, endothelialized MHF bundles, but the data were not significantly different at specific time points.

If a less stringent test for significance is applied, the LSD comparison test, some statistical correlations can be made between groups. At  $t = 1$  minute there is a significant difference between non-endothelialized, non-surface modified MHF bundles and endothelialized, surface modified MHF bundles at 750 RPM ( $p < 0.05$ ). At  $t = 20$  minutes the same is true for MHF bundles rotated at 250 RPM ( $p < 0.05$ ).

Significant differences in  $\text{CO}_2$  accumulation in cell culture medium between endothelialized and non-endothelialized MHF bundles, or bundles rotated at 250 RPM or 750 RPM were not found either (Figure 6-2).

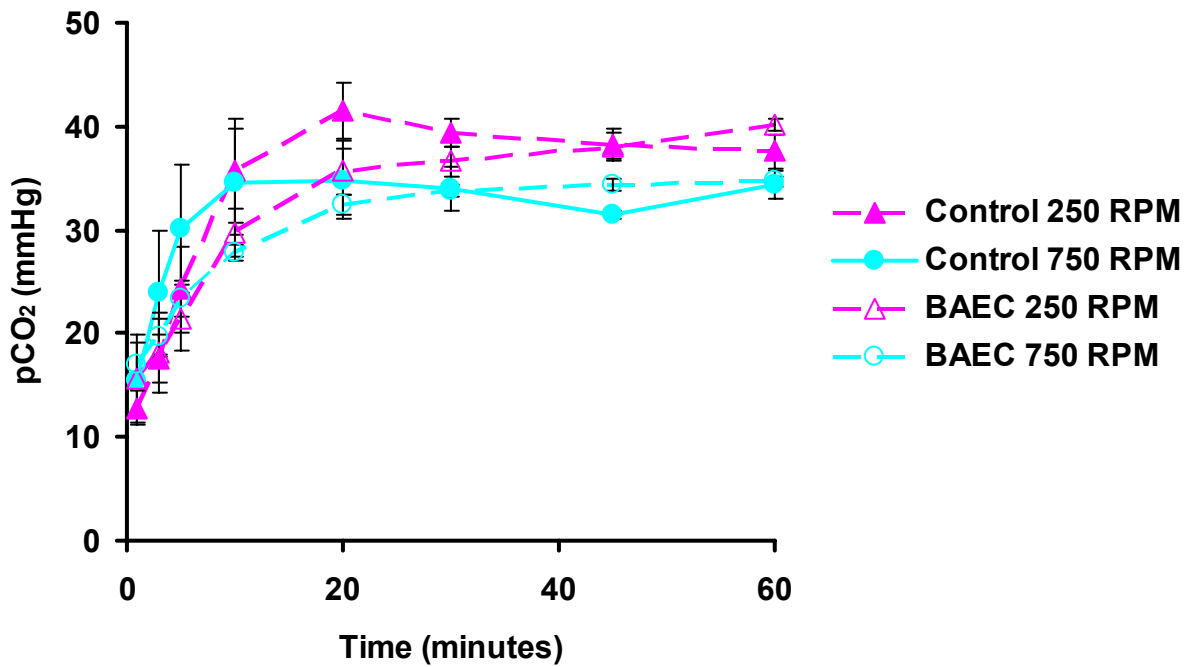


**Figure 6-2** Carbon dioxide accumulation in the biohybrid lung prototype in cell culture medium (95% O<sub>2</sub> & 5% CO<sub>2</sub> mixture, ± SE)

### 6.3.2 Oxygen accumulation in bovine blood in the biohybrid lung prototype

Oxygen accumulation data in blood for MHF bundles with or without BAECs rotated at 250 RPM and 750 RPM are plotted below (Figure 6-3).

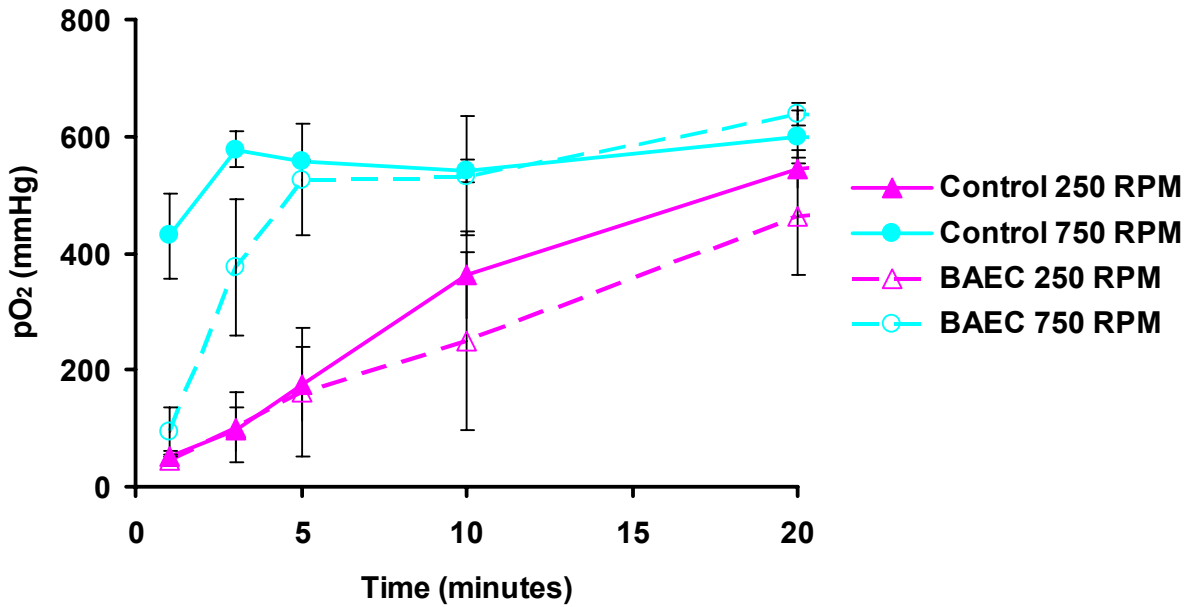


**Figure 6-3** Oxygen accumulation in the biohybrid lung prototype in blood

As in cell culture medium, MHF bundles rotated at 750 RPM result in higher levels of  $pO_2$  for each time point than MHF bundles rotated at 250 RPM. Significant differences are seen between non-endothelialized, non-surface modified MHF bundles at time points of 1 and 3 minutes ( $p < 0.05$ ). At 750 RPM non-endothelialized, non-surface modified MHF bundles have higher  $pO_2$  values than endothelialized, surface modified MHF bundles. A significant difference was observed at the first time point, 1 minute ( $p < 0.05$ ). At 250 RPM  $pO_2$  values coincide for the first 3 time points and are not significantly different at the remaining time points.

Again, if a less rigorous test of significance is applied, the LSD comparison test, more statistical differences can be found between groups. At  $t = 3, 5$  and  $10$  minutes, there is a significant difference between endothelialized, surface modified MHF bundles rotated at 250 RPM and 750 RPM ( $p < 0.05$ ). At  $t = 5$  minutes there is a statistically significant difference between non-endothelialized, non-surface modified MHF bundles rotated at 250 RPM or 750 RPM ( $p < 0.05$ ).

No statistically significant differences were found between rotational speed, or endothelialized versus non-endothelialized MHF bundles for  $CO_2$  accumulation evaluated in cell culture medium (Figure 6-4).

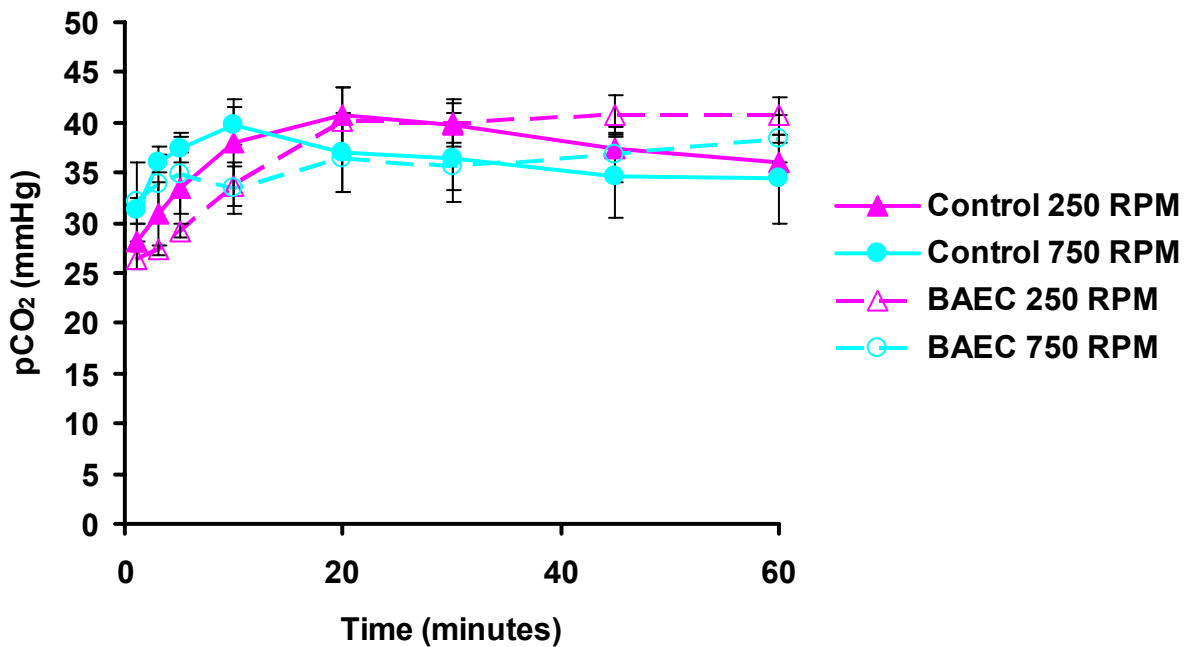


**Figure 6-4** Carbon dioxide accumulation in the biohybrid lung prototype in blood (95% O<sub>2</sub> & 5% CO<sub>2</sub> mixture, ± SE)

### 6.3.3 Evaluation of endothelialized MHF bundles following hyperoxia and bovine blood exposure

Electron micrographs of thrombotic deposition on non-endothelialized/non-surface modified MHF bundles exposed to hyperoxia (panels a,b,c), endothelialized/surface modified MHF bundles (panels d,e,f), and endothelialized/surface modified MHF bundles (panels g,h,i) exposed to hyperoxia rotated at 250 RPM or 750 RPM are shown (Figure 6-5 and Figure 6-6, respectively to speeds). On the inner fiber layer (figure 6-5 a,d,g and figure 6-6 a,d,g) thrombotic deposition is comparable between the three groups. On the middle fiber layer (Figure 6-5 b,e,h and Figure 6-6 b,e,h) and outer fiber layer (panel c, f and i) endothelialized MHFs show equivalent or less thrombotic deposition than non-endothelialized MHFs. Images are representative of the sample population.

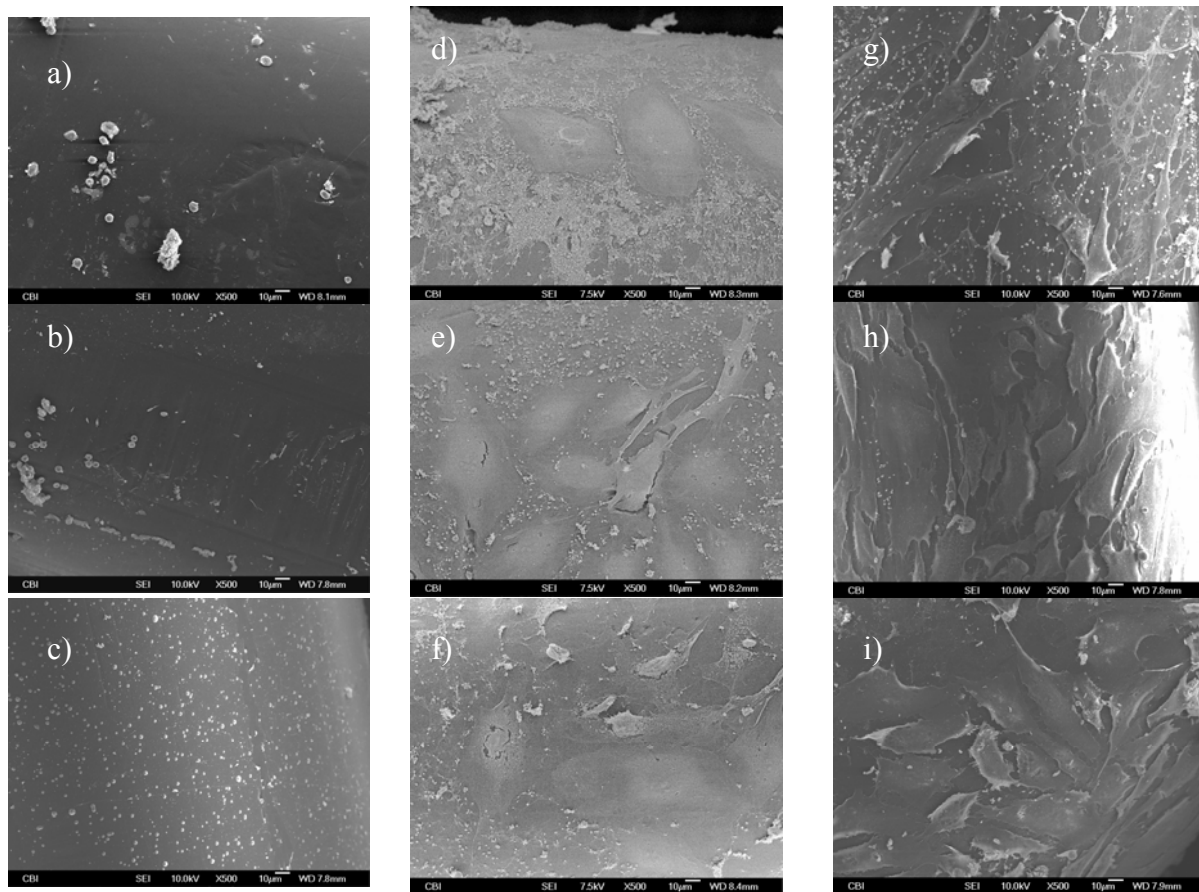


**Figure 6-5** Electron micrographs of MHF modules rotated at 250 RPM exposed to bovine blood and hyperoxia Control without surface modification or endothelialization, with 95% O<sub>2</sub> & 5% CO<sub>2</sub>: a) inner fiber layer, b) middle fiber layer, c) outer fiber layer  
 Surface modified with RFGD treatment and fibronectin adsorption, and endothelialization, without oxygenation: d) inner fiber layer, e) middle fiber layer, f) outer fiber layer  
 Surface modified with RFGD treatment and fibronectin adsorption, and endothelialization, with 95% O<sub>2</sub> & 5% CO<sub>2</sub>: g) inner fiber layer, h) middle fiber layer, i) outer fiber layer

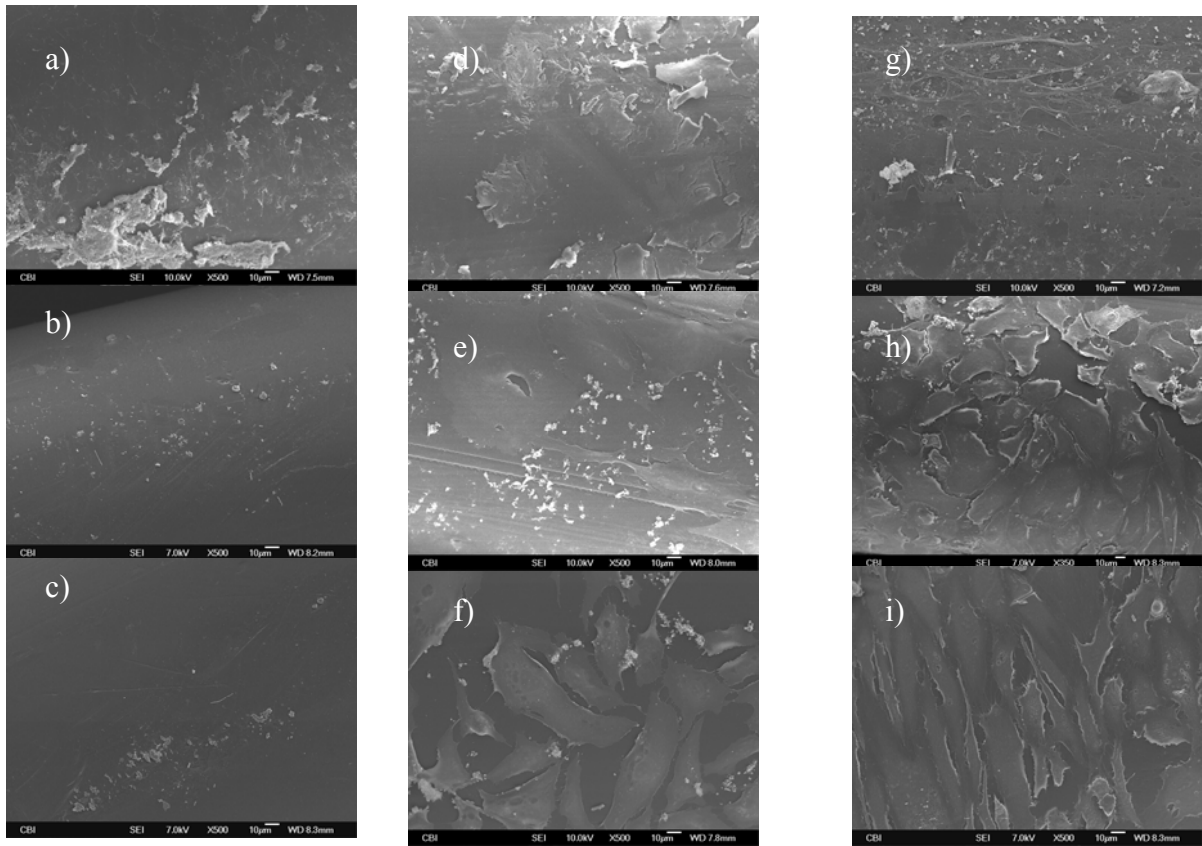


**Figure 6-6** Electron micrographs of MHF modules rotated at 750 RPM exposed to bovine blood and hyperoxia Control without surface modification or endothelialization, with 95% O<sub>2</sub> & 5% CO<sub>2</sub>: a) inner fiber layer, b) middle fiber layer, c) outer fiber layer

Surface modified with RFGD treatment and fibronectin adsorption, and endothelialization, without oxygenation: d) inner fiber layer, e) middle fiber layer, f) outer fiber layer

Surface modified with RFGD treatment and fibronectin adsorption, and endothelialization, with 95% O<sub>2</sub> & 5% CO<sub>2</sub>: g) inner fiber layer, h) middle fiber layer, i) outer fiber layer

Positive and negative controls for e-selectin expression are shown on endothelialized, surface modified MHF patches (Figure 6-7). The positive control was stimulated with IL-1 $\beta$ , an inflammatory cytokine, for 5 hours prior to labeling. The nucleus is shown in blue and e-selectin is shown in green.

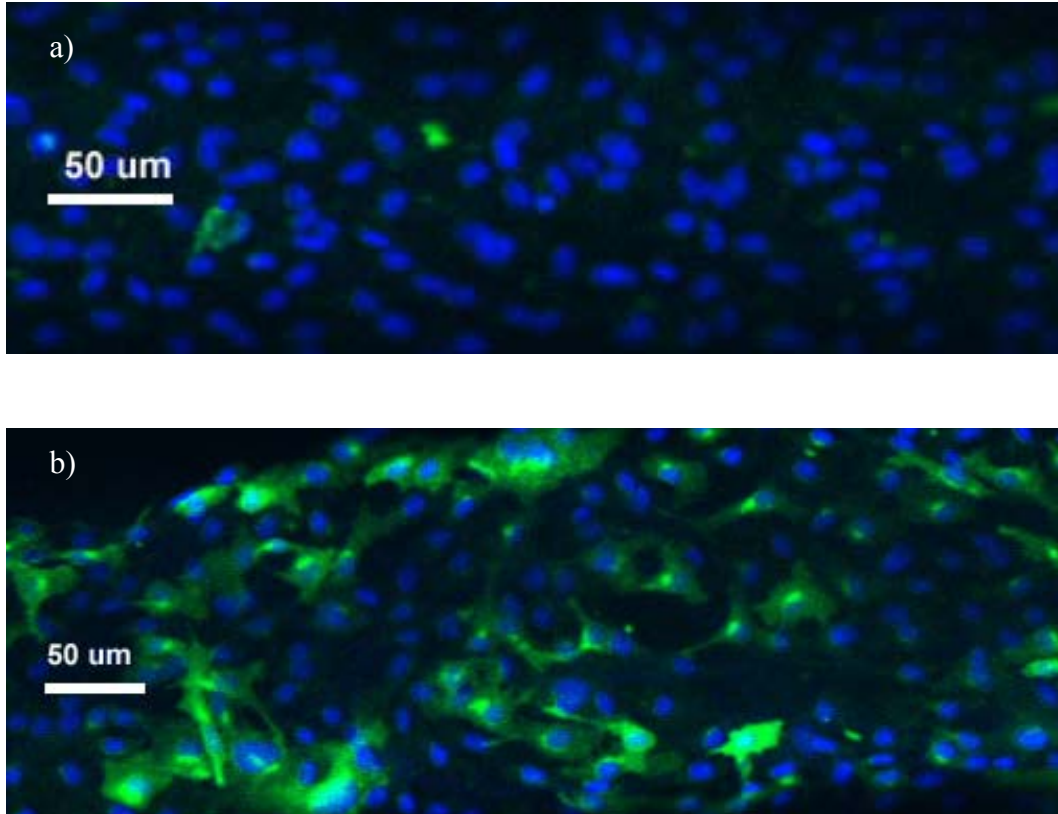
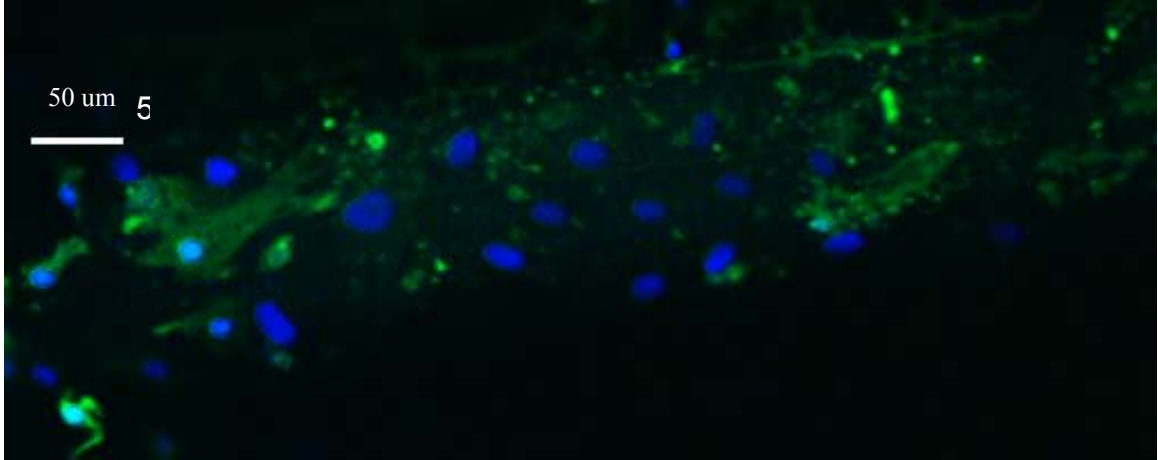


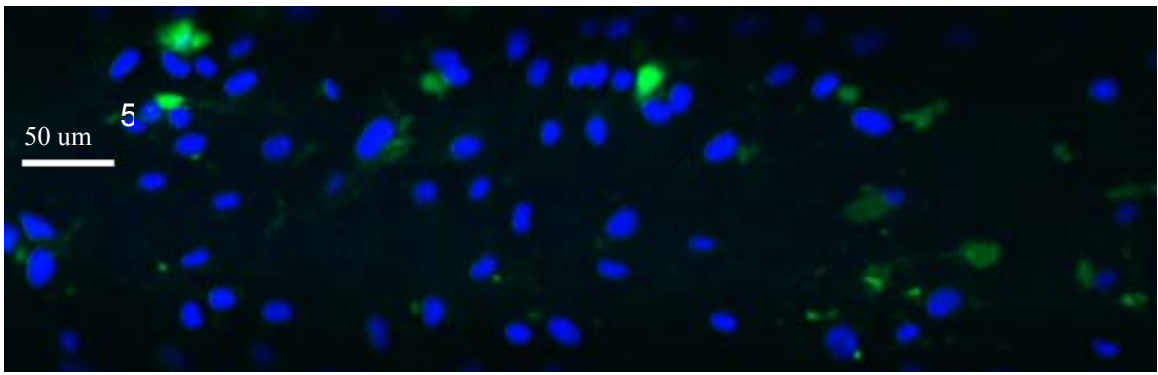
**Figure 6-7** Confocal images of positive and negative immunofluorescent controls for e-selectin MHF patches surface modified with Radio Frequency Glow Discharge and fibronectin adsorption, and endothelialized, E-selectin = green, Rhodamine-Phalloidin = red, DRAQ5 = blue: a) control, b) IL-1 $\beta$  stimulation for 5 hrs

Inner, middle and outer fiber layer of an endothelialized, surface-modified MHF bundle exposed to hyperoxia (95% O<sub>2</sub> & 5% CO<sub>2</sub>) and bovine blood, rotated at 250 RPM (Figure 6-8).

a)



b)



c)

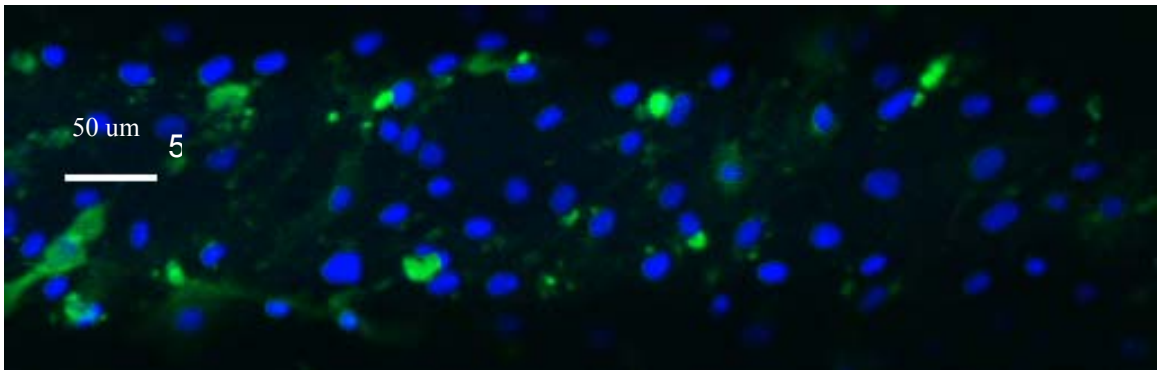


**Figure 6-8** E-selectin expression by ECs on the biohybrid lung prototype MHFs under hyperoxia at 250 RPM

Confocal images of endothelialized MHF bundles surface modified with RFGD treatment and fibronectin adsorption, following rotation at 250 RPM, bovine blood exposure, and 95% O<sub>2</sub> & 5% CO<sub>2</sub> for 24 hrs E-selectin = green, Rhodamine-Phalloidin = red, DRAQ5 = blue: a) inner layer, b) middle layer, c) outer layer

Inner, middle and outer fiber layer of an endothelialized, surface-modified MHF bundle exposed to hyperoxia (95% O<sub>2</sub> & 5% CO<sub>2</sub>) and bovine blood, rotated at 750 RPM are shown (Figure 6-9).

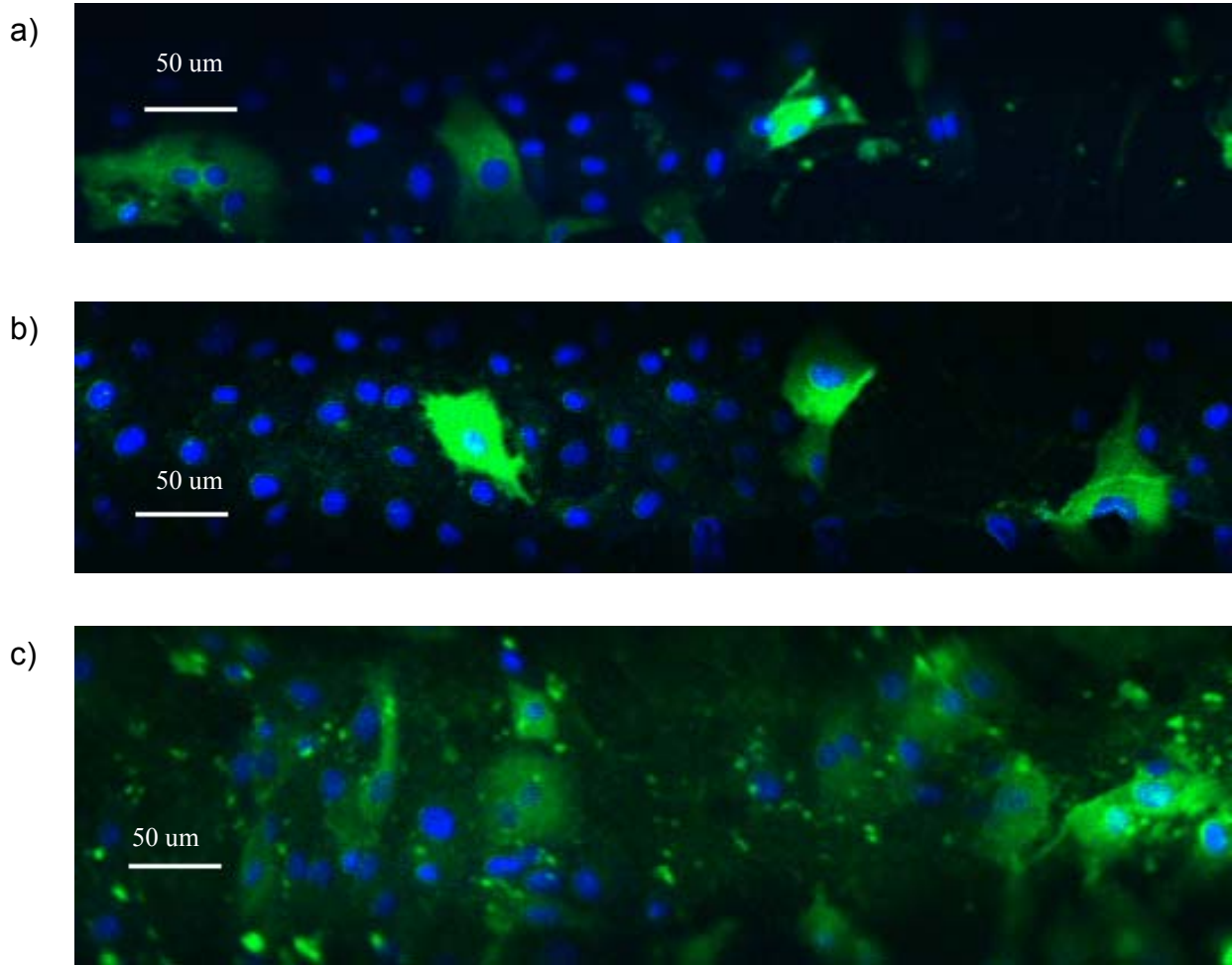


**Figure 6-9** E- selectin expression in the biohybrid lung prototype under hyperoxia at 750 RPM

Confocal images of endothelialized MHF bundles surface modified with RFGD treatment and fibronectin adsorption, following rotation at 750 RPM, bovine blood exposure, and 95% O<sub>2</sub> & 5% CO<sub>2</sub> for 24 hrs E-selectin = green, Rhodamine-Phalloidin = red, DRAQ5 = blue: a) inner layer, b) middle layer, c) outer layer

It should be noted that blood products (i.e. platelets, leukocytes, and erythrocytes) fluoresce green as well. Of particular note is the shape of the green area and location of the blue nucleus to identify BAECs expressing e-selectin. Low to moderate levels of e-selectin expression are shown on the inner and middle fiber layers at both rotational speeds. Moderate levels of e-selectin expression are shown on the outer layer of the MHF bundle rotated at 250 RPM, and high levels of e-selectin expression are shown on the outer layer of the MHF bundle rotated at 750 RPM.

PECAM-1 expression was not observed or observed at very low levels for MHF bundles rotated at both speeds (data not shown).

P-selectin expression of BAECs taken from MHFs rotated at 250 RPM or 750 RPM are shown below (Figure 6-10). Both groups show very low levels of p-selectin expression, as evaluated with flow cytometry.

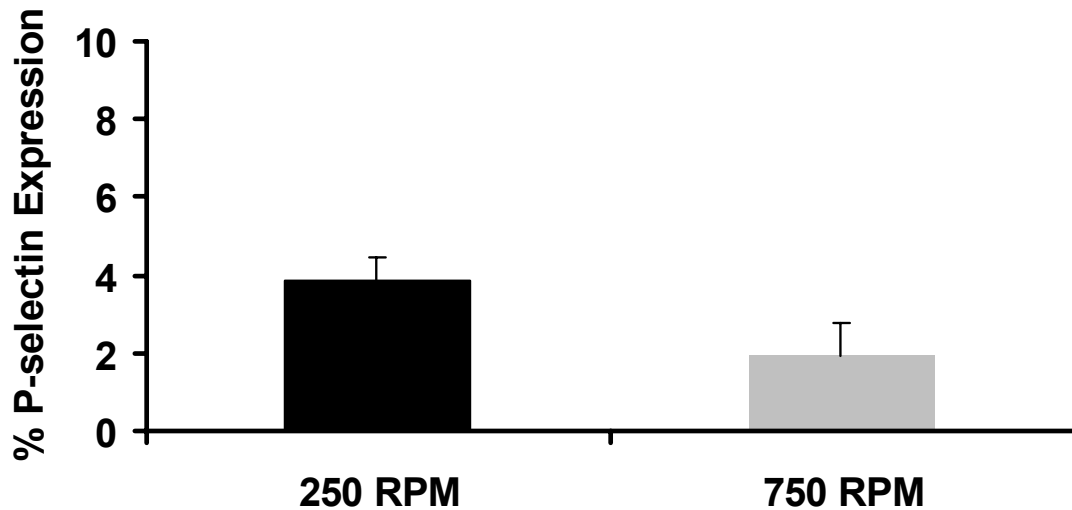


**Figure 6-10** P-selectin expression for BAECs from endothelialized MHF bundles  
MHF bundles were surface modified with RFGD treatment and fibronectin adsorption, and rotated in bovine blood and 95% O<sub>2</sub> + 5% CO<sub>2</sub>: 250 RPM, 750 RPM (+SE)

## 6.4 DISCUSSION

### 6.4.1 Oxygen accumulation in the biohybrid lung prototype

It was anticipated that gas transfer might be somewhat diminished by the presence of an EC layer, as is the case with coatings such as siloxane [39, 67, 141]. To combat lower oxygen delivery rates, sub-confluent endothelialization could be applied, active mixing within the device could be increased, more fibers could be added or a combination of these approaches could be implemented. However, results of oxygen accumulation in cell culture medium and blood did not

show a significant decrease as measured by pO<sub>2</sub> levels between MHF bundles with or without BAECs. It should be noted that BAECs are quite permeable [3, 142], even though they share a similar thickness to synthetic coatings, such as siloxane. BAECs have been measured at 0.2 to 0.4 μm thick [3]. Siloxane coatings on MHFs are typically 0.2 to 2 μm thick [67].

It was also projected that increased speeds of rotation would result in higher levels of pO<sub>2</sub>, or better oxygen delivery into cell culture medium or blood. In bovine blood this trend was apparent, and even statistically significant at initial sampling time points, and may be due to the oxygen carrying capacity of blood related to erythrocytes and hemoglobin. Perhaps with a larger gap between the low and high speeds studied, the experimental evidence would be stronger. The experimental sample size was on the low side (n =3 to n=5) due to the complexity of these experiments. Another factor that could increase pO<sub>2</sub> levels at higher speed could be alternative fiber spacing patterns. In the paracorporeal respiratory assist lung (PRAL) developed by Federspiel et al., oxygen supplied to blood increased by nearly half between 250 RPM and 750 RPM [64].

Additional experiments or controls could have been investigated based on the above findings. The presence of an EC layer may have more of an affect on CO<sub>2</sub> removal than O<sub>2</sub> accumulation, since CO<sub>2</sub> removal is an important factor in oxygenator design and can be limited by the presence of coatings on MHFs [39, 143]. Experiments involving higher percentages of CO<sub>2</sub> and lower percentages of O<sub>2</sub> may have shown significant differences in CO<sub>2</sub> accumulation that were not observed in the experiments utilizing 5% CO<sub>2</sub>. CO<sub>2</sub> levels did reach 38 mmHg (5% CO<sub>2</sub>) in experiments, but O<sub>2</sub> levels did not reach 722 mmHg (95% O<sub>2</sub>). Air bubbles were sometimes present at the higher speeds of rotation in MHF bundles tested in medium, which may have caused some error in these results, however overall data trends do not suggest that this effect had a significant impact. Yet, further investigations could be performed to understand why oxygen levels did not reach equivalent saturation levels in all experiments. In addition, controls of LPS, TNF-α or IL-1β could have been used as positive controls against hyperoxia. Langford et al. have shown BAEC disruption in the presence of LPS [144]. Marsden et al. has shown increased release of endothelin-1 and other alterations in EC phenotype in the presence of TNF-α [145].

#### **6.4.2 Evaluation of endothelialized MHF bundles following hyperoxia and bovine blood exposure**

In terms of biocompatibility, electron micrographs of thrombotic deposition showed a beneficial effect for endothelialized fibers in the biohybrid lung. At both test speeds, 250 RPM and 750 RPM, thrombotic deposition on endothelialized MHF bundles was equivalent or less than thrombotic deposition on non-endothelialized MHF bundles. Elevated levels of PECAM-1 and p-selectin expression are referenced indicators of inflammatory phenotype for ECs as well [77, 79]. PECAM-1 expression evaluated with confocal imaging remained low (refer to Appendix E). Levels of p-selectin expression on BAECs were also very low at both rotational speeds.

Upregulation of e-selectin has been reported in the presence of hyperoxia and inflammation for ECs [139]. Confocal images of MHF bundles rotated at 250 RPM or 750 RPM showed low to moderate levels of e-selectin expression on all fiber layers except the outer fiber layer at 750 RPM. Combined e-selectin, PECAM-1 and p-selectin data suggest that BAECs following 24 hr exposure to hyperoxia at 95% may still possess a non-inflammatory phenotype.

Additional or alternative methods of evaluation were intended for use in evaluation of the BAEC phenotype. This list includes increased flow cytometric expression of the monoclonal antibody against bovine ICAM-1 (Biovendor, RE11228C100), increased flow cytometric expression of the monoclonal antibody against bovine TF (gift of Dr. Stephen Carson at the University of Nebraska Medical Center, Omaha, NE), increased flow cytometric expression of monoclonal antibody against human VCAM-1 (Serotec, MC907S) and evaluation of apoptosis via annexin-v (Sigma, APOAF) binding. All positive controls were stimulated with TNF- $\alpha$  or IL-1 $\beta$  for 5 or more hours. Upregulation of ICAM-1 was observed for positive controls of HUVECs taken from tissue culture flasks, evaluated with flow cytometry. However, ICAM-1 upregulation by BAECs could not be elicited. This was true for a monoclonal antibody against human ICAM-1 as well as a monoclonal antibody against bovines. The selection of antibodies against bovines was quite limited. A monoclonal antibody against bovine TF did not show a response to positive controls for BAECs either, as evaluated with flow cytometry. This antibody, however, was from the 1980's and had not been used for several years. Antibodies against E-selectin and VCAM-1 did not show upregulation for positive controls via flow cytometry. They did show upregulation when observed with immunofluorescence microscopy. VCAM-1 showed a strong response to

stimulation with IL-1 $\beta$  or TNF- $\alpha$  for BAECs seeded on glass coverslips, but this did not translate to observable expression on MHFs viewed with confocal microscopy. Annexin-V could not be shown to exhibit increased binding with flow cytometry techniques either. BAECs stimulated with staurosporine (Sigma, S5921) showed obvious morphological changes that appeared to be apoptosis when viewed under a microscope, but the cells did not fluoresce in response to the annexin-v assay.

There seems to be a difference between hyperoxic affects on ECs *in vivo* as components of the vasculature rather than *ex vivo* or *in vitro* isolated EC exposure. In experiments involving whole lung exposure to hyperoxia, increased leukocyte and blood cell deposition has been reported in mice [110]. As discussed in section 1.5.4, changes in CAMs and cytokine levels were detected in mouse lungs subjected to 95% to 100% oxygen. ECs exposed to hyperoxia under tissue culture conditions do not show many of these deleterious affects [119, 120]. Lack of cell proliferation was the primary observation in hyperoxic *in vitro* cultures [146]. This may be attributed a reduction in plasma membrane fluidity, a mechanism for EC dysfunction [147]. BAECs exposed to 24 hrs of hyperoxia in the biohybrid lung did not incur higher levels of thrombotic deposition in comparison to control bundles. Less thrombotic deposition was observed on endothelialized bundles, which may be the most relevant criteria for evaluation of EC phenotype in the biohybrid lung prototype. This observation combined with overall low levels of e-selectin and p-selectin expression seem to suggest that BAECs maintained a healthy phenotype following multiple days (4-8) of rotation and 24 hrs of exposure to hyperoxia. The period of hyperoxia was shorter in the experiments for this study than for those in the cited literature, but overall strenuous effects on ECs, involving seeding and conditioning to shear stress, were longer.

## 7.0 SUMMARY

### 7.1 CONCLUSIONS

A biohybrid lung prototype was developed to explore a potential treatment option for patients suffering from ARDS. The biohybrid lung prototype allows for oxygenation through a rotating, endothelialized MHF bundle. MHFs were surface modified with RFGD and fibronectin adsorption to support EC attachment and growth for improved blood-surface contact within the device. ECs were then conditioned to withstand shear stress in the physiologic range. Near confluence was maintained at speeds tested up to 1500 RPM, corresponding to 29.6 dynes/cm<sup>2</sup>. The biohybrid lung prototype provides a useful tool to evaluate shear stress on ECs under rotation.

Bovine blood biocompatibility testing with the refined biohybrid lung prototype and MHFs used in the biohybrid lung prototype showed favorable evidence for incorporation of ECs into an extracorporeal device for extended respiratory support. Levels of BAEC coverage as low as approximately 20% showed a significant decrease in thrombotic deposition for MHFs treated with RFGD and fibronectin adsorption or RFGD and gelatin adsorption. It was shown that surface modification of MHFs with RFGD and gelatin or fibronectin adsorption greatly increased EC adherence and proliferation. The presence of ECs greatly reduced thrombotic deposition regardless of full confluence. Within the biohybrid lung, ECs provided equivalent or better blood-surface biocompatibility on MHF bundles modified with RFGD and fibronectin adsorption in comparison to untreated MHF bundles.

Oxygen accumulation curves in cell culture medium and in blood did not show a significant difference between pO<sub>2</sub> levels for endothelialized and non-endothelialized MHF bundles. This finding provides encouraging evidence that a biohybrid lung may not be limited in its ability to provide adequate oxygenation by the EC layer alone. Surface area requirements may

not need to be significantly increased due to the presence of an EC layer. It was also observed that a higher speed of rotation trended towards higher pO<sub>2</sub> levels than the lower test speed. This was statistically significant in blood at early time points. Thrombotic deposition on endothelialized MHF bundles exposed to 95% hyperoxia was equivalent or less than thrombotic deposition on non-endothelialized MHF bundles under 95% hyperoxia. This data in combination with low levels of e-selectin and p-selectin expression from BAECs suggested that the cells retained a non-thrombogenic, non-inflammatory phenotype, crucial to improving the biocompatibility as desired in this application.

The biohybrid lung prototype is novel in its aggressive approach toward modification of ECMO support. It combines active mixing, polymethylpentene MHFs, MHF modification and endothelialization. Other groups are pursuing mass transfer augmentation, use of alternative MHFs, addition of MHF coatings and even development of hybrid systems, independently. These areas of research are generating encouraging results. The biohybrid lung prototype could be altered to incorporate desirable attributes of other artificial lung devices under investigation. For example, the PRAL demonstrated increased gas exchange with increased rotation [64]. The PAL did not [65]. Design specifications, such as fiber spacing, from the PRAL could be incorporated into the biohybrid lung prototype to increase gas transfer. Findings from the hybrid lung under development by Takagi et al. support incorporation of ECs into an artificial lung for improved biocompatibility [72]. The use of PMP fibers to reduce poor wetting is supported by Toomasian et al [70]. An advantage that the biohybrid lung has over the above mentioned technologies is its combined approach to reduce fiber wetting, enhance gas exchange and improve biocompatibility. This comprehensive program may improve mortality rates associated with ARDS much more than approaches that address only one area of device insufficiency.

There are some limitations to the practicality of the biohybrid lung prototype that are not associated with approaches that exclude living cells. Incorporation of the biohybrid lung prototype into the intensive care setting would be a significant task. Integration of cell therapies into hospitals and patient care procedures are in their infant stages. Current cell therapies are limited to direct injection of cells into host tissue. Most facilities are not equipped to handle cell culture and expansion, or maintain *in vitro/ex vivo* cell sterility. Care givers are not trained to work with hybrid devices, and may be unaware of the delicate nature of the cells. For example, if cells are not maintained at approximately  $37 \pm 2^\circ\text{C}$  in the biohybrid lung prototype, they will die.

The extra training, equipment and fragility of the biohybrid lung will result in increased costs associated with the therapy. Insurance providers are hesitant to cover costs associated with cell therapies, unless they fall under approved procedures, such as autologous bone marrow or cell transplants [148]. To date, Medicare coverage for cell therapies is limited to autologous and allogeneic transplants only in severe cases, such as leukemia, lymphoma and neuroblastoma, for example [148]. Therefore it is critical to involve insurance companies in clinical trials to gain approval for future procedure/device reimbursement. Unfortunately, this may allow insurance providers to dictate the “appropriate science” related to a specific the cell therapy [148].

In addition, effective methods for autologous cell harvest and expansion have not been developed to render large cell counts. Fortunately, considerable effort is being expended to address this limitation by several groups to promote other modalities of cell therapy [149, 150]. A positive finding in the research shown within this dissertation is that subconfluent endothelialization may still provide statistically significant decreases of thrombotic deposition in comparison to non-endothelialized MHF bundles. Hurdles associated with incorporation of cell therapies into patient care will eventually be overcome as long as the need for cell therapy and regenerative medicine persists.

## 7.2 FUTURE WORK

Critical *in vitro* observations have been made with the biohybrid lung project, which suggest it should be further pursued in an animal model. The biohybrid lung prototype would require scaling up before it could be tested in the appropriate animal model, such as the bovine. However, it is important to address the limitations associated with the biohybrid lung as much as possible during scale up. It is also valuable to include relevant beneficial findings from other groups. For example, MHF fiber spacing and other design specifications from the PRAL could be incorporated into the scaled up version of the biohybrid lung to augment gas transfer with rotation.

Additional work could be done to improve cooling within the bioreactor. Incorporation of fluid purged seals could decrease heat generation associated with high torque requirements attributed to high levels of rotation. An alternative grip with lower heat conductivity could be

placed on the shaft of the MHF bundle to reduce transfer of heat from the motor through the titanium shaft.

Efforts could be taken to improve overall device biocompatibility. Blood entrance and exit ports could be optimized to decrease blood damage during blood perfusion. Balloon seals and string could be replaced with potentially less thrombogenic materials to separate the gas and liquid pathways within the device. Components such as tubing, the acrylic housing and connectors could be heparin coated, as is often done with PVC tubing and components of clinically used extracorporeal circuits [59].

Animal trials could be run in a bovine model to compare the enhanced/redesigned biohybrid lung prototype to a commercially available oxygenator, such as the heparin coated Maxima Plus oxygenator (Medtronic Inc., Anaheim, CA, USA). *In vivo* trials could initially be performed for 3 days. Based on these findings, trials could be extended to 1 week or multiple weeks.

Cell sources could be investigated, as well. ECs could be derived from an autologous bovine source through bone marrow or skeletal tissue muscle biopsies for precursor cells. Additional work would need to be done to guarantee sterility throughout the process. These cells could be expanded in culture, driven toward the EC phenotype and then seeded onto MHF bundles. Work could also be done to decrease EC seeding and growth time using the autologous source in the MHF bundle seeding process.

With an *in vivo* model more sensitive blood monitoring could be done, such as platelet count, IL-10 levels in serum, TNF- $\alpha$  levels, p-selectin expression on platelets (for platelet activation), CD63 expression (for platelet activation), platelet and leukocyte aggregate quantitation, and other assessments. A better understanding of overall hemostasis related to incorporation of the biohybrid lung and potential reductions in heparin therapy could be developed with an animal model.

## APPENDIX A

### NOMENCLATURE

#### Abbreviations

ACD	Acid Citrate Dextrose
AMMO	Active Mixing Membrane Oxygenator
APC	Activated Protein C
ARDS	Acute Respiratory Distress Syndrome
AT	Antithrombin
BAEC	Bovine Aortic Endothelial Cell
CAL	Chronic Artificial Lung
CAM	Cellular Adhesion Molecule
COPD	Chronic Obstructive Pulmonary Disease
EC	EC
ECMO	Extracorporeal Membrane Oxygenation
eNOS	Endothelial Nitric Oxide Synthase
ETO	Ethylene Oxide
HUVEC	Human Umbilical Vein Endothelial Cell
ICAM-1	Intracellular Adhesion Molecule-1
IL-(1,6,8)	Interleukin-(1,6,8)
IMO	Intravenous Membrane Oxygenator
iNOS	Inducible Nitric Oxide Synthase
IVOX	Intravenous Oxygenator

MHF	Microporous Hollow Fiber
MTT	Methylthiazolyl Diphenyl-tetrazolium
NO	Nitric Oxide
PAI-I	Type I Plasminogen Activator Inhibitor
PAL	Pumping Artificial Lung
PECAM-1	Platelet Endothelial Cell Adhesion Molecule-1
PEEP	Positive End Expiratory Pressure
PMP	Polymethylpentene
PRAL	Paracorporeal Respiratory Assist Lung
RFGD	Radio Frequency Glow Discharge
RGD	Arg-Gly-Asp
ROS	Reactive Oxygen Species
SD	Standard Deviation
SEM	Scanning Electron Micrograph
SE	Standard Error of the Mean
TFPI	Tissue Factor Pathway Inhibitor
TNF- $\alpha$	Tumor Necrosis Factor- $\alpha$
VCAM-1	Vascular Cell Adhesion Molecule-1
vWF	von Willebrand Factor
XPS	X-ray Photoelectron Spectroscopy

### **Symbols**

$a$	width
$b$	length
$C_i$	oxygen concentration of the reservoir
$C_o$	oxygen concentration in the biohybrid lung prototype
$d$	gap width between the inner and outer cylinder of the bioreactor
$d_p$	pore diameter
$D$	diffusion coefficient of the diffusing gas

$D_m$	diffusion coefficient of oxygen in water
$g_o$	gravity effects
$h$	fiber wall thickness
$H_m$	EC thickness
$K$	permeance
$K_{ec}$	permeance of the EC
$K_{ec/fiber}$	coated fiber permeance
$K_{fiber}$	permeance of the fiber
$K_l$	liquid-side permeance
$K_m$	diffusional resistance of the MHF membrane
$K_n$	Knudsen number
$L$	length of the MHF
$M$	molecular weight of the given gas
$Q$	flow rate
$R$	outer radius of the MHF
$R$	gas constant
$R_1$	outer radius of the MHF bundle
$Re$	Reynolds number
$R_i$	radius of the titanium module
$R_o$	radius of the inner wall of the bioreactor housing
$S$	oxygen concentration measured from medium
$S_a$	atmospheric partial pressure
$S_o$	zero oxygen partial pressure
$SA_{EC}$	surface area of an EC
$SA_{MHF}$	surface area of a MHF
$T$	absolute temperature
$Ta$	Taylor number
$U_1$	speed of the inner cylinder in the bioreactor
$v_r$	velocity in the r-direction
$v_o$	velocity in the theta-direction
$\alpha$	solubility coefficient

$\delta$	average boundary layer thickness
$\varepsilon$	porosity
$\theta$	theta-direction
$\lambda$	mean free path length of the diffusing species
$\mu$	dynamic viscosity
$\nu$	kinematic viscosity
$\rho$	density
$\tau$	pore tortuosity
$\Omega$	angular velocity

## APPENDIX B

### CELL COVERAGE CALCULATIONS

Cell coverage on MHFs was estimated from MTT related absorbency values. First, an average absorbency value was calculated from 3 samples of solution read spectrophotometrically. A linear trend line was fit to the MTT calibration curve to obtain the slope of the curve. The value of cells/mL was then calculated from Equation 17.

**Equation 17** Cells/mL calculated from MTT readings

$$\text{Cells/mL} = (\text{average absorbency})/(\text{slope of the MTT calibration curve})$$

The calculation for surface area for MHFs is given in Equation 18. R is the outer radius of the MHF. L is the length of the MHF.

**Equation 18** Surface area of MHFs

$$SA_{MHF} = 2\pi RL(\# \text{ fibers})$$

The value for cells/cm<sup>2</sup> was calculated (Equation 19).

**Equation 19** Cells/cm<sup>2</sup>

$$\text{Cells/cm}^2 = (\text{cells/mL})/(SA_{MHF})$$

The surface area of an individual EC was calculated (Equation 20). Each EC is assumed to be elliptical in shape, where *a* is width (48 μm) and *b* is length (31 μm) [151].

**Equation 20** EC surface area

$$SA_{EC} = \frac{\pi ab}{4}$$

The % (cell) coverage was estimated using Equation 21.

**Equation 21** % Coverage of ECs on MHFs

$$\% \text{ Coverage} = 100[(\text{cells}/\text{cm}^2)/(\text{cells}/ 1 \text{ cm}^2)]$$

## APPENDIX C

### PERFUSION OF THE BIOHYBRID LUNG

Simple calculations were performed to estimate a suitable flow rate for medium perfusion through the biohybrid lung prototype. It was assumed that adequately oxygenated medium (saturated) would flow from a reservoir through silicone tubing through the bioreactor and back. The goal was to provide adequate oxygenation to BAECs on the MHF bundle in the bioreactor. The main determinants for medium flow rate (Q) were number of cells in the bioreactor and the amount of oxygen consumption required by these cells. The total number of cells can be estimated using Equation 22.

**Equation 22** Calculation for number of cells on the MHFs

$$\#Cells = \frac{SA_{MHF}}{SA_{EC}}$$

Steinlechner-Maran et al. referenced 40 pmolO<sub>2</sub>/sec/10<sup>6</sup>cells as the metabolic rate of oxygen consumption [152, 153]. OUR is oxygen consumption rate (Equation 23). Equation 24 gives the estimated flow rate for adequate oxygenation of ECs.

**Equation 23** OUR for ECs in the biohybrid lung prototype

$$OUR = (\text{metabolic rate of oxygen consumption})(\#Cells)$$

**Equation 24** Flow rate

$$Q = \frac{(OUR)(\#Cells)}{C_i - C_o}$$

$C_o$  is the oxygen concentration in the biohybrid lung prototype, which was assumed to be zero.  $C_i$  is the oxygen concentration of the reservoir, and was found experimentally. A  $pO_2$  probe (Unisense) was placed in a reservoir of cell culture medium. Oxygen concentration was measured from the medium and expressed in pico amps. This value was fit into Equation 25 (as variable S) to calculate oxygen concentration.

**Equation 25** Oxygen concentration using a Unisense  $pO_2$  probe

$$C_i = \alpha \cdot (S - S_o) / (S_a - S_o)$$

$\alpha$  is the solubility of oxygen in the liquid, S is the signal recorded,  $S_o$  is zero oxygen partial pressure,  $S_a$  is atmospheric partial pressure.  $C_i$  was calculated from Equation 25 to be 284  $\mu\text{molO}_2/\text{L}$ . A minimum flow rate of 0.18 mL/min was calculated through this exercise for a MHF surface area of 250  $\text{cm}^2$ .

## APPENDIX D

### TAYLOR VORTICES

Taylor-Couette flow can occur in a coaxial cylinder setup when the inner cylinder rotates at a higher speed than an outer cylinder, which leads to toroidal vortices from hydrodynamic instability [129]. Taylor-Couette flow is described by the dimensionless Taylor number ( $Ta$ ) for a rotating cylinder within a stationary cylinder (Equation 26) [128, 129].

**Equation 26** Dimensionless Taylor number

$$Ta = \frac{Re^2 d}{R_1}$$

The gap width ( $d$ ) is the width between the inner and outer cylinders ( $d = 0.004$  m). The inner radius ( $R_1$ ) is the outer radius of the MHF bundle ( $R_1 = 0.0105$  m). The Reynolds number,  $Re$ , is given in Equation 27.

**Equation 27** Reynolds number

$$Re = \frac{U_1 d}{\nu}$$

The speed of the inner cylinder ( $U_1$ ) is given below in Equation 28, and adjusted for time (60 seconds). The kinematic viscosity ( $\nu$ ) for blood is  $2.83 \times 10^{-6}$  m<sup>2</sup>/s [128, 129].

**Equation 28** Speed of the inner cylinder in a Taylor-Couette system

$$U_1 = \frac{(RPM)(2\pi R_1)}{60}$$

Computed Taylor Numbers for speeds of rotation are given below (Table 4).

**Table 4** Taylor number for corresponding RPM in the biohybrid lung prototype

RPM	Velocity (m/s)	Reynolds # (for blood)	Taylor #
50	0.05	79	2348
100	0.11	157	9390
150	0.16	236	21128
200	0.22	314	37560
250	0.27	393	58688
300	0.33	471	84511
350	0.38	550	115029
400	0.44	628	150242
450	0.49	707	190149
500	0.55	785	234752
550	0.60	864	284050
600	0.66	942	338043
650	0.71	1021	396732
700	0.77	1099	460115
750	0.82	1178	528193
800	0.88	1256	600966
850	0.93	1335	678434
900	0.99	1413	760598
950	1.04	1492	847456
1000	1.10	1570	939010
1050	1.15	1649	1035258
1100	1.21	1727	1136202
1150	1.26	1806	1241840
1200	1.32	1884	1352174
1250	1.37	1963	1467202
1300	1.43	2041	1586926
1350	1.48	2120	1711345
1400	1.54	2198	1840459
1450	1.59	2277	1974268
1500	1.65	2355	2112771

High Taylor numbers may be an indication of turbulent flow. Steady vortices are observed at  $Ta < 800$ . Wavy vortices are described as  $800 < Ta < 2000$ . Turbulent vortices are in the range of  $2000 < Ta < 10,000-15,000$ . Turbulence is  $Ta > 15,000$  [129]. Due to the large gap between the MHF bundle and the outer housing of the biohybrid lung prototype, turbulent vortices are most likely present at a rotational speed as low as 50 RPM. Therefore, shear stresses may be higher than estimated in chapter 3.

## APPENDIX E

### PECAM-1 EXPRESSION BY BAECs ON MHF BUNDLES

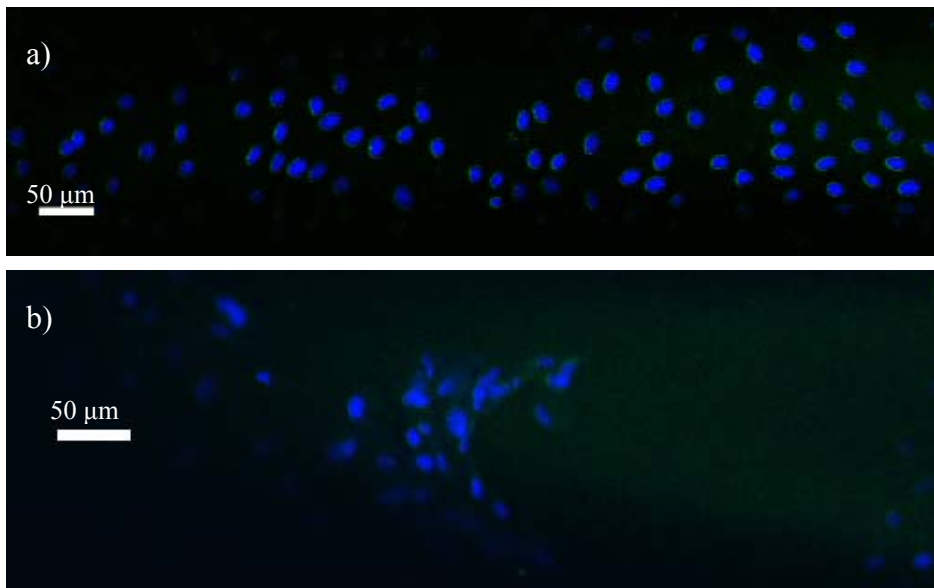


**Figure 7-1** PECAM-1 expression by BAECs on MHF bundles exposed to bovine blood  
Middle fiber layers of MHF bundles rotated at: a) 250 RPM, b) 750 RPM

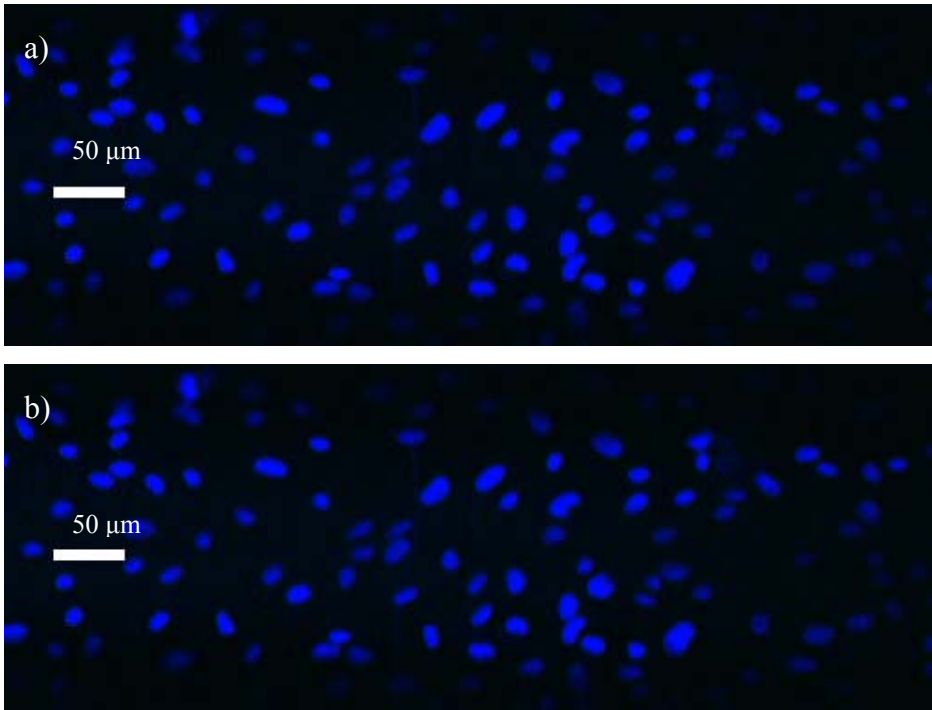


**Figure 7-2** PECAM-1 expression by BAECs on MHF bundles exposed to bovine blood and hyperoxia  
Outer fiber layers of MHF bundles rotated at: a) 250 RPM, b) 750 RPM

## **APPENDIX F**

### **PERMEANCE IN THE BIOHYBRID LUNG PROTOTYPE**

To evaluate oxygen delivery in the biohybrid lung prototype, a permeance test system was initially constructed. Results obtained from the system ultimately demonstrated large amounts of variance that made it difficult to compare permeance values between fiber types, speeds and MHFs with and without endothelialization. This prompted use of the ABL for gas measurements instead. However, the system is worth discussing and may have potential future use with an alternative device or test parameters.

The permeance test system was composed of an oxygen probe (Unisense, OX-500 fast, Aarhus, Germany), tachometer (built specifically for this setup), transducer box (built specifically for this setup), flow meter (Fathom Technologies, model GR116-1-A-PV), LabVIEW software (National Instruments, version 6), PC, data acquisition card (National Instruments, AT-MIO-16E), connector block (National Instruments, CB-68LP) and vacuum pump. A carbon dioxide probe could also be introduced into this system. A schematic of the permeance test system is shown in Figure 7-3.

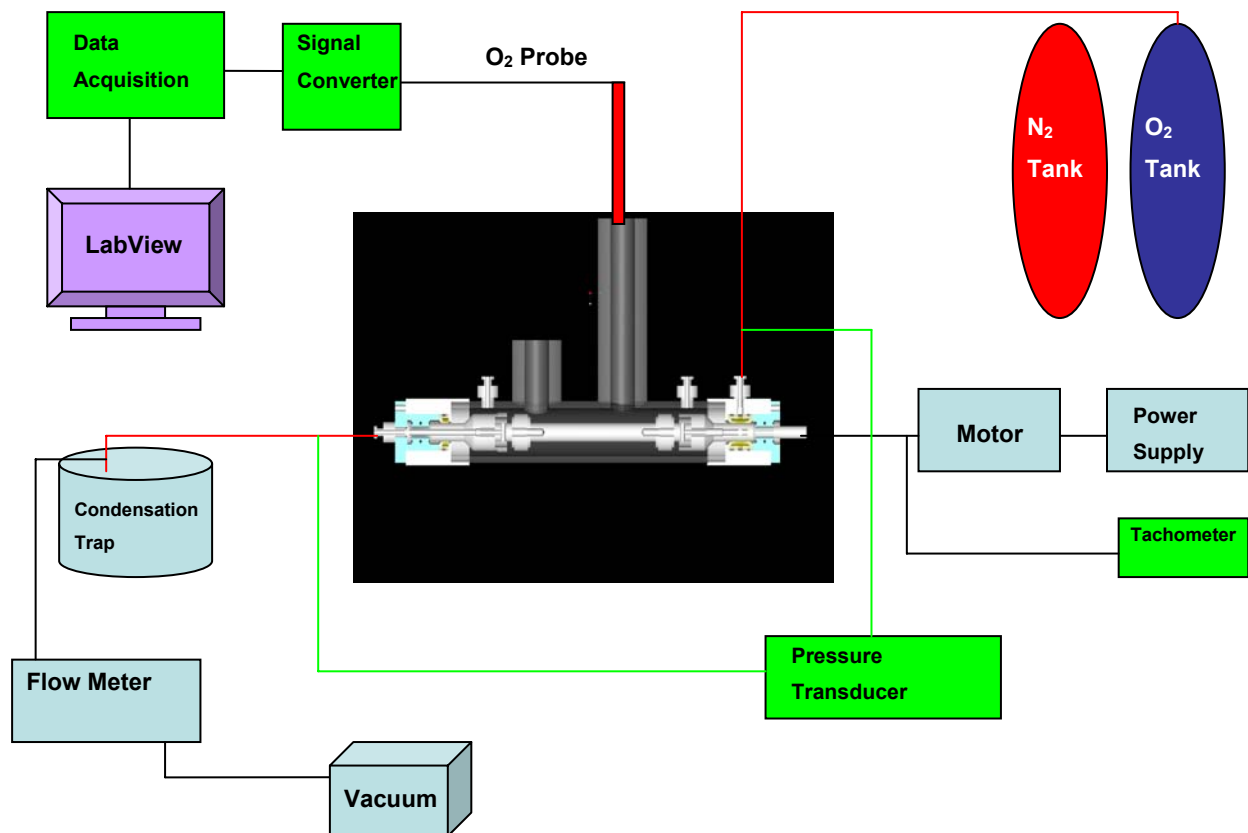


**Figure 7-3** Permeance test system

The permeance was calculated for oxygen by passing the test gas (95% O<sub>2</sub>, 5% CO<sub>2</sub>) through the lumen of the fibers. Once the test gas had built up within the surrounding liquid (water, for data shown below), the pO<sub>2</sub> probe reached a maximum reading. The inflow of gas was then changed from the test gas to a washout gas (95% N<sub>2</sub>, 5% CO<sub>2</sub>), and the decay rate was recorded. The washout rate constant ( $\lambda$ ) was obtained from plotting a log-linear scale of time verses pO<sub>2</sub>, and fitting an exponential curve to the data set. From this method,  $\lambda$  is found independently of the gas flow rate through the MHFs, and  $\lambda$  is proportional to the system permeability.

Permeance was calculated from Equation 29 [154].

**Equation 29** Permeance for the test system

$$K=(\lambda V\alpha)/A$$

The volume (V) of liquid within the biohybrid lung prototype was known. The oxygen solubility coefficient ( $\alpha$ ) is known for water or blood at a given temperature. And the area (A) can be calculated for the MHF bundle (expressed as  $SA_{MHF}$  in Appendix B, Equation 18). Permeance has the units of  $[ml/cm^2/s/cmHg]$ .

Permeance readings, obtained experimentally, are displayed in Figure 7-4.

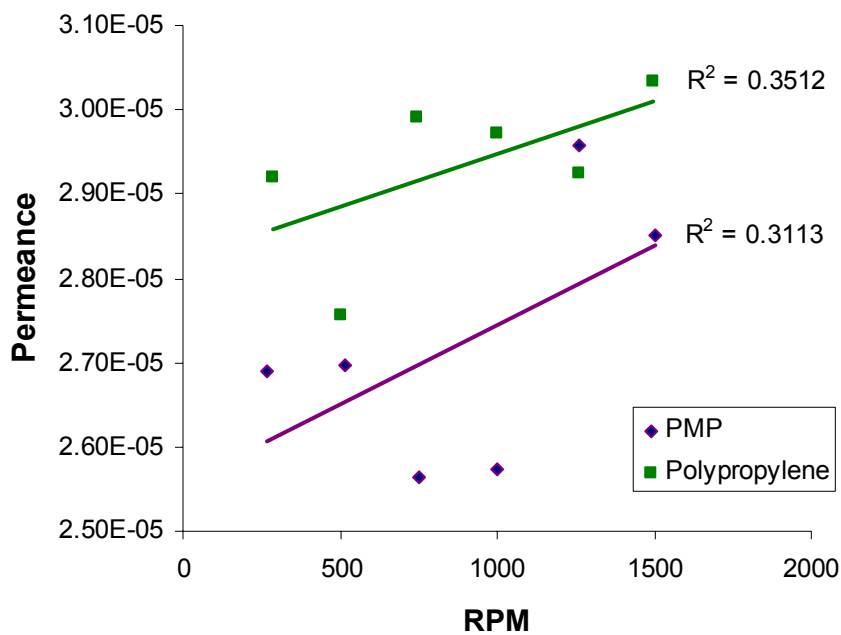


**Figure 7-4** Oxygen permeance of polypropylene and PMP MHFs in water  $pO_2$  was measured from the liquid side of the MHF bundle (n=4 per fiber type, per speed)

Permeance values were computed for increasing speeds of 250 to 1500 RPM for polypropylene (n=4) and PMP fibers (n=4). The data show an overall trend of better permeance with increasing RPM. However, the correlation is pretty poor with  $R^2$  values of 0.35 and 0.31 for polypropylene and PMP fibers, respectively. The data also show higher permeance for polypropylene fibers than PMP fibers. This is expected since polypropylene fibers have a porous surface and PMP fibers do not. The drop in permeance values for PMP fibers at 750 and 1000 RPM, as well as the drop in permeance values for polypropylene fibers at 1000 and 1250 RPM are difficult to explain. This occurrence could be due to experimental error from the sensitivity of

the pO<sub>2</sub> probe. It also could be due to air forming around the MHF bundle at these elevated speeds, which was observed repeatedly.

To further understand permeance variations expected to occur within the biohybrid lung prototype, equations were developed to describe the potential role of an EC layer. Equation 30 provides an estimated oxygen permeance through a single EC based on an assumed thickness (H<sub>m</sub>) of 0.2 μm, diffusion coefficient of oxygen in water (D<sub>m</sub>) and solubility coefficient of oxygen in water (α). Equation 31 combines the permeance of the fiber (K<sub>fiber</sub>) with the estimated permeance of the EC (K<sub>ec</sub>) to give a coated fiber permeance (K<sub>ec/fiber</sub>).

**Equation 30** Permeance for an EC layer

$$K_{ec} = (D_m \cdot \alpha) / H_m$$

**Equation 31** Permeance for a coated MHF

$$K_{ec/fiber} = [(1/ K_{fiber}) + (1/ K_{ec})]^{-1}$$

The calculated K<sub>ec</sub> in oxygen is 4.5x10<sup>-5</sup> ml/cm<sup>2</sup>/s/cmHg. K<sub>fiber</sub> for a PMP fiber (Membrana, Wuppertal, Germany) is 1.08x10<sup>-3</sup> ml/cm<sup>2</sup>/s/cmHg [39]. Therefore the combined permeance (using equation 33) is 4.32x10<sup>-5</sup> ml/cm<sup>2</sup>/s/cmHg. This calculation suggests that the presence of an EC on a MHF will greatly inhibit permeance. However, the EC is a biological entity, and Equation 30 may be a poor model of its permeance.

## BIBLIOGRAPHY

1. Carr, J.J., *Introduction to Biomedical Equipment Technology*. 4 ed. 2001, Columbus, OH: Prentice Hall. 3.
2. Hattler, B.G. *Gas Exchange in the Venous System: Support for the Failing Lung*. 2002. Georgetown.
3. *Eckert Animal Physiology Mechanisms and Adaptations*. 4 ed, ed. B. Randall, French. 1997, New York: W. H. Freeman and Company.
4. *NHLBI Clinical Trial Stopped Early: Successful Ventilator Strategy Found for Intensive Care Patients on Life Support*. 1999, NIH.
5. Ruffini, E., et al., *Frequency and mortality of acute lung injury and acute respiratory distress syndrome after pulmonary resection for bronchogenic carcinoma*. Eur J Cardiothorac Surg, 2001. **20**(1): p. 30-6, discussion 36-7.
6. ARDS. Medical Encyclopedia, MEDLINE Plus Health Information 2002 [cited.
7. Kollef, M.H. and D.P. Schuster, *The acute respiratory distress syndrome*. N Engl J Med, 1995. **332**(1): p. 27-37.
8. Ware, L.B. and M.A. Matthay, *The acute respiratory distress syndrome*. N Engl J Med, 2000. **342**(18): p. 1334-49.
9. Haitsma, J.J. and B. Lachmann, *Lung protective ventilation in ARDS: the open lung maneuver*. Minerva Anesthesiol, 2006. **72**(3): p. 117-32.
10. *Intensive care protocol*, The University Hospital, Newark, NJ: The University Hospital, Newark, NJ.
11. Barry, B.E. and J.D. Crapo, *Patterns of accumulation of platelets and neutrophils in rat lungs during exposure to 100% and 85% oxygen*. Am Rev Respir Dis, 1985. **132**(3): p. 548-55.
12. Kazzaz, J.A., et al., *Cellular oxygen toxicity. Oxidant injury without apoptosis*. J Biol Chem, 1996. **271**(25): p. 15182-6.

13. Welty, S.E., et al., *Increases in lung tissue expression of intercellular adhesion molecule-1 are associated with hyperoxic lung injury and inflammation in mice.* Am J Respir Cell Mol Biol, 1993. **9**(4): p. 393-400.
14. Schultz, M.J., et al., *Pulmonary coagulopathy as a new target in therapeutic studies of acute lung injury or pneumonia--a review.* Crit Care Med, 2006. **34**(3): p. 871-7.
15. Ratner, B.D., *Biomaterials Science; An Introduction to Materials in Medicine.* San 1996, San Diego: Academic Press. 410.
16. Seeger, W., et al., *Alveolar surfactant and adult respiratory distress syndrome. Pathogenetic role and therapeutic prospects.* Clin Investig, 1993. **71**(3): p. 177-90.
17. Sibbald, W., Anderson, RR, Reid, B, *Alveolo-capillary permeability in human septic ARDS: effect of high-dose cortico-steroid therapy.* Chest, 1981. **79**: p. 133-42.
18. Jepsen, S., Herlevsen, P, Knudsen, P, *Antioxidant treatment with N-acetylcysteine during adult respiratory distress syndrome: a prospective, randomized, placebo-controlled study.* Crit Care Med, 1992. **20**: p. 918-23.
19. Slotman, G., Burchard, KW, D'Arezzo, A, *Ketoconazole prevents acute respiratory failure in critically ill surgical patients.* J Trauma, 1988. **28**: p. 648-54.
20. Glauser, F., Polatty, RC, Sessler, CN, *Worsening oxygenation in the mechanically ventilated patient: causes, mechanisms, and early detection.* Am Rev Respir Dis, 1988. **138**: p. 458-65.
21. Montravers, P., Fagon, JY, Gilbert, C, Blanchet, F, *Pilot study of cardiopulmonary risk from pentoxifylline in adult respiratory distress syndrome.* Chest, 1993. **103**: p. 1017-22.
22. Cuthbertson, B.H., et al., *UK guidelines for the use of inhaled nitric oxide therapy in adult ICUs. American-European Consensus Conference on ALI/ARDS.* Intensive Care Med, 1997. **23**(12): p. 1212-8.
23. Rotta, A.T., C.L. Kunrath, and B. Wiryawan, *[Management of the acute respiratory distress syndrome].* J Pediatr (Rio J), 2003. **79 Suppl 2**: p. S149-60.
24. Tan, P.S., et al., *Nitric oxide contamination of hospital compressed air improves gas exchange in patients with acute lung injury.* Intensive Care Med, 2002. **28**(8): p. 1064-72.
25. Gianetti, J., S. Bevilacqua, and R. De Caterina, *Inhaled nitric oxide: more than a selective pulmonary vasodilator.* Eur J Clin Invest, 2002. **32**(8): p. 628-35.
26. Gerlach, H., et al., *Dose-response characteristics during long-term inhalation of nitric oxide in patients with severe acute respiratory distress syndrome: a prospective, randomized, controlled study.* Am J Respir Crit Care Med, 2003. **167**(7): p. 1008-15.

27. Bhandari, V., *The role of nitric oxide in hyperoxia-induced injury to the developing lung*. Front Biosci, 2003. **8**: p. e361-9.
28. Kobayashi, H., et al., *Antiinflammatory properties of inducible nitric oxide synthase in acute hyperoxic lung injury*. Am J Respir Cell Mol Biol, 2001. **24**(4): p. 390-7.
29. Steudel, W., et al., *Expression of nitric oxide synthase isoforms (NOS II and NOS III) in adult rat lung in hyperoxic pulmonary hypertension*. Cell Tissue Res, 1999. **295**(2): p. 317-29.
30. Potter, C.F., et al., *Effects of hyperoxia on nitric oxide synthase expression, nitric oxide activity, and lung injury in rat pups*. Pediatr Res, 1999. **45**(1): p. 8-13.
31. Wickramasinghe, S.R., et al., *Designing blood oxygenators*. Ann N Y Acad Sci, 2003. **984**: p. 502-14.
32. Hashimoto, K., et al., *Strategy for balancing anticoagulation and hemostasis in aortocoronary bypass surgery: blood conservation and graft patency*. Jpn Circ J, 1999. **63**(3): p. 165-9.
33. Miller, M.J., *Membrane Material Used in the Cobe Optima™ Hollow Fiber Membrane Oxygenator*, COBE Cardiovascular, Inc.: Arvada, CO.
34. Schmidt, B., *Membranes in artificial organs*. Artif Organs, 1996. **20**(5): p. 375-80.
35. Lund, L.W., *Is condensation the cause of plasma leakage in microporous hollow fiber membrane oxygenators*. Journal of Membrane Science, 1998. **147**: p. 87-93.
36. Ueyama, K., Y. Niimi, and Y. Nose, *How to test oxygenators for extracorporeal membrane oxygenation: is the Association for the Advancement of Medical Instrumentation's protocol enough?* Artif Organs, 1996. **20**(7): p. 741-2.
37. Segers, P.A., et al., *Clinical evaluation of nine hollow-fibre membrane oxygenators*. Perfusion, 2001. **16**(2): p. 95-106.
38. Welty, J., *Fundamentals of Momentum, Heat and Mass Transfer*. 4th ed. 2001, New York: John Wiley & Sons, Inc.
39. Eash, H.J., et al., *Evaluation of plasma resistant hollow fiber membranes for artificial lungs*. Asaio J, 2004. **50**(5): p. 491-7.
40. Niimi, Y., et al., *The effects of heparin coating of oxygenator fibers on platelet adhesion and protein adsorption*. Anesth Analg, 1999. **89**(3): p. 573-9.
41. Maslow, A. and C. Schwartz, *Cardiopulmonary bypass-associated coagulopathies and prophylactic therapy*. Int Anesthesiol Clin, 2004. **42**(3): p. 103-33.

42. Marcus, A.J. and L.B. Safier, *Thromboregulation: multicellular modulation of platelet reactivity in hemostasis and thrombosis*. *Faseb J*, 1993. **7**(6): p. 516-22.
43. Niimi, Y., *Impact of Oxygenator Membranes on Platelet Adhesion and Activation.* *Artificial Organs*. *Artificial Organs*, 1997. **21**(6).
44. Niimi, Y., et al., *Platelet adhesion to heparin coated oxygenator fibers under in vitro static conditions: impact of temperature*. *Asaio J*, 2001. **47**(4): p. 361-4.
45. de Maistre, E., Y. Gruel, and D. Lasne, *Diagnosis and management of heparin-induced thrombocytopenia: [Le diagnostic et le traitement de la thrombopenie induite par l'heparine]*. *Can J Anaesth*, 2006. **53**(6\_suppl): p. S123-S134.
46. Afshar-Kharghan, V. and P. Thiagarajan, *Leukocyte adhesion and thrombosis*. *Curr Opin Hematol*, 2006. **13**(1): p. 34-9.
47. Andrews, D.A. and P.S. Low, *Role of red blood cells in thrombosis*. *Curr Opin Hematol*, 1999. **6**(2): p. 76-82.
48. Paparella, D., S.J. Brister, and M.R. Buchanan, *Coagulation disorders of cardiopulmonary bypass: a review*. *Intensive Care Med*, 2004. **30**(10): p. 1873-81.
49. Lasne, D., B. Jude, and S. Susen, *From normal to pathological hemostasis: [De l'hemostase normale a l'hemostase pathologique]*. *Can J Anaesth*, 2006. **53**(6\_suppl): p. S2-S11.
50. Linden, M.D., *The hemostatic defect of cardiopulmonary bypass*. *J Thromb Thrombolysis*, 2003. **16**(3): p. 129-47.
51. Rubens, F.D., et al., *Effects of methylprednisolone and a biocompatible copolymer circuit on blood activation during cardiopulmonary bypass*. *Ann Thorac Surg*, 2005. **79**(2): p. 655-65.
52. Ask, A., D. Holt, and L. Smith, *In vivo comparison study of FDA-approved surface-modifying additives and poly-2-methoxyethylacrylate circuit surfaces coatings during cardiopulmonary bypass*. *J Extra Corpor Technol*, 2006. **38**(1): p. 27-32.
53. Medtronic, *Medtronic Cardiovascular Surgery - Arrested Heart - Overview - Product Overview*.
54. Ladowski, J.S., et al., *Clinical heparin coated cardiopulmonary bypass: reduction of systemic heparin requirements for redo cardiac surgery*. *Asaio J*, 1996. **42**(1): p. 34-6.
55. Sobieski, M.A., 2nd, et al., *Prospective study on cardiopulmonary bypass prime reduction and its effect on intraoperative blood product and hemoconcentrator use*. *Perfusion*, 2005. **20**(1): p. 31-7.

56. Allen, S., et al., *A clinical, renal and immunological assessment of surface modifying additive treated (SMART) cardiopulmonary bypass circuits*. *Perfusion*, 2005. **20**(5): p. 255-62.
57. Hsu, L.C., *Heparin-coated cardiopulmonary bypass circuits: current status*. *Perfusion*, 2001. **16**(5): p. 417-28.
58. Fukutomi, M., et al., *Changes in platelet, granulocyte, and complement activation during cardiopulmonary bypass using heparin-coated equipment*. *Artif Organs*, 1996. **20**(7): p. 767-76.
59. Johnell, M., R. Larsson, and A. Siegbahn, *The influence of different heparin surface concentrations and antithrombin-binding capacity on inflammation and coagulation*. *Biomaterials*, 2005. **26**(14): p. 1731-9.
60. Yamanaka, J., et al., [*The evaluation of the bio-compatibility and the clinical usefulness of heparin-coated cardiopulmonary bypass circuits*]. *Nippon Kyobu Geka Gakkai Zasshi*, 1996. **44**(1): p. 47-53.
61. Spiess, B.D., et al., *Heparin-coated bypass circuits (Carmeda) suppress the release of tissue plasminogen activator during normothermic coronary artery bypass graft surgery*. *J Cardiothorac Vasc Anesth*, 1998. **12**(3): p. 299-304.
62. Gartner, M. *The chronic artificial lung*. in *ASAIO*. 2003. Washington, D.C.
63. Wu, Z., *Progress toward an ambulatory pump-lung*. *J Thorac Cardiovasc Surg*, 2005. **130**(4): p. 973-8.
64. Svitek, R.G., B.J. Frankowski, and W.J. Federspiel, *Evaluation of a pumping assist lung that uses a rotating fiber bundle*. *ASAIO J*, 2005. **51**(6): p. 773-80.
65. Makarewicz, A., *A pumping intravascular artificial lung with active mixing*. *ASAIO J*, 1993. **39**(3): p. M466-9.
66. Makarewicz, A., *New design for a pumping artificial lung*. *Asaio J*, 1996. **42**(5): p. M615-9.
67. Niimi, Y., et al., *Effects of ultrathin silicone coating of porous membrane on gas transfer and hemolytic performance*. *Artif Organs*, 1997. **21**(10): p. 1082-6.
68. Iida, M., et al., *A newly developed silicone-coated membrane oxygenator for long-term cardiopulmonary bypass and cardiac support*. *Artif Organs*, 1997. **21**(7): p. 755-9.
69. Maeda, T., et al., *Preclinical evaluation of a hollow fiber silicone membrane oxygenator for extracorporeal membrane oxygenator application*. *Asaio J*, 2000. **46**(4): p. 426-30.

70. Toomasian, J.M., et al., *A polymethylpentene fiber gas exchanger for long-term extracorporeal life support*. *Asaio J*, 2005. **51**(4): p. 390-7.
71. Niwa, M., et al., *Development of a novel polyimide hollow-fiber oxygenator*. *Artif Organs*, 2004. **28**(5): p. 487-95.
72. Takagi, M., et al., *Hydrodynamically stable adhesion of endothelial cells onto a polypropylene hollow fiber membrane by modification with adhesive protein*. *J Artif Organs*, 2003. **6**(3): p. 222-6.
73. Pearson, J.D., *Endothelial cell function and thrombosis*. *Baillieres Best Pract Res Clin Haematol*, 1999. **12**(3): p. 329-41.
74. Ruggeri, Z.M., *Von Willebrand factor, platelets and endothelial cell interactions*. *J Thromb Haemost*, 2003. **1**(7): p. 1335-42.
75. Valujskikh, A. and P.S. Heeger, *Emerging roles of endothelial cells in transplant rejection*. *Curr Opin Immunol*, 2003. **15**(5): p. 493-8.
76. Jutila, M.A., et al., *Cell surface P- and E-selectin support shear-dependent rolling of bovine gamma/delta T cells*. *J Immunol*, 1994. **153**(9): p. 3917-28.
77. Blann, A.D., S.K. Nadar, and G.Y. Lip, *The adhesion molecule P-selectin and cardiovascular disease*. *Eur Heart J*, 2003. **24**(24): p. 2166-79.
78. Van Kampen, C. and B.A. Mallard, *Regulation of bovine E-selectin expression by recombinant tumor necrosis factor alpha and lipopolysaccharide*. *Vet Immunol Immunopathol*, 2001. **79**(3-4): p. 151-65.
79. Gong, N. and S. Chatterjee, *Platelet endothelial cell adhesion molecule in cell signaling and thrombosis*. *Mol Cell Biochem*, 2003. **253**(1-2): p. 151-8.
80. van der Zijpp, Y.J., A.A. Poot, and J. Feijen, *ICAM-1 and VCAM-1 expression by endothelial cells grown on fibronectin-coated TCPS and PS*. *J Biomed Mater Res A*, 2003. **65**(1): p. 51-9.
81. Mathur, A.B., G.A. Truskey, and W.M. Reichert, *Synergistic effect of high-affinity binding and flow preconditioning on endothelial cell adhesion*. *J Biomed Mater Res A*, 2003. **64**(1): p. 155-63.
82. Pratt, K.J., et al., *Kinetics of endothelial cell-surface attachment forces*. *J Vasc Surg*, 1988. **7**(4): p. 591-9.
83. Larsen, C.C., et al., *The effect of RGD fluorosurfactant polymer modification of ePTFE on endothelial cell adhesion, growth, and function*. *Biomaterials*, 2006. **27**(28): p. 4846-55.

84. Hatakeyama, H., et al., *Bio-functionalized thermoresponsive interfaces facilitating cell adhesion and proliferation*. *Biomaterials*, 2006.
85. Pierschbacher, M.D. and E. Ruoslahti, *Cell attachment activity of fibronectin can be duplicated by small synthetic fragments of the molecule*. *Nature*, 1984. **309**(5963): p. 30-3.
86. Celej, M.S., G.G. Montich, and G.D. Fidelio, *Conformational flexibility of avidin: the influence of biotin binding*. *Biochem Biophys Res Commun*, 2004. **325**(3): p. 922-7.
87. Kojima, N., T. Matsuo, and Y. Sakai, *Rapid hepatic cell attachment onto biodegradable polymer surfaces without toxicity using an avidin-biotin binding system*. *Biomaterials*, 2006. **27**(28): p. 4904-10.
88. Lawley, T.J. and Y. Kubota, *Induction of morphologic differentiation of endothelial cells in culture*. *J Invest Dermatol*, 1989. **93**(2 Suppl): p. 59S-61S.
89. Wang, D.A., et al., *In situ immobilization of proteins and RGD peptide on polyurethane surfaces via poly(ethylene oxide) coupling polymers for human endothelial cell growth*. *Biomacromolecules*, 2002. **3**(6): p. 1286-95.
90. Chung, T.W., et al., *Enhancing growth human endothelial cells on Arg-Gly-Asp (RGD) embedded poly (epsilon-caprolactone) (PCL) surface with nanometer scale of surface disturbance*. *J Biomed Mater Res A*, 2005. **72**(2): p. 213-9.
91. Zhu, Y., et al., *Endothelium regeneration on luminal surface of polyurethane vascular scaffold modified with diamine and covalently grafted with gelatin*. *Biomaterials*, 2004. **25**(3): p. 423-30.
92. Mooradian, D.L., et al., *Effect of glow discharge surface modification of plasma TFE vascular graft material on fibronectin and laminin retention and endothelial cell adhesion*. *J Surg Res*, 1992. **53**(1): p. 74-81.
93. Pratt, K.J., S.K. Williams, and B.E. Jarrell, *Enhanced adherence of human adult endothelial cells to plasma discharge modified polyethylene terephthalate*. *J Biomed Mater Res*, 1989. **23**(10): p. 1131-47.
94. Sipehia, R., et al., *Enhanced attachment and growth of human endothelial cells derived from umbilical veins on ammonia plasma modified surfaces of PTFE and ePTFE synthetic vascular graft biomaterials*. *Biomater Artif Cells Immobilization Biotechnol*, 1993. **21**(4): p. 455-68.
95. Tseng, D.Y. and E.R. Edelman, *Effects of amide and amine plasma-treated ePTFE vascular grafts on endothelial cell lining in an artificial circulatory system*. *J Biomed Mater Res*, 1998. **42**(2): p. 188-98.

96. Nerem, R.M., et al., *Hemodynamics and vascular endothelial biology*. J Cardiovasc Pharmacol, 1993. **21 Suppl 1**: p. S6-10.
97. Davies, P.F., Robotewskyj, A., Griem, M. L. , *Quantitative studies of endothelial cell adhesion*. J Clin Invest, 1994. **93**: p. 2031-2038.
98. Davies, P.F., Remuzzi, A., Gordon, E. J., Dewey, C. F. Jr., Gimbrone, M. A. Jr., *Turbulent fluid shear stress induces vascular endothelial cell turnover in vitro*. Proc Natl Acad Sci USA, 1986. **83**: p. 2114-2117.
99. Lin, K., et al., *Molecular mechanism of endothelial growth arrest by laminar shear stress*. Proc Natl Acad Sci U S A, 2000. **97**(17): p. 9385-9.
100. Ueda, A., et al., *Effect of shear stress on microvessel network formation of endothelial cells with in vitro three-dimensional model*. Am J Physiol Heart Circ Physiol, 2004. **287**(3): p. H994-1002.
101. Ballermann, B.J., et al., *Shear stress and the endothelium*. Kidney Int Suppl, 1998. **67**: p. S100-8.
102. Nerem, R.M., et al., *The study of the influence of flow on vascular endothelial biology*. Am J Med Sci, 1998. **316**(3): p. 169-75.
103. Jankowski, R.J., et al., *Effect of retroviral transduction on human endothelial cell phenotype and adhesion to Dacron vascular grafts*. J Vasc Surg, 1997. **26**(4): p. 676-84.
104. Kriegelstein, C.F. and D.N. Granger, *Adhesion molecules and their role in vascular disease*. Am J Hypertens, 2001. **14**(6 Pt 2): p. 44S-54S.
105. Van Kampen, C. and B.A. Mallard, *Regulation of bovine intercellular adhesion molecule 1 (ICAM-1) and vascular cell adhesion molecule 1 (VCAM-1) on cultured aortic endothelial cells*. Vet Immunol Immunopathol, 2001. **79**(1-2): p. 129-38.
106. Ni, C.W., et al., *Shear flow attenuates serum-induced STAT3 activation in endothelial cells*. J Biol Chem, 2003. **278**(22): p. 19702-8.
107. Fisher, A.B., et al., *Endothelial cellular response to altered shear stress*. Am J Physiol Lung Cell Mol Physiol, 2001. **281**(3): p. L529-33.
108. Piedboeuf, B., et al., *Increased endothelial cell expression of platelet-endothelial cell adhesion molecule-1 during hyperoxic lung injury*. Am J Respir Cell Mol Biol, 1998. **19**(4): p. 543-53.
109. DeLisser, H.M. and S.M. Albelda, *The function of cell adhesion molecules in lung inflammation: more questions than answers*. Am J Respir Cell Mol Biol, 1998. **19**(4): p. 533-6.

110. Barazzone, C., et al., *Hyperoxia induces platelet activation and lung sequestration: an event dependent on tumor necrosis factor-alpha and CD11a*. Am J Respir Cell Mol Biol, 1996. **15**(1): p. 107-14.
111. Barazzone, C., et al., *Plasminogen activator inhibitor-1 in acute hyperoxic mouse lung injury*. J Clin Invest, 1996. **98**(12): p. 2666-73.
112. Perkowski, S., et al., *Gene expression profiling of the early pulmonary response to hyperoxia in mice*. Am J Respir Cell Mol Biol, 2003. **28**(6): p. 682-96.
113. Shackelford, R.E., W.K. Kaufmann, and R.S. Paules, *Oxidative stress and cell cycle checkpoint function*. Free Radic Biol Med, 2000. **28**(9): p. 1387-404.
114. Lum, H. and K.A. Roebuck, *Oxidant stress and endothelial cell dysfunction*. Am J Physiol Cell Physiol, 2001. **280**(4): p. C719-41.
115. Zhao, X., *Redox regulation of endothelial barrier integrity*. Am J Physiol Lung Cell Mol Physiol 2001. **281**(4): p. L879-86.
116. Weissman, M.H. *Blood Oxygenation I: Fundamentals*. in AIOCE Symposium. 1972.
117. Kunicki, T., *Platelet membrane glycoproteins and their function: an overview*. Blut, 1989. **59**(1): p. 30-4.
118. Stevens, T., et al., *Mechanisms regulating endothelial cell barrier function*. Am J Physiol Lung Cell Mol Physiol, 2000. **279**(3): p. L419-22.
119. Klein, C.L., et al., *Comparative studies on vascular endothelium in vitro. 2. Hypoxia: its influences on endothelial cell proliferation and expression of cell adhesion molecules*. Pathobiology, 1995. **63**(1): p. 1-8.
120. Lee, S.L., et al., *Ultrastructural changes in bovine pulmonary artery endothelial cells exposed to 80% O<sub>2</sub> in vitro*. In Vitro, 1983. **19**(9): p. 714-22.
121. Colman, R.W., *Hemostatic complications of cardiopulmonary bypass*. Am J Hematol, 1995. **48**(4): p. 267-72.
122. Waxler, B., *Cell Stroma Interactions in Aortic Endothelial Cell Cultures*. Laboratory Investigation, 1979. **41**(2): p. 128-134.
123. *Product Information, MTT Product No. M 5655*, Sigma.
124. Shimono, T., et al., *Silicone-coated polypropylene hollow-fiber oxygenator: experimental evaluation and preliminary clinical use*. Ann Thorac Surg, 1997. **63**(6): p. 1730-6.
125. *Alamar Blue<sup>TM</sup> Product Analysis Sheet*, Biosource International: USA.

126. Gloeckner, H., Jonuleit, T, Lemke, H, *Monitoring of cell viability and cell growth in a hollow-fiber bioreactor by use of the dye Alamar Blue<sup>TM</sup>*. Journal of Immunological Methods, 2001. **252**: p. 131-138.
127. Bird, R., *Transport Phenomena*. 2 ed. 2002, New York: John Wiley & Sons, Inc.
128. Batten, W., *Numerical simulations of the evolution of Taylor cells from a growing boundary layer on the inner cylinder of a high radius ratio Taylor-Couette system*. Physical Review, 2002. **66**: p. 066302-1 - 066302-5.
129. Baier, G., *Prediction of mass transfer rates in spatially periodic flows*. Chemical Engineering Science, 1999. **54**: p. 343-355.
130. Samet, M.M., Chick, D. M., Chistensen, C. W., Lelkes, P. I., *Morphology and integrity of endothelial cell monolayers inside a ventricle shaped perfusion chamber*. ASAIO J, 1993. **39**(3): p. M403-9.
131. Frame, M.D., Sarelius, I. H., *Flow-induced cytoskeletal changes in endothelial cells growing on curved surfaces*. Microcirculation, 2000. **7**: p. 419-427.
132. *Lung Injury Mechanisms, Pathophysiology and Therapy*, ed. R.H. Notler, Finkelstein, J. N., Holm, B. A. Vol. 196. 2005, Boca Raton: Taylor and Francis Group.
133. Hertfelder, H.J., et al., *Perioperative monitoring of primary and secondary hemostasis in coronary artery bypass grafting*. Semin Thromb Hemost, 2005. **31**(4): p. 426-40.
134. Jagneaux, T., D.E. Taylor, and S.P. Kantrow, *Coagulation in sepsis*. Am J Med Sci, 2004. **328**(4): p. 196-204.
135. Harker, L.A., *Mechanism of abnormal bleeding in patient undergoing cardiopulmonary bypass: Acquired transient platelet dysfunction associated with selective alpha-granule release*. Blood, 1980. **56**: p. 824-834.
136. Khuri, S.F., *Hematologic changes during and after cardiopulmonary bypass and their relationship to the bleeding time and nonsurgical blood loss*. J Thorac Cardiovasc Surg, 1992. **104**: p. 94-107.
137. Fuglsang, J., et al., *Platelet activity and in vivo arterial thrombus formation in rats with mild hyperhomocysteinaemia*. Blood Coagul Fibrinolysis, 2002. **13**(8): p. 683-9.
138. Ohata, T., et al., *Hybrid artificial lung with interleukin-10 and endothelial constitutive nitric oxide synthase gene-transfected endothelial cells attenuates inflammatory reactions induced by cardiopulmonary bypass*. Circulation, 1998. **98**(19 Suppl): p. II269-74.
139. Zund, G., et al., *Hypoxia enhances stimulus-dependent induction of E-selectin on aortic endothelial cells*. Proc Natl Acad Sci U S A, 1996. **93**(14): p. 7075-80.

140. Bernard, R., *Fundamentals of Biostatistics*. 5th ed, ed. C. Crockett. 2000, Pacific Grove: Duxbury Thomson Learning.
141. Kanamori, T., et al., *Estimate of gas transfer rates of an intravascular membrane oxygenator*. *Asaio J*, 2000. **46**(5): p. 612-9.
142. Dumas, D., et al., *Membrane fluidity and oxygen diffusion in cholesterol-enriched endothelial cells*. *Clin Hemorheol Microcirc*, 1999. **21**(3-4): p. 255-61.
143. Federspiel, W.J. and B.G. Hattler, *Sweep gas flowrate and CO<sub>2</sub> exchange in artificial lungs*. *Artif Organs*, 1996. **20**(9): p. 1050-2.
144. Langford, P.R., Szabo, M., Moxon, E. R., *In vitro cytotoxicity of Haemophilus influenza lipopolysaccharides for bovine aortal endothelial cells*. *FEMS Microbiol Lett*, 1991. **65**(2): p. 161-4.
145. Marsden, P.A., Brenner, B. M., *Transcriptional regulation of the endothelin-1 gene by TNF-alpha*. *Am J Physiol*, 1992. **262**(4 Pt 1): p. C854-61.
146. Bjerkvig, R., et al., *Effects of hyperoxia on human endothelial cell proliferation and morphology in vitro*. *Undersea Biomed Res*, 1992. **19**(6): p. 415-26.
147. Block, E.R., et al., *Hyperoxia reduces plasma membrane fluidity: a mechanism for endothelial cell dysfunction*. *J Appl Physiol*, 1986. **60**(3): p. 826-35.
148. Norton, K. *Utilizing Clinical Trials to Foster Payer Adoption*. in *Regenerate World Congress on Tissue Engineering and Regenerative Medicine*. 2006. Pittsburgh.
149. Parker, A.M., Katz, A. J., *Adipose-derived stem cells for the regeneration of damaged tissues*. *Expert Opin Biol Ther*, 2006. **6**(6): p. 567-78.
150. Sugrue, M.W., Hutcheson, C. E., Fisk, D. D., Roberts, C. G., Mageed, A., Wingard, J. R., Moreb, J. S., *The effects of overnight storage of leukapheresis stem cell products on cell viability, recovery, and cost*. *J Hematother*, 1998. **7**(5): p. 431-6.
151. Schneider, *Rapid aldosterone-induced cell volume increase of endothelial cells measured by the atomic force microscope*. *Cell Bio International*, 1997. **21**(11): p. 759.
152. Steinlechner-Maran, R., *Oxygen dependence of respiration in coupled and uncoupled endothelial cells*. *American Journal of Physiology (Cell Physiology)*, 1996. **271**: p. 2053.
153. Martin, Y. and P. Vermette, *Bioreactors for tissue mass culture: design, characterization, and recent advances*. *Biomaterials*, 2005. **26**(35): p. 7481-503.
154. Lund, L.W., et al., *A novel method for measuring hollow fiber membrane permeability in a gas-liquid system*. *Asaio J*, 1996. **42**(5): p. M446-51.